The Dissertation Committee for Rex Young Nielson Certifies that this is the approved version of the following dissertation:

Nonlinear Laser Microfabrication in Biological Environments

Committee:

Jason B. Shear, Supervisor

Richard M. Crooks

James A. Holcombe

Christine E. Schmidt

David A. Vanden Bout

Nonlinear Laser Microfabrication in Biological Environments

by

Rex Young Nielson, B.S.; M.S.

Dissertation

Presented to the Faculty of the Graduate School of

The University of Texas at Austin

in Partial Fulfillment

of the Requirements

for the Degree of

Doctor of Philosophy

The University of Texas at Austin

December 2007

Dedication

This dissertation is dedicated to my wife, Rhonda

Acknowledgements

I would like to thank my advisor, Jason Shear, for his immeasurable help and patience. I would also like to thank the members of my committee for their consideration and time. I thank the exceptional people I have had the privilege of working with in the Shear Lab. Drs. Richard Allen and Bryan Kaehr were generous enough to allow me to collaborate with them on the material described in Chapters 3 and 4 respectively. They, along with the other graduate students who were in the Shear Lab when I arrived, Drs. Dana Wise, Ryan Hill, and Matt Plenert answered many of my questions and taught me a great deal. I would like to thank the current members of the lab Eric Ritschdorff, Samira Moorjani, Stephanie Seidlets, Eric Spivey, Zhou Lu, Todd Hoppe and Jodi Connell. It has been a pleasure to work with them for the last several years. I have enjoyed getting to know our bright and enthusiastic first year students Michelle Fox and Maryam Ali. The department's resident electronics wizard Tim Hooper deserves many thanks, without him the project described in Chapter 4 would have amounted to nothing more than a voided warranty on a digital projector. My sincerest gratitude goes to my parents and the rest my family including my wife, whose help with this dissertation has gone beyond spousal love and support; she assisted in the preparation of many of the figures. Financial support for this work was provided by the National Institute of Health and the Welch Foundation.

Nonlinear Laser Microfabrication in Biological Environments

Publication No._____

Rex Young Nielson, Ph.D.

The University of Texas at Austin, 2007

Supervisor: Jason B. Shear

Microscope optics have long been used to observe biological samples, when used in conjunction with a laser light source, they can also be a powerful means to probe and manipulate cells. This dissertation describes the development of methodologies for laser-based microfabrication in biological environments. These techniques use pulsed laser light at a wavelength transparent to the experimental medium except in a region with submicron dimensions defined by the focus of a high numerical aperture objective. At the focal region, high intensity light can modify sample material. The localized nature of this energetic event allows it to be accomplished in the vicinity of living cells, enabling microfabrication strategies that are used to probe and modify extracellular environments with high resolution. The basic principles of this process are explored and its use in several applications for cell culture manipulation are described. In one methodology the focused laser induces physical and chemical events that lead to the formation of a micron-scale solid from a precursor protein solution. By translating the relative position of the beam in the solution, arbitrary

three-dimensional structures can be formed. The use of protein microstructures as a platform for probing and manipulating cellular microenvironments is investigated and an advanced method of rapidly patterning elaborate structures with a spatial light modulator is demonstrated. The high intensity laser focus is used in a second strategy to create microfluidic conduits in a device consisting of two stacked flow channels, one containing adherent cells in buffer and the other a reagent solution. With laser ablation of a pore, highly defined reagent plumes are directed into the cell-containing chamber where they can dose multiple specifically targeted regions with subcellular specificity. The unique microfabrication technologies described in this dissertation could prove to be of use for researchers developing diagnostic and therapeutic devices and could lead to more advanced tools for studying the basic biology of cells.

Table of Contents

List of Figures

Chapter 1: Introduction

1.1 BIOLOGICAL MICROFABRICATION

There is a broad interest in developing microfabrication techniques for use in biological contexts. Building on the micro-scale has proven profoundly successful for the development of electronic devices. Here, microfabrication led to increasingly powerful instruments, with more uses, which can be manufactured more quickly, and less expensively. Researchers developing microfabrication techniques for the life sciences and related areas of chemistry hope to find analogous benefits. Chemical and biological procedures generally involve the transport and processing of materials, making artificial miniaturization more challenging than it is for electronics. However, significant advantages could be realized for bioanalytical and medical devices that could duplicate some of the precision, modularity, and amenability to mass production seen in microelectronics.

A wide range of chemical and biological research fields rely to a significant extent on microfabrication techniques. For example, micro-total-analysis or "lab-on-a-chip" approaches seek to build biological and chemical analysis systems where multiple analytical processes are integrated onto a single microfabricated platform [1, 2]. Likewise, some tissue engineering approaches use microfabrication techniques to mimic the microstructural details of natural tissue in the development of designed materials with controlled biological response [3, 4]. Microarrays probably represent the most developed

application of microfabrication technologies to biological analysis. Microarrays are a commonly used research tool, and may one day play a key role in the development of personalized medicine [5]. The development and characterization of microfabrication techniques with unique biological capabilities could potentially be useful in a broad range of areas, from tissue engineering therapies to microarray based diagnostics.

Microfabrication techniques are becoming important for the study of cells. With conventional cell culture methodologies, cells are introduced, allowed to differentiate, and are tested on a planer surface bathed in homogeneous solutions. While the ability to examine cells *in vitro* is a highly important biological technique, it has limitations. Animal cells in a monolayer on a two-dimensional substrate can behave differently than they would in tissue. Cells cultured in systems able to mimic aspects of the complex three-dimensional (3D) environment of tissue exhibit phenotypes and express molecules different from cells in 2D cell culture [6, 7]. Microfabrication offers promising routes for extending the capabilities of conventional cell culture by adding 3D topographical features, and gradients of immobilized and diffusible chemicals. The ability to mimic some of the complex features of tissue leads to new ways to analyze and control cells [8, 9]. Enhancement of cell culture techniques with microfabrication shows promise in a variety of applications. For example, microfabrication of cell culture analogs that mimic the drug transport properties of tissue have been studied as a possible route to more efficient drug screening methodologies [10] and microfabricated platforms have shown the ability to influence the proliferation and differentiation of stem cell populations [11]. While most microfabrication techniques introduce cells onto prefabricated substrates, the

Shear Lab has developed a unique niche in cell culture microfabrication technologies—microfabrication in live cell culture.

The Shear Lab works on the development of laser-based microanalytical techniques for the study of biomolecules and cells. This includes capillary electrophoresis to track the expression of cell metabolites, fast separations for the analysis of transient states of biological molecules, and work on sensor arrays [12-14]. The lab has also developed microfabrication schemes that can be accomplished in biological environments [15]. The harsh processes necessary for the formation or removal of microsolids are relegated to the femtoliter volume at the beam waist of a laser focused though high numerical aperture (NA) objective. This allows microfabrication in cellular buffers, in the vicinity of living cells.

Techniques of direct modification of cellular microenvironments are important for biological investigations. The development of new tools for molecular biology, such as expression cloning and polymerase chain reaction, has facilitated a dramatic growth in the knowledge of the molecular workings inside of the cell. However, many of the common methods of manipulating the external microenvironments of cells remain relatively primitive. For example, often micropipettes are simply manipulated into the vicinity of the cell to release reagents.

Microfabrication techniques effectively gentle enough to be accomplished in the presence of cells could potentially lead to new ways of testing and manipulating cells in a manner more efficient and effective than achieved using current technologies. This could enable new types of studies of how cells sense and respond to their local environments. There are many examples of why this is an important area of study. For instance, during

animal development dividing and migrating cells acquire dynamic positional information from their local environments to find their properly incorporated position in the organism. Localized signals in the extracellular environment also can play a detrimental role for the organism, as when cancer cells induce angiogenesis which supports tumor growth [16, 17]. Insight into important biological events could be gained from methodologies that can, in an experimentally controlled cell culture environment, efficiently probe and analyze cells at the same scales as the natural phenomena in question.

1.2 MICROFABRICATION TECHNIQUES

The work presented in this dissertation describes development of two microfabrication techniques. The first is a microfabrication technique based on the phase change of protein, from solvated in aqueous solution, to a solid with micro-scale dimensions. The photon flux of a pulsed laser focused through a microscope objective into a protein solution can be high enough to lead to nonlinear absorption and deposition of laser energy at the focal volume. This leads to the formation of a protein particle with micron-scale dimensions. By scanning the focal volume in the sample with beam directing galvano mirrors and/or x,y,z stage micropositioning 3D microstructures can be built. Aqueous protein is a uniquely biocompatible precursor material for microfabrication. This dissertation describes experiments in which the activities and morphologies of cells, bathed in protein-based microfabrication solutions, remain unaffected for hours. The fabrication process is also highly compatible with cells because

of its extremely localized nature. The processes leading to protein condensation are relegated to small enough regions that structures can be made within microns of cells.

Though the protein microsolids have not been fully characterized it is clear that they retain characteristics of their solution phase precursors. This work describes experiments that use an avidin precursor for microstructure fabrication. After laser processing, the avidin incorporated into a designed matrix maintains a strong affinity for its ligand, biotin. This outcome is useful for functionalizing the structures with biotin-linked enzymes. Decoration of avidin structures with various biotin-linked reagents is a way to build chemically active 3D structures. Since a degree of the solution phase protein characteristics are maintained after laser processing, it should be feasible to directly fabricate microstructures with desired chemistries by using the appropriate precursor material. This could provide a useful tool in the design of 3D cell environments with defined chemical and structural characteristics.

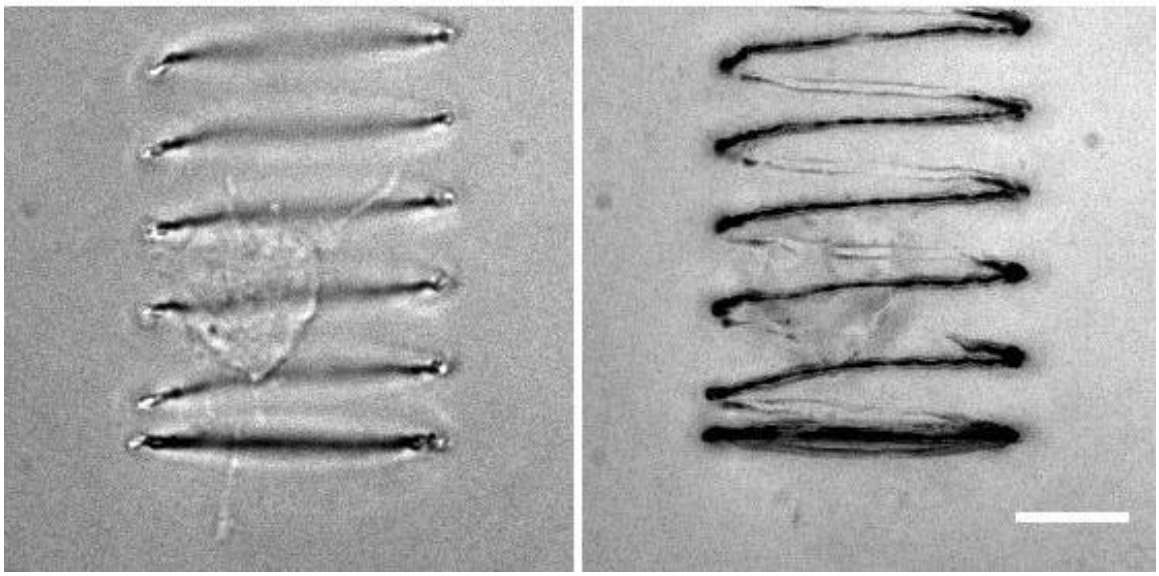

Figure 1.1 Example of biocompatible microfabrication. The images show a coil-like protein structure that was made around a cell suspended in a Matrigel™ matrix. The left image shows a plane with the cell in focus. The right image is an average of a series of images at various planes along the z axis that better shows the protein microstructure. Scale bar, 20 μm.

This dissertation also describes the use of pulsed lasers for a process that involves microfabrication of pores in a membrane that separates two microfluidic channels. On one surface of the membrane, adherent cells are bathed in a flow of buffer while various reagents are pumped through the chamber on the opposing side of the membrane. Upon laser induced formation of a pore, upstream from a targeted cell, a plume of reagent emerges into the cell containing channel. Taking advantage of the highly laminar nature of fluid flow in microchannels, the micron width plumes can be targeted to subcellular regions of the adherent cells. The result is a reagent application method with a unique combination of resolution and the ability to dose multiple sites simultaneously.

It is anticipated that the techniques described in this dissertation will be the subject of further development and eventually prove to be of use for researchers laboring in the important tasks of advancing therapeutics, diagnostics, and the basic understanding of cell biology.

1.3 Overview of the Chapters

This chapter outlined the motivations and techniques of the research described in this dissertation. Chapter 2 reviews the mechanisms of nonlinear interactions of high intensity lasers in aqueous media. Estimates are provided of the levels of energy deposition for various experimental configurations and some of the likely physical and chemical processes underlying the microfabrication schemes are discussed. This chapter is meant to provide a guide for future experimental characterizations of the microfabrication processes.

Cell compatible additive microfabrication is the topic of Chapter 3. Protein microfabrication in cellular environments is demonstrated including the enzymatic functionalization of protein microstructures and the use of protein microstructures as guides to control the movements of motile cells.

Chapter 4 describes a method for rapid patterning of protein microstructure using a digital micro-mirror array from Texas Instruments to spatially and temporally control laser exposure at the focal plane. The use of commercial video projection instrumentation in conjunction with custom image manipulation and presentation software enables arbitrary 3D microstructures to be designed and prototyped at a high rate.

Chapter 5 describes a unique cell dosing system based on a stacked microfluidic channel geometry. It is demonstrated that with the device, adherent cells can be dosed with high precision with a variety of reagents. Also, a scheme to control the reagent plumes with a more complicated microfluidic geometry is presented.

.

1.4 REFERENCES

1. Whitesides, G.M., *The origins and the future of microfluidics.* Nature, 2006. **442**(7101): p. 368-373.

2. Dittrich, P., K. Tachikawa, and A. Manz, *Micro total analysis systems. Latest advancements and trends.* Analytical Chemistry, 2006. **78**(12): p. 3887-908.

3. Vozzi, G., et al., *Fabrication of PLGA scaffolds using soft lithography and microsyringe deposition.* Biomaterials, 2003. **24**(15): p. 2533-40.

4. Khademhosseini, A., et al., *Microscale technologies for tissue engineering and biology.* Proceedings of the National Academy of Sciences, 2006. **103**(8): p. 2480-2487.

5. Muller, U. and D. Nicolau, *Microarray technology and its applications*. 2005: Springer.

6. Cukierman, E., et al., *Taking cell-matrix adhesions to the third dimension.* Science, 2001. **294**(5547): p. 1708.

7. Winters, B., et al., *Three-dimensional culture regulates raf-1 expression to modulate fibronectin matrix assembly.* Molecular Biology of the Cell, 2006. **17**(8): p. 3386.

8. Sims, C. and N. Allbritton, *Analysis of single mammalian cells on-chip.* Lab on a Chip, 2007. **7**: p. 423-440.

9. El-Ali, J., P. Sorger, and K. Jensen, *Cells on chips.* Nature, 2006. **442**(7101): p. 403-411.

10. Viravaidya, K., A. Sin, and M. Shuler, *Development of a microscale cell culture analog to probe naphthalene toxicity.* Biotechnology Progress, 2004. **20**(1): p. 316-323.

11. Chung, B., et al., *Human neural stem cell growth and differentiation in a gradient-generating microfluidic device.* Lab Chip, 2005. **5**: p. 401-406.

12. Wise, D. and J. Shear, *Quantitation of nicotinamide and serotonin derivatives and detection of flavins in neuronal extracts using capillary electrophoresis with multiphoton-excited fluorescence.* Journal of Chromatography A, 2006. **1111**(2): p. 153-158.

13. Sohn, Y., et al., *A microbead array chemical sensor using capillary-based sample introduction: toward the development of an "electronic tongue".* Biosensors and Bioelectronics, 2005. **21**(2): p. 303-312.

14. Plenert, M. and J. Shear, *Microsecond electrophoresis.* Proceedings of the National Academy of Sciences, 2003. **100**(7): p. 3853-3857.

15. Kaehr, B., et al., *Guiding neuronal development with in situ microfabrication.* Proceedings of the National Academy of Sciences, 2004. **101**(46): p. 16104-16108.

16. Dvorak, H., *How tumors make bad blood vessels and stroma*. American Journal of Pathology, 2003. **162**: p. 1747-1757.

17. Cairns, R., R. Khokha, and R. Hill, *Molecular mechanisms of tumor invasion and metastasis: an integrated view.* Curr Mol Med, 2003. **3**(7): p. 659-671.

Chapter 2: Mechanisms of High Intensity Laser Processing of Biological Substrates

This dissertation describes the use of high intensity light as a tool for submicron resolved modification of biologically relevant substrates. At a sufficient intensity level, light energy can be deposited into an otherwise transparent material. Experimentally, high intensity levels are achieved by use low duty cycle pulsed lasers and by focusing the beam to a small cross-sectional area by means of a high numerical aperture (NA) lens system. The threshold intensity for nonlinear effects relegates the affected area to a microscopically resolved 3D volume, which provides a unique tool to probe and modify biological environments. This chapter surveys some of the physical and chemical events involved in this process.

2.1 INTRODUCTION

The response of materials to high intensity light can be a complex process that involves energy gradients and phase transformations that evolve on sub-nanosecond time scales. This chapter does not seek to furnish a comprehensive or quantitative description of these processes, but is an attempt to provide some elements of a conceptual framework to guide future experiments. Increased understanding of the mechanisms involved in laser microfabrication in biological media will allow more control of the process, which will be important for the further development of the technologies. The nonlinear laser interactions described in this dissertation involve three intensity regimes. The lowest

intensity levels involve multiphoton absorption. Here photons with energies lower then those required for direct absorption by a molecular species induce electronic excitation when the sum of their energies is combined in a near simultaneous absorption event. The probability of this event is very small, therefore it only happens at any significant frequency with a high photon flux, such as can be achieved at the beam waist of a focused, pulsed laser. With the excitation of an appropriate fluorophore this process can provide emission from a region that is microscopically resolved in three-dimensions. Scanning the fluorescence emitting focal volume is the basis of a commonly employed strategy for optical slicing and imaging known as *multiphoton microscopy*.

Typically, higher laser intensities are used for experiments where light focused into a protein solution results in the formation of solid matrix whose initial size can be restricted to submicron dimensions of the focal volume. By scanning the laser focus in the protein solution, arbitrary 3D microstructures can be fabricated. This process can be described as *additive microfabrication*.

Generally the highest intensity levels, used in experiments described in this dissertation, are for a type of *subtractive microfabrication*. In this case a laser is focused into a polymer membrane that is used as a cell culture substrate. The membrane substrate is ionized at the laser focus which leads to heating, melting, cavitation and the removal of material. The resulting microscopically defined pore is used as a conduit for the targeted dosing of cells with reagent.

The processes mentioned above are initiated by the generation and spatio-temporal localization of laser energy. The next two sections will discuss how this is accomplished.

2.2 LASER SYSTEMS

Laser systems have a remarkable capacity for effectively concentrating power. The average power outputs of the lasers described in this dissertation are relatively low, in the 10's to 100's of milliwatts. However, the lasers are pulsed and have low duty cycles meaning that the power during a pulse is much higher than the time averaged power. When the lasers are tightly focused with a high NA lens, the flux of photons at the beam waist can be extremely high. The intensity values of the focused laser light in some applications described here can exceed 1 TW cm^{-2} (10^{12} W cm^{-2}). At such intensities, light that is transparent to the bulk of the sample can be absorbed in the focal volume, leading to photochemical and photophysical events in and near the focal volume. These events include, fluorescence, photochemistry and optical breakdown.

Figure 2.1 shows the layout of the equipment used for focusing and scanning a laser beam within a sample. Two basic light sources were used for the experiments described in this dissertation. Most of the initial work was accomplished with mode-locked titanium sapphire (Ti:S) lasers which provided red light in ~150 fs pulses with repetition rates of ~76 MHz. The second source used was a Q-switched, frequency doubled (532 nm), microchip Nd:YAG (Neodymium Yttrium Aluminum Garnet) laser which has a pulse frequency of 7.7 kHz, with a pulse width of 0.6 ns. The Nd:YAG's energy was distributed over longer pulse widths in comparison to the Ti:S laser. However, the energy of each pulse was larger (μJ vs. nJ) so the intensities of both lasers were within an order of magnitude of each other.

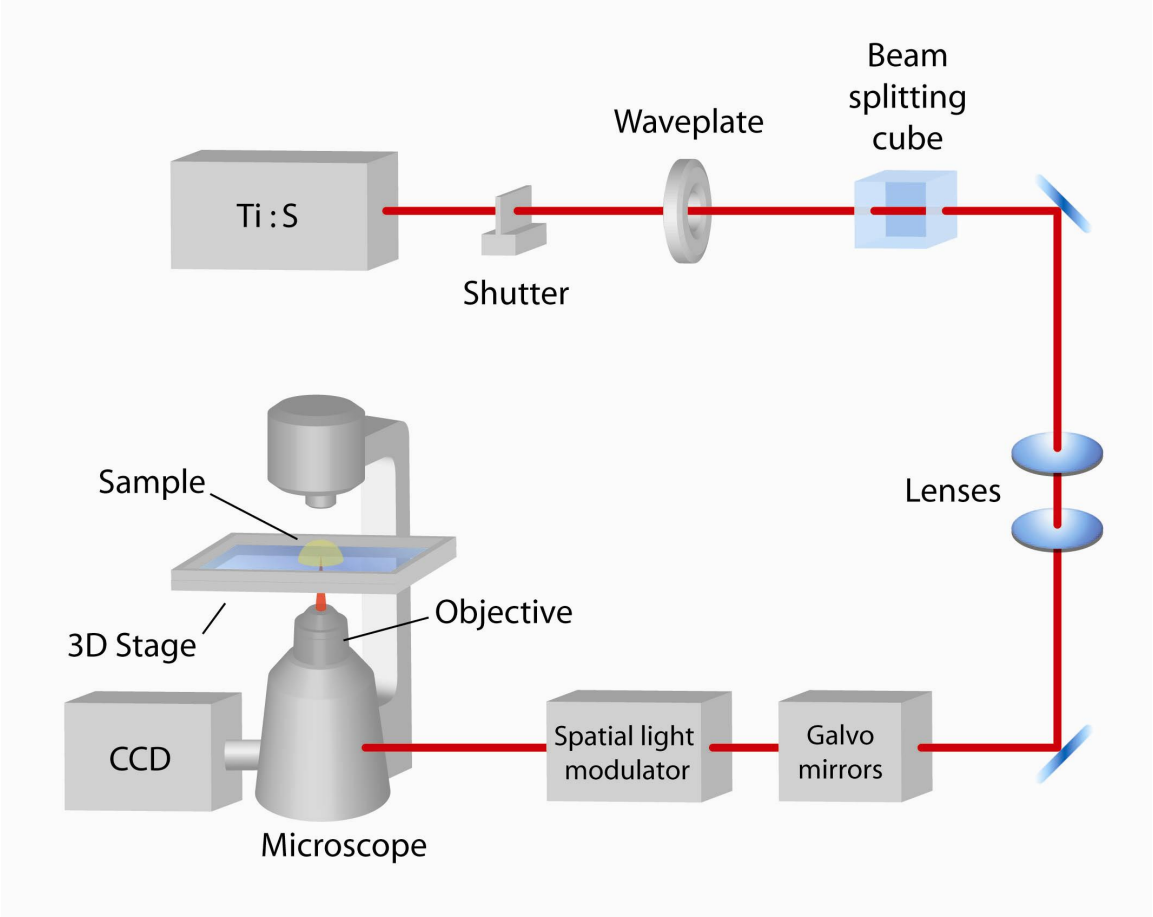

Figure 2.1: A schematic of the instrumentation used for laser microfabrication

The laser output was directed by mirrors into a half wave plate and beam splitting cube which were used to control the average power of the laser beam. A pair of lenses served as a telescope to expand and collimate the beam. The beam was then directed onto a dichroic mirror mounted inside a microscope, which aligned the laser with the microscope's optical train. The microscope and its attached CCD camera were used to observe and record processes at the focal plane of the objective. During experiments, the focal volume was scanned by means of a motorized microscope stage or a piezo driven

3D scanner. Chapter 4 describes the addition of beam scanning galvano mirrors and a spatial light modulator. Positioned before the microscope, these components allowed rapid patterning of the light in the focal plane of the microscope objective. The distribution of light at the focal plane region is a critical component of these experiments and is the subject of the next section.

2.3 INTENSITY PROFILE

The point spread function describes the intensity distribution in the vicinity of the front focal plane of a microscope objective. This is most accurately described as a vector field. However, a rigorous description of a femtosecond laser pulse brought to a focus through multiple dielectric interfaces is complex. Researchers studying the high intensity transformation of materials with focused light have often found it convenient to take the simplifying step of approximating the intensity distribution in Gaussian terms, similar to what is shown below [1-4]. While Gaussian approximations simplify calculations and make available straight forward analytical expressions, it should be noted that more rigorous vectorial approaches are available [5, 6].

The high intensity region at the laser beam waist has a prolate spheroidal shape where the long axis is aligned with the optical axis. Its dimensions can be described by the Rayleigh length z_o

$$z_o = \frac{w_o^{\,2}\pi\eta}{\lambda} \tag{1}$$

where η is the refractive index of the sample medium, λ is the laser wavelength, and w_o is the beam waist which for a diffraction limited focus can be described by

$$w_o = 0.61\frac{\lambda}{NA} \tag{2}$$

A parameter necessary to estimate the intensity distribution is the incident power of a laser pulse which is known a "peak power" P_o

$$P_o = \frac{P_{avg}\varphi}{\tau\,\omega} \tag{3}$$

here P_{avg} is the average power measured at the back aperture of the objective, φ is the throughput of the objective for the given wavelength, τ is the pulse width, and ω is the pulse repetition rate ($\tau\omega$ is the duty cycle). Typical functions describing the temporal variation of power during a laser pulse to not vary largely from the assumption of constant power during a square pulse [7]. Thus, for simplicity, it is assumed that power is constant during a pulse and these equations are not written explicitly as functions of time.

The peak intensity I_o is found by dividing the peak power by the beam waist area. The multiple of *2* gives the maximum for a Gaussian distribution.

$$I_o = \frac{2P_o}{w_o^{\,2}\pi} \tag{4}$$

A typical protein cross-linking experiment might use a Ti:S laser tuned to 740 nm with a pulse width of 150 fs, a pulse frequency of 76 MHz, and an average power of 30 mW. Focusing the laser using a 1.3 NA objective with an 80% transmittance at the wavelength of light would give a peak intensity value of 1.1 TW cm^{-2}.

The Gaussian-Lorentzian (GL) formula performs as well as other Gaussian estimates for approximating the intensity distribution of a diffraction limited focus [8]. This equation is commonly used to describe diffraction limited focal volumes in fluorescence correlation spectroscopy [9-11] because it is straightforward to integrate (which is done below). The GL also provides an accurate physical description of the spatial intensity profile with the non-diffraction limited focus that results from underfilling the back aperture of the objective [12], a format used for some of the experiments described in this dissertation. Figure 2.2a shows the axial view of the GL spatial intensity distribution as described by the formulas:

$$w(z) = w_o \sqrt{1 + \left(\frac{z}{z_o}\right)^2} \tag{5a}$$

$$S(r,z) = w_o^2 \frac{\exp(-2r^2/w(z)^2)}{w(z)^2} \tag{5b}$$

$$I(r,z) = I_o\, S(r,z) \tag{5c}$$

Here r and z are the radial and axial coordinates respectively, equation (5a) characterizes the beam divergence, and equation (5b) describes a unitless spatial distribution function. The intensity distribution can be obtained by multiplying $S(r,z)$ by the peak intensity I_o as shown in equation (5c). The nonlinear response of the medium to light intensity means that the affected region is potentially more confined then the intensity distribution. The response of the medium to an n-photon process can be effectively described by raising the intensity distribution function to the nth power [1, 12, 13]. The decreased spatial distribution for a for a two-photon process $I(r,z)^2$ is shown in figure 2.2b.

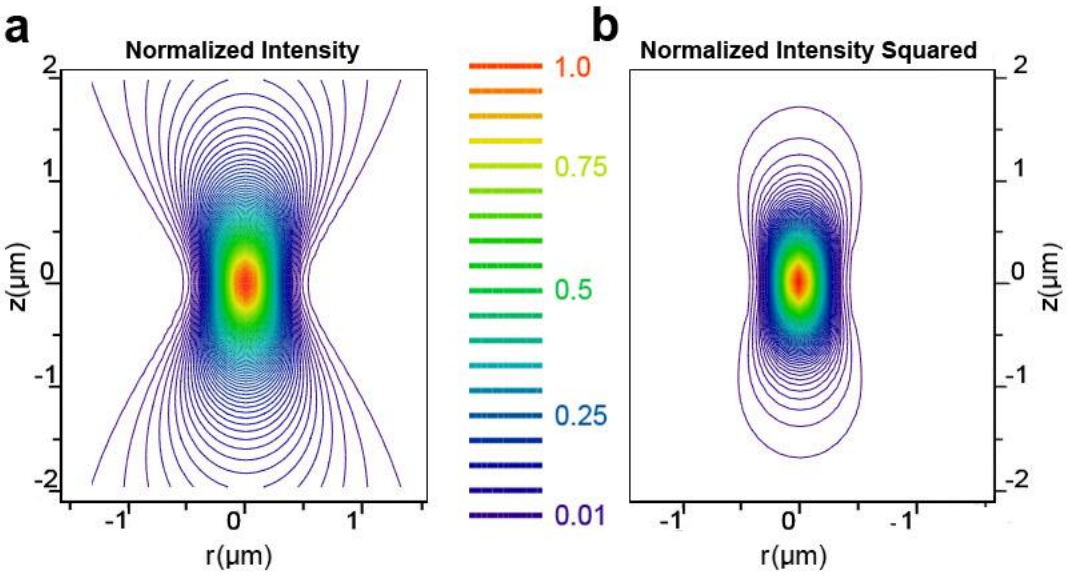

Figure 2.2: Focused light and affected region. (a) Optical axis cross-section of a beam waist for a GL intensity distribution. (b) The same function squared to depict the region of response for a two-photon process. Calculations were for a 1.3 NA objective and a laser wavelength of 740 nm. Both functions were normalized to one.

2.4 Absorption of Light Energy

2.4.1 Electronic Excitation and Ionization

Figure 2.3 depicts mechanisms for electronic excitation and ionization. Linear absorption is depicted by figure 2.3a. Here the energy of the photon is equal to energy separation between the ground and the excited state. This describes a medium that is not transparent to impinging photons.

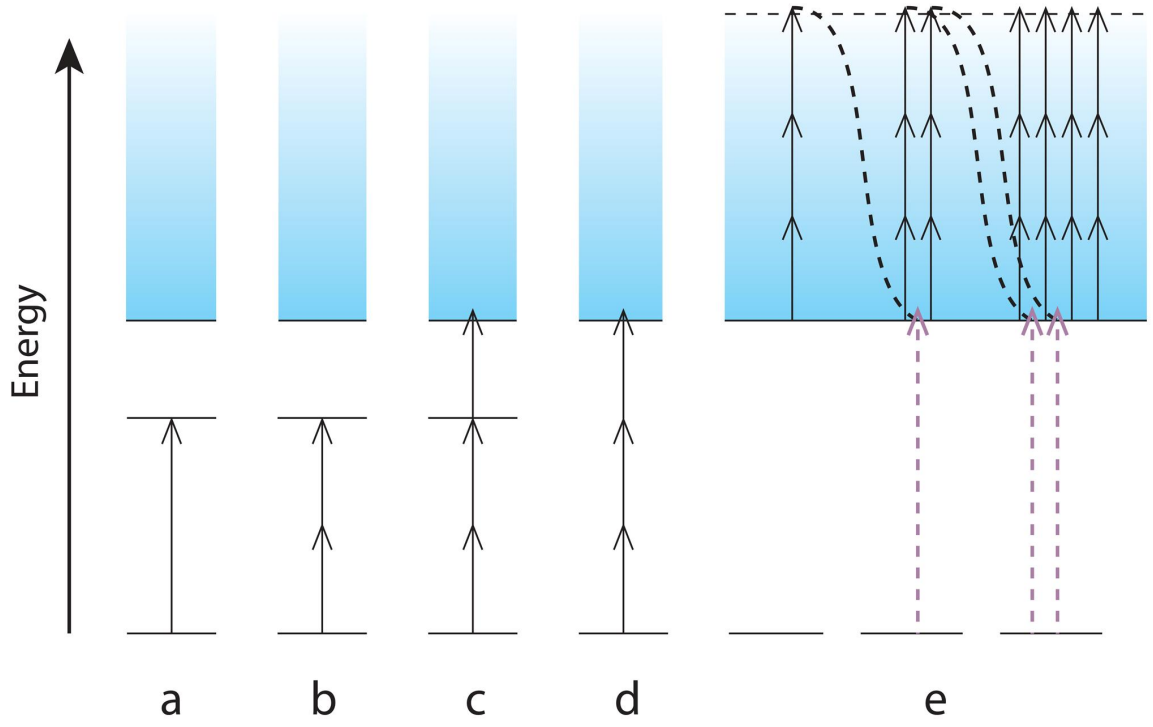

Figure 2.3: Processes for frequency dependent photon deposition in material. (a) one photon absorption, (b) two-photon absorption, (c) multiphoton ionization with an intermediate resonant level, (d) non-resonant multiphoton ionization, (e) Avalanche ionization: initially free electron absorbs photons gaining enough energy to promote a valence electron through impact (depicted by dashed arrows). The process is repeated with the newly promoted electrons.

Figure 2.3b depicts two-photon absorption. For multiphoton processes, the bound electron is promoted to a higher energy level by the near simultaneous absorption of n photons, the sum of whose energies nhv is equal to or greater then the transition energy

(*hv* is the energy of a photon). Multiphoton absorption was not experimentally observed until after the invention of the laser due to the requirement of extremely high intensities for it to be achieved at significant rates.

The photon absorption rate W_n (photons/sec) for one or multiple photon processes can be described with the phenomenological term.

$$W_n \propto \sigma_n F^n \tag{6}$$

Here F is the laser flux (photons cm^{-2} sec^{-1}), and σ_n is the nth-order cross-section (cm^{2n} sec^{n-1} $photon^{-(n-1)}$ $molecule^{-1}$). The simple F^n dependence where n is an integer does not hold for stepwise nonlinear transition, such as depicted by Figure 2.3c. In this case an intermediate resonant level generally decreases the flux necessary to achieve a given transition rate [14]. The next section will discuss the multiphoton absorption process in detail.

2.4.2 Multiphoton Absorption

Experimentally, multiphoton processes are easiest to monitor by observing the fluorescent decay of excited states. Unlike one-photon processes transmittance is difficult to measure because a relatively small fraction of the incident light is attenuated in the sample. Typical two-photon cross-section values for molecular fluorophores are within an order of magnitude of 10^{-50} cm^4 s $photon^{-1}$, and three-photon cross-sections generally have significantly smaller absolute values [12, 15]. Fluorophores allow observation of the

multiphoton processes by proxy. Light emission by a fluorophore excited by n photons is proportional to the photon absorption rate. This allows laboratory measurement of the intensity range for a given nonlinear absorption process. At laser powers too low, no signal is detected, and for a power too high, fluorescence loses F^n dependence. This can happen because of saturation, intersystem crossing, photobleaching or the onset of higher order processes. A typical peak intensity range for multiphoton fluorescence of a stable fluorophore excited by ~150 femtosecond near-IR pulses is approximately 0.01 to 0.2 TW cm^{-2}.

The formula predicting the n-photon absorption rate has the form of equation (6) written as a function of the illuminated sample volume with an additional term for the number concentration of absorbers C (molecules cm^{-3}). Assuming σ_n and C are constants and that F^n has axial symmetry the equation can be given [12, 16]:

$$W_n = \sigma_n C \int F^n(r,z)dV \tag{7}$$

To describe two-photon absorption with terms defined above, the equation has the form:

$$W_2 = \sigma_2 \frac{C}{(h\nu)^2} I_o^2 \int S^2(r,z)dV \tag{8}$$

Here dividing photon flux F by the photon energy $h\nu$ converts the variable to peak intensity. The assumption of time and space independence for the femtosecond pulse

allows us to equate the spatial intensity distribution with the peak intensity I_o (equation 4) multiplied by the spatial distribution function S (equation 5c) [12]. The integral of the square of the spatial distribution function can be evaluated analytically by writing the integral in cylindrical coordinates. Because the focal region is typically much smaller then the beam path through the sample the limits of integration can be written as infinite.

$$\begin{aligned} \int S(r,z)^2 dV &= \int_{-\infty}^{\infty}\int_{0}^{\infty} S^2(r,z) 2\pi r \, dr dz \\ &= \frac{\eta \pi^3 w_O^4}{4\lambda} \end{aligned} \tag{9}$$

This useful result gives the volume of the two-photon excitation profile plotted in Figure 2.2b. However, this definition of the focal volume must be used with some caution, sometimes additional factors are calculated which can change the result several fold [8, 12]. For the rough estimates we require, equation (9) will suffice.

The time averaged two-photon absorption rate can be found by substituting equation (9) into equation (8), writing the peak intensity I_o in terms of peak power (equation 4) and multiplying by laser duty cycle $\tau\omega$.

$$W_2 = \frac{\pi C P_0^2 \eta \sigma_2}{(h\nu)^2 \lambda} \tau\omega \tag{10}$$

Notably, the focal volume dimensions drop out of the equation. Conceptually, the reason for this is that a larger focal volume compensates with greater numbers of absorbing species for what it lost in photon flux.

The two-photon absorption rate is related to the measured time averaged two-photon fluorescence F_{luor} by the equation:

$$F_{luor} = \frac{1}{2}\Phi D_f W_2 \tag{11}$$

where Φ is the quantum efficiency of the fluorophore, D_f is a factor that characterizes the spatial and temporal efficiency of the detection system, and the factor of ½ accounts for the fact that two laser photons have to be absorbed to promote the fluorescence emission of a single photon.

We can estimate the energy per unit volume deposited by a single pulse by dividing the absorption rate (equation 8) by the focal volume (equation 9) and multiplying by the pulse width and the energy of a photon as shown:

$$\varepsilon_{TPE} = \sigma_2 C I_O^2 \tau (h\nu)^{-1} \tag{12}$$

The energy density absorbed per pulse with multiphoton excitation is relatively small. Assuming an absorber with a two-photon cross-section of 10^{-49} (cm^4 s molecule^{-1} photon^{-1}), a concentration of 10 mM, a laser wavelength of 740 nm, a pulse width of 150 fs, an average power of 10 mW, a presumptively diffraction

limited focus with a 1.3 NA objective that has an 80% throughput, and the use of equations (2), (3), (4), and (12); yields an energy density per pulse of 0.046 J cm^{-3}.

2.4.3 Nonlinear Ionization

Multiphoton ionization (Figure 2.3d) is essentially the same as multiphoton excitation except the molecule is ionized instead of electronically excited. Often this requires a higher transition energy, meaning more instantaneously absorbed photons are required. Tunneling ionization, another form of direct photoionization is not considered here because, at visible wavelengths, it is not important until peak intensities several orders of magnitude higher then those described here are reached [17].

With a strong enough applied electric field any material will undergo the process of dielectric breakdown and will develop a conduction band populated with charge carriers. Populations of unbound electrons that interact freely with light can similarly evolve during an intense laser pulse. In aqueous media such *free* electrons are very transient and will exist as a significant population only during a high intensity laser pulse, afterward recombining, or solvating, or forming new chemical species within a few picoseconds [3]. Free electrons play an important role in the deposition of laser energy into materials through avalanche ionization. This process, diagrammed in Figure 2.3e, operates on "seed" electrons already in the conduction band. In an intense laser pulse the most likely source of seed electrons is promotion by photoionization [17]. Free electrons can gain energy from a laser field through free-free absorption which is also known as the inverse bremsstrahlung process. Bremsstrahlung (German for "braking radiation") describes electromagnetic radiation produced when electrons decelerate after collisions

with heavier particles such as atomic nuclei [18]. Inverse bremsstrahlung describes the opposite effect where radiation is absorbed by a free electron when it collides with a heavier particle. This increases the energy of the electron. In this manner electrons can gain enough energy from the laser field to ionize atoms during a collision, and repetitions of this process lead to a rapid multiplication of ionized electrons. The result is the formation of a plasma in the region of the laser focus [19].

Whether photoionization or avalanche ionization plays a larger role in generation of free electrons depends on the conditions. For lasers with femtosecond pulses, photoionization can play a stronger role because the process occurs almost instantaneously. Free electrons grow exponentially with avalanche ionization but the process takes longer to establish. The relative contribution of the two mechanisms in the femtosecond pulse regime is the subject of differing viewpoints among researchers [17, 20, 21]. However, in pulses more than a few picoseconds in length, avalanche ionization dominates [22, 24].

To calculate energy absorption from two photons it is typically assumed that the two-photon cross-section is independent of the intensity (refer to equation 7). This is not the case with the absorption coefficient at intensity exposures capable of producing avalanche ionization. With the onset of avalanche ionization, the medium at the focus becomes significantly opaque and linearly absorbs photons. The concentration of free electrons increases rapidly until a threshold is reached where the plasma reflects instead of absorbs incident photons. The typical estimate for the free electron concentration when this occurs is around 10^{21} cm^{-3} [3, 22, 23]. This is called the *critical electron density* and it sets an upper bound for the free electron population of laser generated plasma. Vogel

and coworkers provide plots of the calculated maximum electron density achieved during a laser pulse, versus the laser intensity [13]. According to their calculations, the electron density generated by a laser with a 6 ns pulse width will increase eight orders of magnitude to reach the critical density over a very small intensity range. For lasers with nanosecond pulse widths, plasma formation is a threshold phenomenon and the focal volume is either highly ionized or not at all. The same plots for femtosecond laser pulses show the electron density evolving more gradually with laser intensity until critical density is reached. According to the calculations a significant population of free electrons a "low density plasma" can exist during a pulse before the critical electron density is reached [24].

2.5 HEATING

2.5.1 Heating from Electronic Excitation

Some of the laser energy absorbed by a sample is transformed into heat, and it is possible that a rapid increase in local temperature plays a part in the processes or side effects of cell compatible microfabrication. It is useful to look at the events of laser interaction with matter as a step wise process consisting of excitation of electrons, relaxation of electrons, and subsequent chemical reaction or physical change. The short pulses of the Ti:S laser (150 fs) make this view especially convenient because excitation and relaxation steps are effectively separated, a femtosecond pulse is over by the time any significant electronic relaxation occurs. The relatively long pulses (0.6 ns) of the

microchip Nd:YAG source complicate this picture because that the laser interacts with the sample even as electrons relax to lower energy levels. This is diagramed in Figure 2.4 where the Nd:YAG pulse width and the electron thermalization time overlap.

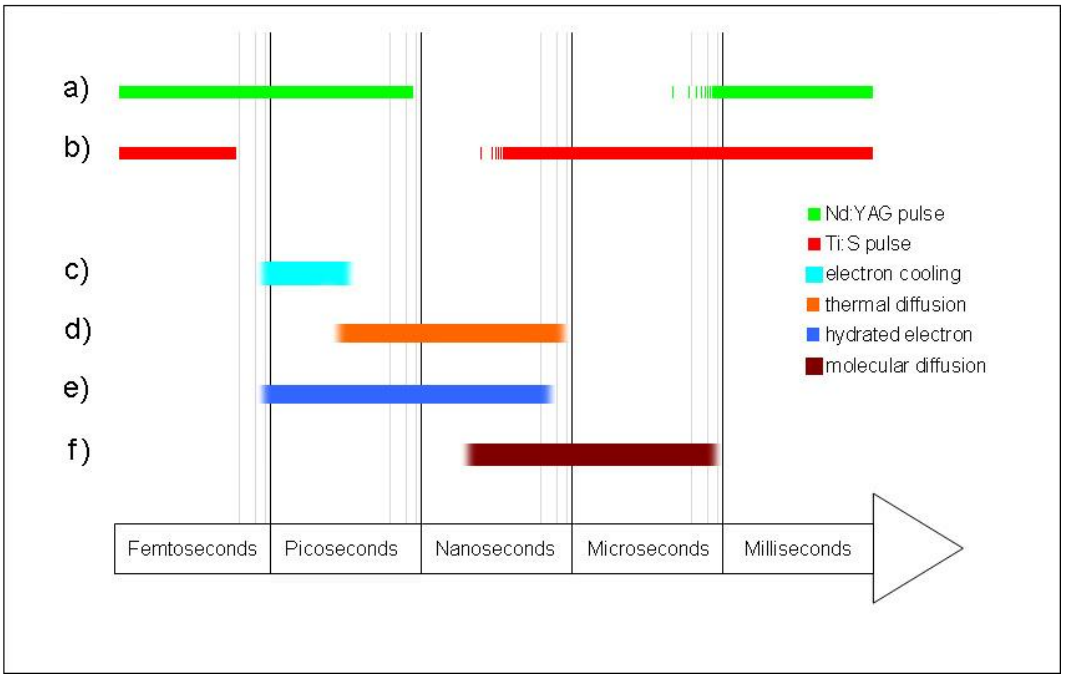

Figure 2.4: Time scales of events for high intensity laser interaction with water. (a) Depiction of series of 600 ps pulses at 7.7 kHz (b) Series of 150 fs pulses at 76 MHz. (c) Electron thermalization, sub to low ps time scale [25]. (d) Thermal diffusion time in water from region defined by 1.3 NA voxel, sub to low µs time scale [13]. (e) lifetime of solvated electron in oxygenated water, 300 ns [26]. (f) diffusion time of molecule from region defined by 1.3 NA voxel, ~600 µs (equation (14), using the diffusion coefficient of 10^{-6} cm^2 s^{-1}).

In the case of two-photon absorption, the temperature rise for a single femtosecond pulse can be estimated from the energy density from a single pulse calculated with equation (12) [27].

$$\Delta T = \frac{\varepsilon}{\rho_w B_w} \tag{13}$$

Here ε is the energy density, ρ_w is the mass density of the medium and B_w is the heat capacity. Using the density and heat capacity values for water, ρ_w = 1.0 g cm^{-3}, B_w = 4187 J K^{-1} kg^{-1} and the result from the sample calculation for equation (12) (0.046 J cm^{-3}), we find a temperature rise of 0.011 K. This assumes that all the energy absorbed was transformed to heat.

The accumulation of heat from multiple pulses would depend on the rate of heat transport from the focal volume. This can be roughly assessed with an equation to estimate the thermal diffusion time t_d from the focal volume [3].

$$t_d = \frac{w_o^2}{2\kappa} \tag{14}$$

The variable κ is the thermal diffusivity of water (1.4 x 10^{-3} cm^2 s^{-1}). For the beam waist radius of a diffraction limited focus of a 1.3 NA objective, the diffusion time is ~400 ns. With a pulse repetition rate of 76 MHz there are pulses every 13 ns, so it would be expected that heat would accumulate at the focal spot. Temperature evolution in the focal region as a function of 3D space and time was modeled by Vogel *et al.* for an energy density of 1 J cm^{-3} being deposited by a 100 fs pulse at a repetition rate of 80 MHz. According to their calculations the temperature stabilized in less than 100 μs [13]. The increase in temperature after a long series of pulses for a diffraction limited 1.3

NA objective was calculated to be only 36% higher then the temperature increase of a single pulse. For the larger focal volume of a 0.6 NA objective, heat transport would not be as efficient. In this case the accumulated heating after a long series of pulses was predicted to be approximately seven-fold that for a single pulse. With a tightly focused laser the cumulative increase in temperature with exposure to a series of pulses is limited.

Multiphoton microscopy typically uses femtosecond pulses at MHz repetition rates, with light near-IR focused using high NA objectives, at powers chosen to optimize fluorescence signal-to-noise. The lack of heating produced by the technique during examination of sensitive biological samples has long been considered one of its advantages. Linear absorption of the near infra-red light by water has been more of a concern as a source of heating than multiphoton absorption [15]. However, a sophisticated analysis by the Schönle and Hell did not find heating through linear absorption to be significant in the experimental conditions typical for multiphoton microscopy [28].

2.5.2 Heat Generation from Ionization

For high energy laser interactions, heating takes place when the energy carried by free electrons is transferred to the medium, a process that is accomplished in a few picoseconds [29]. This process can lead to some readily observable events if the electron density is sufficiently high. The result is damage to the substrate that is known as *optical* or *laser-induced breakdown*. The series of events in the laser mediated breakdown of a dielectric are heating of the substrate, explosive expansion, and emission of a shock wave [3, 19]. These micro-explosions have been a familiar feature of the experiments described

in this dissertation. Sometimes optical breakdown has been used in microfabrication processes and other times it has been a side effect. The temperature increase threshold for bubble formation, from exposure to femtosecond pulses focused with a 1.3 NA objective to be has been estimated to be ~130 °C, starting from water at 20 °C [13].

The 600 ps pulse of the frequency doubled Nd:YAG laser has the capacity for generating more heat than do the shorter pulses of the Ti:S source. For pulse widths above several picoseconds, the laser energy deposition process and the response of the medium become intertwined. Electrons transfer energy to the lattice during the course of pulse. This results in expansion of material which is further heated by the laser [30]. Laser-material interaction in the these regimes is dominated by thermal decomposition [31]. The microchip Nd:YAG laser used in experiments described in this dissertation, at calculated peak intensity levels approaching 1 TW cm^{-2}, ablates glass coverslips. This is not something that the Ti:S source can do even though the laser is capable of considerably higher peak intensity levels. This is indicative of the longer pulse length of the Nd:YAG leading to more heating and more substrate damage.

The pulse repetition rate of 7.7 kHz for the 532 nm Nd:YAG means that the delay between pulses is orders of magnitude longer then the estimated thermal diffusion time (which for a diffraction limited focus with a 1.3 NA objective would be ~1 μs). It is therefore anticipated that in an aqueous solution there would be no cumulative heating from a series of pulses. It should be noted that cumulative effects still occur, most likely through physical modification of a solid substrate or through accumulation of light modified solution phase compounds, since molecular diffusion is much slower than heat diffusion.

2.6 MECHANISMS OF SUBTRACTIVE MICROFABRICATION

This dissertation describes a microfludic cell dosing scheme based on laser fabricated micropores in a polymer membrane. Figure 2.5 shows a scanning electron microscope (SEM) image of a characteristic pore formed in a 2.5 μm thick Mylar membrane. The pore was fabricated using the Ti:S oscillator. In more recent experiments pores have been fabricated with the 532 nm microchip Nd:YAG. Analysis of the finished pores with optical microscopy indicates they have similar morphologies, which consists of an aperture 3 to 4 microns in diameter that is rimmed with a raised burr of material.

The typical intensities values for pore fabrication were ~4 TW cm^{-2} for the Ti:S and ~0.6 TW cm^{-2} for the Nd:YAG. With the Ti:S laser there was a threshold for apparent damage to the membrane, with peak intensites below ~1 TW cm^{-2} not damaging the membrane under typical experimental conditions. Since the damage threshold was above the intensities needed to fabricate protein structures, it was feasible to direct write microstructures on the membrane with the Ti:S source. It was not feasible to do this with the Nd:YAG microchip laser where damage occurred to the membrane even at very low average powers. While the bulk optical properties of the membrane are transparent at visible wavelengths, for packaging purposes they are coated with microscopic inorganic particles of proprietary composition. If these impurities were easily ionized at 532 nm, it would greatly enhance optical breakdown by providing seed electrons for avalanche ionization. Materials with easily ionized impurities can have very low and hard to define thresholds for optical damage by picosecond and nanosecond lasers [17].

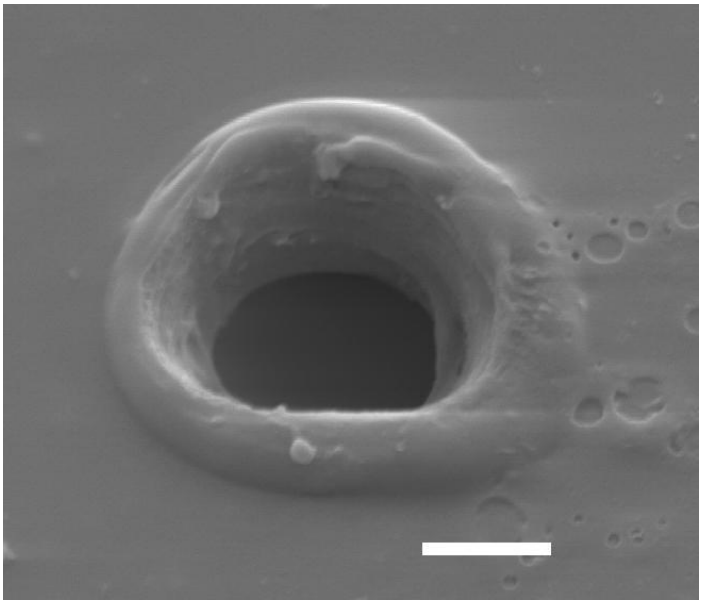

Figure 2.5 Pore fabricated on 2.5 μm thick Mylar by laser induced breakdown with Ti:S 76 MHz oscillator at 750 nm and ~4 TW cm^{-2}. Scale bar, 2 μm.

The events observed during pore formation include a visible flash (in the case of the microchip laser) and the formation of a small gas bubble. The finished pore provides evidence of energetic removal of material. The diameter of the pore, while microscopically defined, occupies an area many times larger then the beam waist calculated in equation (2). This indicates a transport of energy outwards from the region of the highest intensity. A burr surrounding the pore, indicates melting and resolidification have occurred. These features point to a predominantly thermal component of pore formation. Substrate damage by lasers in the picosecond and nanosecond time regimes is considered to be generally caused by a thermal mechanisms [32-34].

The similar morphologies of the pores made by the femtosecond and picosecond pulsed lasers most likely indicate similar mechanisms of fabrication. While heat is generated less efficiently during femtosecond pulses compared to picosecond pulses, temperatures considerably higher then the melting point of Mylar (~250° C [35]) are predicted to be reached with the femtosecond laser, as ionized electrons approach critical density [13]. It seems reasonable that the primary mechanism for the formation of pores made with the picosecond and femtosecond lasers is thermalized energy deposited by avalanche ionization which leads to melting and ablation of the membrane. The next section will investigate the possibility that avalanche ionization also plays a role in additive microfabrication.

2.7 PROSPECTIVE ADDITIVE MICROFABRICATION MECHANISMS

2.7.1 Multiphoton Lithography

As first described by Wu *et al*. in 1992 the nonlinear absorbance of light in the focal region of a high NA objective can change a liquid phase precursor to a solid with submicron dimensions. Focal volume scanning can then be used to create 3D microstructures [36]. Several years after the initial demonstration the Kawata lab published a highly influential paper that includes a striking SEM image of a bull micro-sculpture on the dimensions of a red blood cell [37]. The increasing citations of this paper (over 100 in 2006 according to the Scifinder Scholar database) are indicative of the growing interest in the field [38, 39].

Published work has described this basic method by several different acronyms including, 2PP, TPIP, MAP, MPE fabrication, TPA lithography, MPP and DLW (respectively: "Two-photon polymerization" [2], "two-photon induced polymerization" [40], "Multiphoton absorption polymerization" [41], "Multiphoton excitation fabrication" [42], "Two-photon absorbed lithography" [43], "Multiphoton polymerization" [44], and "Direct laser writing" [45]).

The materials for multiphoton lithography most often have consisted of a prepolymer resin in the form of viscous organic liquids, solids or gels. The resins are often based on commercial compounds designed for UV polymerization. Usually they are mixtures consisting of monomers (such as acrylates or methacrylates) and photoinitiators or photosensitizers which are compounds designed to absorb light and promote photochemical reactions. The distinction between photoinitiators are photosensitizers is that the former is consumed during the reaction while a photosensitizer can initiate multiple reactions by cycling from excited to ground states [46]. After fabrication, the excess material is usually washed away, typically with ethanol or acetone [4]. Since the liquids often used in these processes are organic they are clearly not conducive for sustenance of biological cells. Multiphoton lithography was first demonstrated in aqueous protein solutions by Pitts *et al.* [47]. The Shear lab developed protein solution-based multiphoton lithography into a microfabrication technique that could be accomplished in cell culture providing a means to dynamically modify and influence the environments of living cells [48-50]. Under typical conditions of protein microfabrication described in this work, the peak intensity values for both the Ti:S and the Nd:YAG lasers were several hundred GW/cm^2. Figure 2.6a shows a grid pattern fabricated from a solution of bovine

serum albumin (BSA). The Shear lab has fabricated microstructures out of a wide range of protein starting materials including BSA, lysozyme, myoglobin, and avidin.

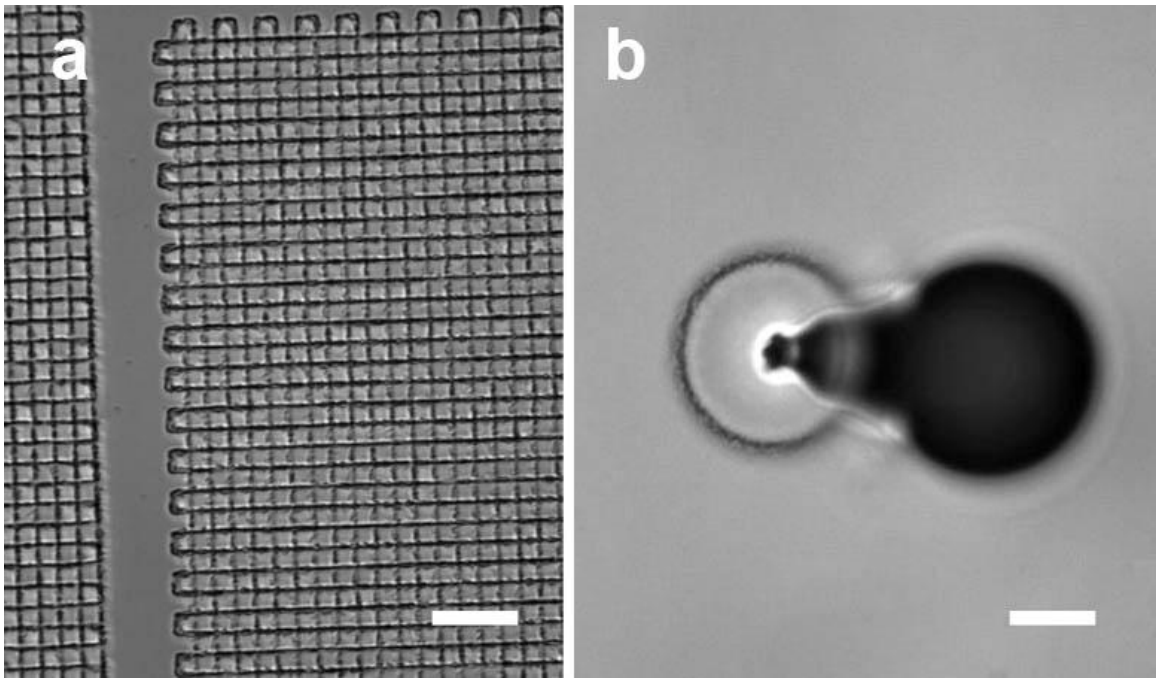

Figure 2.6 BSA structures. (a) grid structure laser fabricated from BSA solution. (b) bubble and ring of material generated in BSA solution by prolonged exposure to ~1 TW cm^{-2} Ti:S pulses. The scale bars are 20 μm.

2.7.2 Reactive Species Produced via Multiphoton Absorption

Because processes at the focal volume are limited in space and time, the photochemical events taking place there are not easily subjected to direct analysis. When assessing the potential mechanisms of protein microfabrication, the Shear lab and other workers have looked to better characterized one-photon photochemical systems [47, 48]. The photo-excitation of methylene blue (MB) and rose bengal is known to generate singlet oxygen through energy transfer from triplet states [51, 52]. Singlet oxygen can subsequently oxidize protein residues leading to reactive species, cross-linking, and the formation of high molecular weight aggregates [53, 54]. Photoexcited sensitizers can also react directly with protein residues leading to the formation of radicals and cross-links between residues [55, 56]. Photosensitized reactions with a singlet oxygen intermediary are known as *type 2* processes, while direct radical formation through interaction between the photosensitizer and substrate are known as *type 1* reactions. Both pathways can occur at the same time, with their relative importance dictated by experimental conditions [57].

The Nd:YAG laser can effectively generate structures in protein solutions with no photosensitizer. Possible mechanisms for this process can be found in the literature describing linear absorption of UV light by the major chromophoric amino acids. The absorption of UV light can lead to formation of radical amino acid species via reactive triplet states [58]. Also, there is evidence that UV absorption by tryptophan can generate singlet oxygen, which means that type 2 processes could potentially occur in protein and amino acid solutions even without a specific photosensitizer added [59]. The two-photon cross-sections of some proteins and amino acids at 532 nm have been reported to be reasonably large [60, 61].

It can be seen in the literature that there are several plausible mechanisms by which electronically excited states could lead to the generation of radicals and cross-linking of proteins. It would also seem plausible that these reactive pathways could be attained through multiphoton absorption.

2.7.3 Free Electron Induced Reactive Species

If a significant level of ionization occurs with the conditions used for protein microfabrication, and if ionization could induce processes leading to the condensation of protein from solution, then laser mediated ionization could play a role in the microfabrication process. This possibility will be assessed for protein microfabrication with the Ti:S source. Literature describing optical breakdown in aqueous solutions with picosecond pulsed lasers is not specific to our experimental conditions, so discussion of fabrication with the microchip Nd:YAG laser will be placed aside.

The estimated peak intensity levels used for protein microfabrication with the Ti:S laser vary with experimental conditions but are typically in the high 100's of GW cm^{-2} range. This is a significant fraction of published breakdown intensity thresholds for ~150 fs near-IR pulses in pure water (4.8 to 8.6 TW cm^{-2}) [62, 63]. The threshold intensity levels for the solutions typically used in my dissertation studies could be lower, as they generally contained millimolar photosensitizer concentrations, levels expected to substantially facilitate ionization. Indeed generation of microscopic bubbles is

commonplace during the protein microfabrication process. As noted above it has been estimated that the temperature increase required for localized phase change and formation of a bubble of with femtosecond near-IR pulses brought to a diffraction limited focus with a 1.3 NA objective is ~130 ºC [13]. The temperature increase from two-photon absorption can be estimated with equations (12) and (13) and the relevant experimental parameters including concentration and two-photon cross-section of the photosensitizer. For typical protein fabrication conditions in this dissertation's studies the predicted temperature increase with these calculations is insignificant (millikelvins) making heat generation from multiphoton absorption a poor candidate for the observed phase change. Localized microscopic bubble formation at the laser focus is therefore a result of optical breakdown stemming from photoionization and avalanche ionization. In fact bubble formation is a common criterion for determining optical breakdown in water induced by femtosecond pulsed lasers [24, 63].

As described above, a significant number of free electrons can populate the focal volume during femtosecond pulses at intensity levels below the threshold for optical breakdown [3, 62]. Often, in this dissertation's protein microfabrication experiments, intensity levels are optimized by adjusting the average laser power to just below the level at which the formation of microscopic bubbles are observed. It is therefore feasible that protein fabrication can take place in a partially ionized focal volume.

The thermalization of free electrons after the termination of the pulse could lead to heating. This could have an effect on the protein fabrication process, it has been demonstrated that the heat induced coagulation of albumin can occur on the time scale of 100's of μs [64]. A partially ionized focal volume could also result in chemical effects.

The laser induced breakdown of aqueous solutions accomplished with UV sources results in the formation of many reactive species including solvated electrons (e^-_{aq}) and reactive oxygen species such as the hydroxyl radical (OH·), hydrogen peroxide (H_2O_2), and superoxide ($O_2^{\cdot -}$) [26, 65]. Pulse radiolysis studies have shown that these reactive species (most notable the hydroxyl radical) will react with solution phase proteins leading, in some cases, to cross-linking between proteins and the formation of high molecular weight aggregates [66-70]. With a significant population of free electrons in the focal volume, there might also be direct changes to the protein, for instance, biomolecules can form transient molecular anions with exposure to free electrons, subsequently leading to the formation of radicals [71, 72]. Considering solutions of up to 400 mg ml^{-1} protein are used which result in an environment densely crowded with solvated protein, such effects could be important.

There are viable pathways leading the formation of cross-linked protein structures both with multiphoton absorption and with photoionization and avalanche ionization. However, considering the evidence that cross-linking can take place in conditions of relatively high energy densities and that multiphoton absorption, in the experimental conditions of this dissertation, is predicted to only deposit a small amount of energy, processes stemming from ionization could be more important.

2.8 CONCLUSION

The possibility that protein microstructures form in a highly ionized focal volume would, in some ways, make the process more difficult to control. It seems likely, that

instead of cross-links between specific protein residues, a more energetic reaction environment would result in less discriminate events. For instance, the involvement of heating could not be precluded. In some ways, this could make the microfabrication process more difficult to predict and control but it might also produce new opportunities for analysis. Because the amount of energy that can be deposited in ionization processes is much higher that that of multiphoton processes, it seems reasonable to anticipate that proportionally more reactive species could be generated for analysis. This could ease some of the challenges of analyzing the small amount of material typically produced in the focal volume. There are various strategies for detecting the products of water lysis which could prove applicable for studies of focal volume processes. For instance the hydroxyl radical can be analyzed with fluorescence methods [73], chemoluminescently [74], and by capillary electrophoresis [75]. These analytical techniques provide possible routes for characterizing products generated by an ionized focal volume.

There are many important types of characterizations that would help elucidate the processes involved in protein microfabrication. This chapter has focused on the physical and chemical events that could potentially underlie the fabrication process. However, there are features of the structures themselves that require characterization. These include the nature of the bonds that knit the protein structures together, and the mechanical characteristics of the microstructures. These questions present many exciting research opportunities.

2.9 REFERENCES

1. Zipfel, W., R. Williams, and W. Webb, *Nonlinear magic: multiphoton microscopy in the biosciences.* Nature Biotechnology, 2003. **21**(11): p. 1369-1377.

2. Serbin, J., et al., *Femtosecond laser-induced two-photon polymerization of inorganic-organic hybrid materials for applications in photonics.* Optics Letters, 2003. **28**(5): p. 301-303.

3. Vogel, A., G. Hiittman, and G. Paltauf, *Femptosecond plasma-mediated nanosurgury of cells and tissues.* Laser Ablation and Its Applications, C. Phipps, Editor. 2007, Springer: New York.

4. Wu, S., J. Serbin, and M. Gu, *Two-photon polymerisation for three-dimensional micro-fabrication.* Journal of Photochemistry and Photobiology. A, Chemistry, 2006. **181**(1): p. 1-11.

5. Hess, S. and W. Webb, *Focal volume optics and experimental artifacts in confocal fluorescence correlation spectroscopy.* Biophysical Journal, 2002. **83**(4): p. 2300-2317.

6. Gu, M., *Advanced optical imaging theory*. 2000, New York: Springer.

7. Birge, R., *One-photon and two-photon excitatioin spectroscopy.* Ultrasensitive Laser Spectroscopy. Edited by David S. Kliger. Published by Academic Press, a subsidiary of Harcourt Brace Jovanovich, New York, 1983, p. 109, 1983.

8. Nagy, A., J. Wu, and K. Berland, *Observation volumes and gamma-factors in two-photon fluorescence fluctuation spectroscopy.* Biophysical Journal, 2005. **89**(3): p. 2077-2090.

9. Gratton, E., et al., *Fluctuation correlation spectroscopy in cells: determination of molecular aggregation.* Biophotonics-Optical Science and Engineering for the 21st Century, 2004, Springer.

10. Berland, K., P. So, and E. Gratton, *Two-photon fluorescence correlation spectroscopy: method and application to the intracellular environment.* Biophysical Journal, 1995. **68**(2): p. 694-701.

11. Chirico, G., F. Olivini, and S. Beretta, *Fluorescence excitation in two-photon microsccopy by autocorrelation spectroscopy and photon counting histogram.* Applied Spectroscopy, 2000. **54**(7): p. 1084-1090.

12. Xu, C. and W. Webb, *Multiphoton excitation of molecular fluorophores and nonlinear laser microscopy.* Topics in Fluorescence Spectroscopy, J. Lakowicz, Editor. 1997, Springer: New York. p. 471–540.

13. Vogel, A., et al., *Mechanisms of femtosecond laser nanosurgery of cells and tissues.* Applied Physics B-Lasers and Optics, 2005. **81**(8): p. 1015-1047.

14. Parker, D., *Laser ionization spectroscopy and mass spectrometry.* Ultrasensitive Laser Spectroscopy, D. Kliger, Editor. 1983, Academic Press: New York. p. 234-307.

15. Denk, W., D. Piston, and W. Webb, *Two-photon molecular excitation in laser-scanning microscopy.* Handbook of Biological Confocal Microscopy, J. Pawley, Editor. 1995, Plenum Press: New York.

16. Fang, H. and R. Swofford, *The thermal lens in absorption spectroscopy*. Ultrasensitive Laser Spectroscopy, D. Kliger, Editor. 1983, Academic Press: New York.

17. Schaffer, C., A. Brodeur, and E. Mazur, *Laser-induced breakdown and damage in bulk transparent materials induced by tightly focused femtosecond laser pulses.* Measurement Science and Technology, 2001. **12**(11): p. 1784-1794.

18. Haug, E. and W. Nakel, *The elementary process of bremsstrahlung*. World Scientific Notes in Physics. Vol. 73. 2004, London: World Scientific.

19. Shen, R.Y., *The principles of non-linear optics*. 1983, New York: John Wiley and Sons.

20. Joglekar, A.P., et al., *A study of the deterministic character of optical damage by femtosecond laser pulses and applications to nanomachining.* Applied Physics B-Lasers and Optics, 2003. **77**(1): p. 25-30.

21. Kaiser, A., et al., *Microscopic processes in dielectrics under irradiation by subpicosecond laser pulses.* Physical Review B, 2000. **61**(17): p. 11437-11450.

22. Cremers, D. and L. Radziemski, *Handbook of laser-induced breakdown spectroscopy*. 2006: John Wiley.

23. Stuart, B., et al., *Nanosecond-to-femtosecond laser-induced breakdown in dielectrics.* Physical Review B, 1996. **53**(4): p. 1749-1761.

24. Noack, J., A. Vogel, and M. Lubeck, *Laser-induced plasma formation in water at nanosecond tofemtosecond time scales: calculation of thresholds, absorptioncoefficients, and energy density.* Quantum Electronics, IEEE Journal of, 1999. **35**(8): p. 1156-1167.

25. Shah, L., et al., *Self-focusing during femtosecond micromachining of silicate glasses.* Quantum Electronics, IEEE Journal of, 2004. **40**(1): p. 57-68.

26. Nikogosyan, D., D. Oraevsky, and V. Rubasov, *Two-photon ionization and dissociation of liquid water by powerful laser UV radiation.* Chemical Physics, 1983. **77**(1): p. 131-143.

27. Vogel, A., et al., *Mechanisms of femtosecond laser nanosurgery of cells and tissues.* Applied Physics B: Lasers and Optics, 2005. **81**(8): p. 1015-1047.

28. Schönle, A. and S. Hell, *Heating by absorption in the focus of an objective lens.* Optics Letters, 1998. **23**: p. 325-327.

29. Ben-Yakar, A., et al., *Thermal and fluid processes of a thin melt zone during femtosecond laser ablation of glass: the formation of rims by single laser pulses.* Journal of Physics D: Applied Physics, 2007. **40**(5): p. 1447-1459.

30. Schou, J., S. Amoruso, and J. Lunney, *Plume dynamics.* Laser Ablation and Its Applications, C. Phipps, Editor. 2007, Springer. p. 67.

31. Baudelet, M., et al., *Femtosecond time-resolved laser-induced breakdown spectroscopy for detection and identification of bacteria: A comparison to the nanosecond regime.* Journal of Applied Physics, 2006. **99**: p. 084701.

32. Tien, A., et al., *Short-pulse laser damage in transparent materials as a function of pulse duration.* Physical Review Letters, 1999. **82**(19): p. 3883-3886.

33. Stuart, B., et al., *Laser-induced damage in dielectrics with nanosecond to subpicosecond pulses.* Phys. Rev. Lett, 1995. **74**: p. 2248.

34. Chichkov, B., et al., *Femtosecond, picosecond and nanosecond laser ablation of solids.* Applied Physics A: Materials Science & Processing, 1996. **63**(2): p. 109-115.

35. Amborski, L. and D. Flierl, *Physical properties of polyethylene terephthalate films.* Industrial & Engineering Chemistry, 1953. **45**(10): p. 2290-2295.

36. Wu, E., et al., *Two-photon lithography for microelectronic application.* SPIE Proc, 1992. **1674**: p. 776.

37. Kawata, S., et al., *Finer features for functional microdevices - Micromachines can be created with higher resolution using two-photon absorption.* Nature, 2001. **412**(6848): p. 697-698.

38. Sun, H. and S. Kawata, *Two-photon photopolymerization and 3D lithographic microfabrication.* Adv. Polym. Sci, 2004. **170**: p. 169-273.

39. Li, L. and J. Fourkas, *Multiphoton polymerization.* Materials Today, 2007. **10**(6): p. 30-37.

40. Kuebler, S., et al. *Optimizing two-photon initiators and exposure conditions of three-dimensional lithographic microfabrication*. Photopolymer Science and Technology, 2001. Chiba, Japan.

41. LaFratta, C., L. Li, and J. Fourkas, *Soft-lithographic replication of 3D polymeric microstructures created with MAP.* Proceedings of SPIE, 2007. **6462**: p. 646210.

42. Basu, S. and P. Campagnola, *Enzymatic activity of alkaline phosphatase inside protein and polymer structures fabricated via multiphoton excitation.* Biomacromolecules, 2004. **5**(2): p. 572-9.

43. Teh, W., et al., *Effect of low numerical-aperture femtosecond two-photon absorption on (SU-8) resist for ultrahigh-aspect-ratio microstereolithography.* Journal of Applied Physics, 2005. **97**: p. 054907.

44. Baldacchini, T., *Acrylic-based resin with favorable properties for three-dimensional two-photon polymerization.* Journal of Applied Physics, 2004. **95**(11): p. 6072.

45. Seet, B., et al., *Three-dimensional spiral-architecture photonic crystals obtainedby direct laser writing.* Microporous Mesoporous Mater, 2003. **58**: p. 105.

46. Allen, R., *Pertubation and analysis of biological microenvironments.* School of Biological Sciences, 2005, University of Texas: Austin. p. 160.

47. Pitts, J., et al., *Submicron multiphoton free-form fabrication of proteins and polymers: studies of reaction efficiencies and applications in sustained release.* Macromolecules, 2000. **33**(5): p. 1514-1523.

48. Kaehr, B., et al., *Guiding neuronal development with in situ microfabrication.* Proceedings of the National Academy of Sciences of the United States of America, 2004. **101**(46): p. 16104-16108.

49. Kaehr, B., et al., *Direct-write fabrication of functional protein matrixes using a low-cost q-switched laser.* Analytical Chemistry (Washington, DC), 2006. **78**(9): p. 3198-3202.

50. Allen, R., et al., *Catalytic three-dimensional protein architectures.* Analytical Chemistry (Washington, DC), 2005. **77**(16): p. 5089-5095.

51. Kochevar, I. and R. Redmond, *Photosensitized production of singlet oxygen.* Methods Enzymol, 2000. **319**: p. 20-8.

52. Gabrielli, D., et al., *Binding, aggregation and photochemical properties of methylene blue in mitochondrial suspensions.* Photochemistry and Photobiology. **79**(3): p. 227-232.

53. Shen, H., et al., *Photodynamic crosslinking of proteins. I. Model studies using histidine-and lysine-containing N-(2-hydroxypropyl) methacrylamide copolymers.* J Photochem Photobiol B, 1996. **34**(2-3): p. 203-10.

54. Davies, M., *Reactive species formed on proteins exposed to singlet oxygen.* Photochem. Photobiol. Sci, 2004. **3**(1): p. 17–25.

55. Knowles, A. and S. Gurnani, *A study of the methylene blue-sensitized oxidation of amino acids.* Photochem Photobiol, 1972. **16**(2): p. 95-108.

56. Shen, H., et al., *Photodynamic crosslinking of proteins. II. Photocrosslinking of a model protein-ribonuclease A.* J Photochem Photobiol B, 1996. **35**(3): p. 213-9.

57. Verweij, H. and J. van Steveninck, *Model studies on photodynamic cross-linking.* Photochem. Photobiol, 1982. **35**: p. 265–267.

58. Davies, M. and R. Truscott, *Photo-oxidation of proteins and its role in cataractogenesis.* J Photochem Photobiol B, 2001. **63**(1-3): p. 114-25.

59. Igarashi, N., S. Onoue, and Y. Tsuda, *Photoreactivity of amino acids: tryptophan-induced photochemical events via reactive oxygen species generation.* Analytical Sciences, 2007. **23**(8): p. 943-948.

60. Xu, Y., et al., *Fluorescence of proteins induced by two-photon absorption.* J Photochem Photobiol B, 1987. **1**(2): p. 223-7.

61. Sengupta, P., et al., *Determination of the absolute two-photon absorption cross section of tryptophan.* Proc. SPIE, 2001. **4262**: p. 336-339.

62. Vogel, A., et al., *Plasma formation in water by picosecond and nanosecond Nd: YAG laserpulses. I. Optical breakdown at threshold and superthreshold irradiance.* Selected Topics in Quantum Electronics, IEEE Journal of, 1996. **2**(4): p. 847-860.

63. Juhasz, T., et al., *Time-resolved observations of shock waves and cavitation bubbles generated by femtosecond laser pulses in corneal tissue and water.* Lasers Surg Med, 1996. **19**(1): p. 23-31.

64. Pfefer, T., et al., *Dynamics of pulsed holmium: YAG laser photocoagulation of albumen.* Physics in Medicine and Biology, 2000. **45**(5): p. 1099-1114.

65. Nikogosyan, D. and H. Gorner, *Laser-induced photodecomposition of amino acids and peptides: extrapolation to corneal collagen.* Selected Topics in Quantum Electronics, IEEE Journal of, 1999. **5**(4): p. 1107-1115.

66. Getoff, N., *Pulse radiolysis of aromatic amino acids—State of the art.* Amino Acids, 1992. **2**(3): p. 195-214.

67. Garrison, W., *Reaction mechanisms in the radiolysis of peptides, polypeptides, and proteins.* Chemical Reviews, 1987. **87**(2): p. 381-398.

68. Schüssler, H., S. Navaratnam, and L. Distel, *Pulse radiolysis studies on histones and serum albumin under different ionic conditions.* Radiation Physics and Chemistry, 2001. **61**(2): p. 123-128.

69. Davies, K., *Protein damage and degradation by oxygen radicals. I. general aspects.* Journal of Biological Chemistry, 1987. **262**(20): p. 9895-9901.

70. Schüssler, H. and M. Puchala, *Oxygen effect in the radiolysis of proteins: v. histones.* Radiation Physics and Chemistry, 2004. **69**(1): p. 45-53.

71. Huels, M., et al., *Single, double, and multiple double strand breaks induced in DNA by 3-100 eV electrons.* J. Am. Chem. Soc, 2003. **125**(15): p. 4467–4477.

72. Boudaïffa, B., et al., *Resonant formation of DNA strand breaks by low-energy (3 to 20 eV) electrons.* Science, 2000. **287**(5458): p. 1658.

73. Manevich, Y., K. Held, and J. Biaglow, *Coumarin-3-carboxylic acid as a detector for hydroxyl radicals generated chemically and by gamma radiation.* Radiation Research, 1997. **148**(6): p. 580-591.

74. Tsai, C., et al., *Rapid and specific detection of hydroxyl radical using an ultraweak chemiluminescence analyzer and a low-level chemiluminescence emitter: application to hydroxyl radical-scavenging ability of aqueous extracts of food constituents.* J Agric Food Chem, 2001. **49**(5): p. 2137-41.

75. Cao, Y., Q. Chu, and J. Ye, *Determination of hydroxyl radical by capillary electrophoresis.* Anal Bioanal Chem, 2003. **376**: p. 691-695.

Chapter 3: Protein-based Microfabrication for the Perturbation and Analysis of Cells

This chapter presents work in which we demonstrate a strategy for microfabricating three-dimensional matrixes composed of protein in cellular and microfluidic environments. In this approach, the high intensity focal region of a pulsed laser focused into protein or protein/photosensitizer solution results the formation of solid, three-dimensionally defined volumes. In this manner, it is possible to fabricate protein microparticles with dimensions on the order of the multiphoton focal volume (less than 1 μm^3) or, by scanning the position of a laser focal point relative to a specimen, to generate surface-adherent matrixes or cables that extend through solution for hundreds of micrometers. We show that protein matrixes can be functionalized, by decoration of avidin matrixes with biotinylated enzymes, or by cross-linking biotinylated proteins that then are linked to biotinylated enzymes via an avidin couple. Several formats are explored, including three-dimensional enzymatic structures, protein pads that generate product gradients within cell cultures, and protein fences to guide the migration of selected motile cells.

3.1 INTRODUCTION

A cell senses and responds to external environmental features that are defined across a broad range of spatial dimensions, from the gross anatomical to nanoscale physical and chemical characteristics. The particular range represented by micrometer scale features is an important level of biological organization. Cellular response to signals

with microscopic spatial resolution plays important roles in development, homeostasis, and in response to disease or injury [1-4]. Microenvironmental signals can be transmitted by diffusible or immobilized chemical gradients or through mechanical coupling [5-7]. The ability to reproduce and study the effects of localized signaling in a controlled cell culture environment could further our understanding of these processes. To this end, various strategies that produce spatiotemporal chemical gradients or physical perturbations have been developed. Modification of extracellular environments in three-dimensions is possible, for example, through directed solution delivery from micropipettes [8] and manipulation of chemically defined microspheres [9]. Although useful for some applications, these techniques are not easily amenable to parallel examination of multiple sites and can suffer in terms of precision. Techniques that incorporate microfabrication can be superior to techniques that involve the careful positioning of pipettes and probes in some respects. For instance, microfluidic techniques can dose cells with very high resolution [10, 11]. Also, highly parallel levels of cell analysis can be achieved with strategies based on the lithographic patterning of surface biomolecules on substrates which can result in expansive arrays of high resolution patterns. These approaches can influence cell behavior including migration, division and metabolic activity [12-15].

While conventional microfabrication strategies can provide high resolution modification of substrates, there are several drawbacks. The environment of a cell within an organism is three-dimensional and dynamically modified. Many current microfabrication strategies are based on lithographic technologies that can only modify two dimensional surfaces. Also, the process of modification of the experimental substrate

is generally accomplished before the cells are introduced. This precludes changing microfabricated features to investigate cellular response, or localizing microfabricated objects to target cellular features at specific locations or time points.

To address such limitations, we have developed a technique based on protein cross-linking induced by the nonlinear absorption of light from a high intensity pulsed laser. This technique enables fabrication of chemically active structures with micrometer three-dimensional resolution in cellular environments. Until recently, microarchitectures fabricated using nonlinear absorption induced photochemistry were based on synthetic resins and were fashioned into structures such as exquisitely detailed (but chemically inert) artwork [16, 17], high-aspect-ratio towers [18], and micromachines [19]. As a biomolecular alternative, Campagnola and coworkers demonstrated that similar structures could be created using nonlinear absorption of high intensity Ti:S light to cross-link proteins such as alkaline phosphatase and fibrinogen [20, 21]. Although these structures were shown to retain some native protein activity, the fabrication solutions contained toxic photosensitizers (e.g., rose bengal), limiting possibilities for application to living cellular environments [21]. Rose bengal and methylene blue facilitate the fabrication of protein microstructures but can be both phototoxic [22] and cytotoxic (in the absence of irradiation) at low micromolar levels [23]. The Shear lab has explored the use of flavins and other noncytotoxic biological compounds for facilitating protein photo-cross-linking. These naturally occurring compounds largely avoid issues related to nonphotonic cytotoxicity. Work from the Shear lab has demonstrated the effectiveness of flavin adenine dinucleotide (FAD) for facilitating the protein cross-linking process within cultures of living cells. The utility of this approach has been demonstrated by influencing

neuronal development in real time [24]. The Shear lab also has explored the use of an inexpensive frequency doubled microchip Nd:YAG laser for protein microfabrication. It has been demonstrated that with this laser it is feasible to fabricate protein structures without added photosensitizer [25].

Here, we investigate the capabilities of this microfabrication strategy for localizing enzymatic reactions within cellular milieus, establishing the feasibility for creating chemical gradients within cell cultures. Chemical localization is achieved via strategies that exploit avidin-biotin conjugation chemistry. In addition to surface-adherent lines and platforms, the geometry of protein matrixes created using this approach ranges from suspended micrometer-thick cables with lengths greater than 100 μm, to the creation of dense three-dimensional fences to guide cell migration. The wide range of protein architectures and chemical functionalities possible with this method opens important opportunities for characterizing and controlling extracellular microenvironments.

3.2 EXPERIMENTAL METHODS

3.2.1 Matrix Fabrication

Protein structures were fabricated using the output from a femtosecond Ti:S laser (Coherent Mira, Santa Clara, CA) operating at ~750 nm (pulse width ~150 fs, pulse repetition rate ~76 MHz). The Ti:S beam was aligned into a Zeiss Axiovert 135 (inverted) microscope. The beam was adjusted to approximately fill the back aperture of a 40× objective (Olympus UPlanFl, 0.75 NA) with average powers of 50 to 100 mW at

the back aperture of the objective resulting in estimated intensities at the beam waist of 0.5 to 1 TW cm^{-2}. By scanning the position of the specimen relative to the laser focus with a Prior motorized stage (Proscan 2), extended structures of different dimensionality could be fabricated. Except where otherwise noted, matrixes were fabricated using solutions that contained protein (100-300 mg/ml) and flavin adenine dinucleotide (FAD) at 5 mM as a photosensitizer in Hepes-buffered saline (HBS; 10 mM Hepes, 135 mM NaCl, 5 mM KCl, 2 mM MgCl2, 2 mM CaCl2, 10 mM D-glucose, pH 7.4). Cables were fabricated using similar protein concentrations, but typically used 1 mM methylene blue (MB) as a photosensitizer due to its superior cross-linking abilities. Although the specific photophysical and photochemical causes have not been delineated, we find that lines fabricated using MB are consistently thicker at a constant protein concentration and scan speed than are lines produced using FAD.

An alternative laser fabrication system was used for the experiments involving keratocyte migration. Here, a microchip frequency doubled (532 nm) Nd:YAG (pulse width 0.6 ns, pulse repetition rate 7.7 kHz) was aligned into a Nikon Eclipse (TE2000-E) microscope. Sample translation was accomplished by means of a Physik Instrumente (P-527) nanopositioning stage. Laser exposure was controlled by Uniblitz shutter (UHS1,Vincent Associates). Both the nano-positioning stage and shutter were controlled with custom software written with Labview (National Instruments, Austin Texas).

3.2.2 Chemicals and Materials

Except where noted, all chemicals were purchased from Sigma-Aldrich (St. Louis, MO). BSA and biotinylated calf intestinal alkaline phosphatase (biotin-AP, 29339) were obtained from Equitech-Bio (Kerrville, TX) and Pierce Biotechnology, Inc. (Rockford, IL), respectively. Avidin was purchased from Molecular Probes, Inc. (Eugene, OR).

3.2.3 Biotin-BSA Cables

BSA was biotinylated via reaction with excess 6-((biotinoyl)amino)hexanoic acid succinimidyl ester (biotin-X SE) in 100 mM carbonate buffer (pH 9.9) followed by dialysis against HBS to remove unreacted substrates. After fabrication, cables were functionalized with alkaline phosphatase (AP) by treatment with avidin (1.0 mg/ml; 2 min) followed by biotin-AP (0.1 mg/ml; 2 min) in HBS.

3.2.4 Cell Culture

Neuroblastoma-glioma (NG108-15) cells were purchased from the American Type Culture Collection (Manassas, VA) and cultured in DMEM (Mediatech, Inc., Herndon, VA) supplemented with 10% fetal bovine serum (FBS), penicillin (100 mg/L), and streptomycin (100 kunits/L) purchased from Invitrogen (Carlsbad, CA). Flasks were maintained at 37 °C in a 10% CO_2 atmosphere with saturated H_2O. NG108-15 cells were seeded on 0.01% (w/v) poly(L-lysine)-coated glass coverslips and incubated for 1-3 days in a low-serum (1% FBS) growth medium.

An established protocol was followed to obtain the keratocyte cells [26]. Briefly, scales were extracted by tweezers from a sacrificed Black Tetra (Gymnocorymbus ternetzi) tropical fish and placed flat on a flame sterilized coverslip. Before the cells could dry, they were perfused with Hepes-modified DMEM (Sigma Aldrich) supplemented with 20% FBS. The cells were then incubated overnight at 30 °C and the sample was used the next day after ~2 min treatment with 0.25 % (wt./v) Trypsin, 2.21 mM EDTA (Cellgro).

3.2.5 PDMS Microchamber Fabrication.

To minimize the surface area subjected to nonspecific protein adsorption in extracellular-gradient experiments, NG108-15 cultures were grown on coverslips that could be transferred to flow cells after fabrication of protein structures. In this approach, adapted from Folch *et al.* [27], a stencil with a 1.5 mm pore was formed from PDMS (Polydimethylsiloxane, 10:1 RTV615A to RTV615B; GE Silicones, Niskayuna, NY) and was placed on a 22 × 22 mm coverslip (no. 1; Erie Scientific, Portsmouth, NH). This procedure created a well (~1 mm deep) into which NG108-15 cells were seeded at ~15000 cells ml^{-1}.

For protein structure fabrication, the medium was removed and a blocking solution of BSA (200 mg ml^{-1}) in HBS was added and incubated for 10 min before addition of photo-cross-linking solution (avidin and FAD). After photofabrication, the pore was washed extensively with HBS. To functionalize the avidin structure, the pore was filled with a 0.1 mg ml^{-1} solution of biotin-AP in HBS for 2 min and then rinsed

several times with HBS. After the stencil was removed, a small droplet of HBS was left on the NG108-15 field, ensuring the cells remained submersed in buffer. An open-sided channel fashioned from PDMS (see below) was aligned over the droplet, and the entire system was gently compressed in an aluminum clamping block to strengthen the seal between the coverslip and PDMS, after which the channel could be flooded with HBS and used as a flow cell.

The negative master for the PDMS channel was prepared by affixing a section of a no. 1 1/2 coverslip (cut to the same dimensions as the desired channel) to the floor of a 3.5-cm-diameter Petri dish using epoxy. Teflon tubing (0.35 mm i.d., 0.65 mm o.d.; Zeus TFE) was affixed to both ends of the channel master coverslip to create voids in PDMS through which solutions could be introduced into the cell containing channels. The Petri dish was filled with PDMS solution, degassed, and cured at 60 °C for 1 h. This process resulted in channels ~170 µm high, 3.5 mm wide, and 20 mm long, which could be placed over cultures of NG108-15 cells.

3.2.6 Cell Imaging

After matrix fabrication, initial inspection of structures, and placement of the flow cell, extracellular product gradients were imaged using a Photometrics CCD (Coolsnap FX) on a Nikon Eclipse (TE2000-E) microscope using a DAPI filter set.

3.2.7 Sample Preparation for Electron Microscopy

Samples were prepared for electron microscopy by exchanging fabrication solutions with Tris-buffered saline (TBS; pH 8.5) containing 15% (w/v) glutaraldehyde. After incubation for 10 min, solution exchanges were performed using, in sequence, 100% H2O, ~50% H2O/50% ethanol, 100% ethanol, 100% methanol (×2); each solution was allowed to incubate for 20 min before being replaced. The specimen was allowed to air-dry for 5 days after the final methanol wash, and the dry sample was coated using a Au/Pd target to a nominal thickness of 8 nm.

3.3 RESULTS AND DISCUSSION

3.3.1 Large-Aspect-Ratio Cross-Linked Structures

Cultured cells display differential patterns of development according to the physiochemical structure of their environment; experiments with two-dimensional and 3D culture systems have demonstrated effects of cell-cell and cell-matrix interactions on neuronal stem cell differentiation [28, 29]. The ability to alter the 3D cellular microenvironment through on-demand fabrication would extend the reach of traditional tissue engineering methods as well as our understanding of cells in biomimetic systems.

To explore the capabilities of nonlinear laser cross-linking for fabricating large-aspect-ratio protein matrixes in various configurations, BSA cables were constructed that bridged gaps between coplanar or parallel glass surfaces spaced by distances greater than 100 μm (Figure 3.1). The thickness (cross-sectional diameter) of such cables is largely determined by laser power and the speed at which the laser focus is translated through the

protein solution, with higher translation speeds and lower powers yielding thinner structures. At a scan speed of ~10 $\mu m\ s^{-1}$ and 100 mW average laser power, cables fabricated from BSA and MB displayed an average thickness of ~2 μm. We also have fabricated cables using the photosensitizer FAD, although such structures generally require significantly greater care to avoid damage during washes.

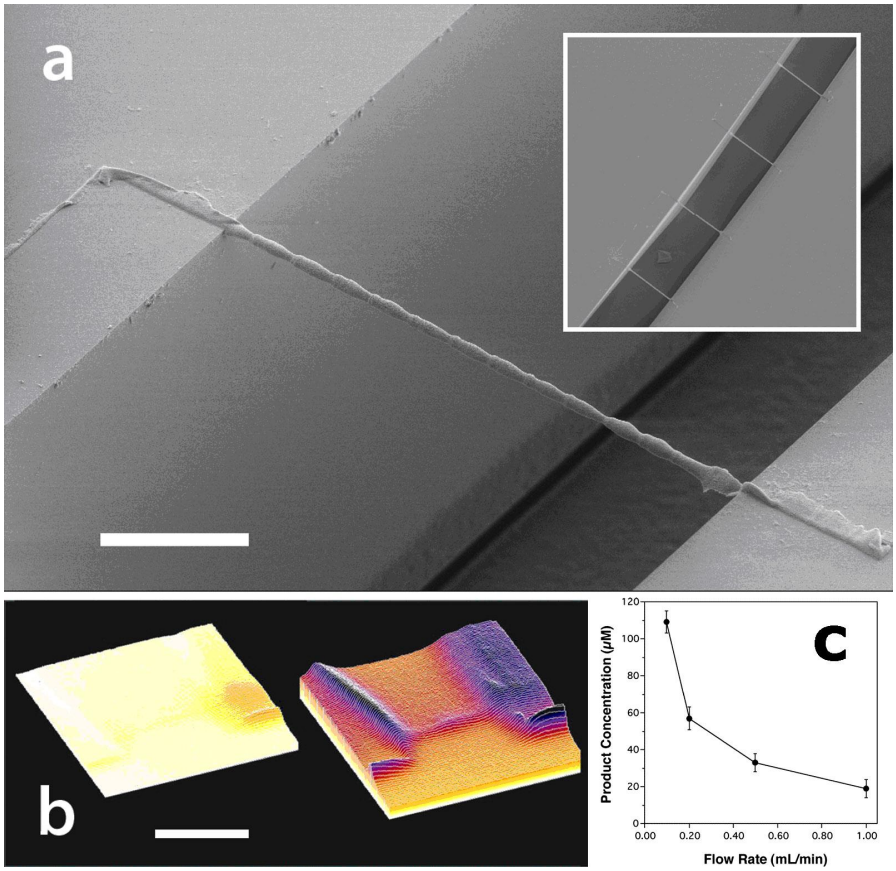

Figure 3.1: Large-aspect-ratio protein cables. (a) SEM micrograph of a BSA cable fabricated across a gap between coplanar borosilicate coverslips. Scale bar, 30 μm. Inset: Low magnification SEM image of the same specimen demonstrating a series of parallel cables. (b) Catalytically active protein cables. A cable was fabricated from biotinylated BSA across a ~180 μm gap between glass coverslips and was labeled with biotin-AP via an avidin sandwich approach. The sample then was treated with the fluorogenic AP substrate, 4-methylum belliferyl phosphate (4-MUP) (100-200 μM), which is catalytically converted to fluorescent 4-MU by AP. The intensity plot on the left was produced from a wide-field fluorescence image acquired under high flow conditions, in which steady-state product concentrations remain low. By reducing flow rates (right intensity plots), an increasing accumulation of 4-MU product can be attained. Background signal from the coverslips is caused by biotin-AP retained as a result of nonspecific adsorption of biotin-BSA. Scale bar, 200 μm. (c) Product concentrations (4-MU) measured 20 μm downstream of an AP-functionalized cable as a function of solution flow rate. Point measurements were made using multiphoton excitation. A volume flow rate of 1.0 ml min^{-1} in the flow cell used here corresponds to a linear flow rate of ~30 mm s^{-1} at the cable.

Figure 3.1b demonstrates the enzymatic activity of a functionalized protein cable under a flow of 4-methylum belliferyl phosphate (4-MUP). This bridge, fabricated using a biotin-BSA conjugate, was decorated with biotin-AP via bridging avidin molecules. 4-MUP was catalytically converted to fluorescent 4-methylumbelliferone (4-MU) by biotin-AP immobilized to the cable. Accumulation of fluorescent product can be seen both in the vicinity of the cable and from coverslip-associated enzyme (the result of nonspecific biotin-BSA adsorption). Product accumulation downstream from the functionalized cables as a function of flow rate was measured (Figure 3.1c). To evaluate whether protein cables were merely accumulating fluorescent product generated at the coverslip surface, control cables were fabricated using nonbiotinylated BSA alongside functionalized cables (data not shown); unlabeled structures displayed no significant 4-MU fluorescence.

3.3.2 In Situ Chemical Gradients

The ability to selectively expose a cell or a small population of cells with a specific chemical effector could potentially have broad utility, particularly if dosing could be achieved with arbitrary spatial control. To explore the potential applicability of biocompatible microfabrication to this goal, we have performed proof-of-concept studies in which a real-time gradient of fluorescent 4-MU molecules are created through localization of a biotinylated enzyme to cross-linked avidin structures. Here, a structure (60 μm × 30 μm × 1 μm) composed of cross-linked avidin was fabricated in a field of NG108-15 cells and functionalized by treatment with 0.1 mg ml^{-1} biotin-AP for 2 min

(Figure 3.2). The structure and cell field then were enclosed in a PDMS microchannel (cross-sectional area, 0.6 mm^2), and a stream of 4-MUP was introduced at a flow rate of ~0.5 ml min^{-1} (~14 mm s^{-1} average linear flow rate). As shown in Figure 3.2, 4-MUP was converted to fluorescent 4-MU principally at the structure, which was carried by the flow in a stream.

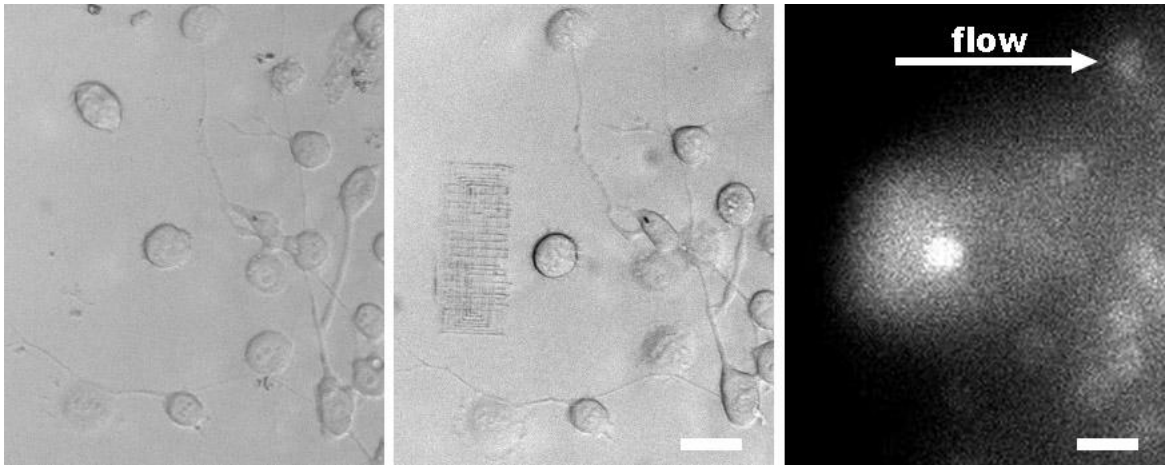

Figure 3.2: Generation of chemical gradients within cellular cultures. The image on the left is a transmission image (10× objective with a 1.5 times magnifier) showing a field of cultured NG108-15 cells before fabrication of a photo-cross-linked avidin scaffold. The middle image shows the same field after fabrication of protein structure and decoration with biotin-AP. On the right is a fluorescence image of the same field subjected to a directional flow of 4-MUP (arrow denotes flow path). Fluorescent 4-MU product can be seen extending from the scaffold along the flow path and bathing downstream cells, several which develop high fluorescence due to dye uptake. The scale bars represent 20 μm.

To characterize such product plumes under controlled conditions, a similar protein structure was fabricated in the absence of cells, and multiphoton fluorescence point measurements using a 100× objective were performed both downstream and upstream of the structure at varying heights. For the flow conditions and reagent

concentration (200 μM 4-MUP) used in these studies, the concentration of fluorescent product immediately adjacent to a structure was ~10 fold greater within the plume (32 ± 7 μM) than on the upstream side of the structure. Similarly low product levels were measured 10-20 μm both above and lateral to the plume so long as moderate flow rates were maintained.

As evidenced by the downstream cell in Figure 3.2 that has accumulated significant 4-MU product, this approach can be used to differentially dose desired cells within cultures that were unpatterned before plating. Other cells in the shown field also have developed cytosolic fluorescence at somewhat lower levels, likely a result of nonspecific ecto-phosphatase activity. The use of biocompatible microfabrication to localize enzyme reactors within cellular environments could eventually be extendable to biologically relevant systems. For example, diffusible molecules can play critical roles in the differentiation of stem cells [30]. With the appropriate enzyme/substrate couple this system could be uniquely capable of producing, in cell culture, the localized gradients stem cells experience *in vivo*. Moreover, although relatively large structures were fabricated in the current proof-of-concept studies for ease of visualization, submicrometer spatial resolutions - suitable for subcellular dosing - should be feasible using multiphoton fabrication.

At present, the principal limitation in the spatio-temporal localization of chemical gradients is the nonspecific adsorption of protein, the result of exposing unprotected glass and fused-silica surfaces to very high protein concentrations (typically at least 100 mg $m1^{-1}$) during the photo-cross-linking process. To avoid prohibitive nonlocalized enzyme activity throughout a fabrication chamber, extensive washing procedures were

required, in some cases causing the release of adherent cells from surfaces. Even with such treatment, residual enzyme levels in some cases can generate significant steady-state product concentrations, particularly under stagnant conditions. Various passivation strategies have been investigated by the Shear lab, such as competitive binding with surfactants, and use of proteins for microstructure fabrication that are designed to be more resistant to nonspecific adsorption (such as streptavidin). These strategies have met with limited results. One challenge is that many conventional methods such as covalent attachment of poly(ethylene glycol) also prohibit cell adhesion. An alternative approach currently being pursued is the photoincorporation of biotin conjugated to a photoreactive benzophenone moiety into protein matrixes as they are created. This may be useful for fabricating structures with high avidin-binding capacities while reducing background associated with nonspecific protein adsorption. Small molecules are generally less prone to nonspecific adsorption than are proteins, which should, in principle, allow biotin to be more effectively washed off,

3.3.3 Topographic Guidance of Cell Migration

Along with microscopically defined chemical gradients, physical features in the extracellular microenvironment can have a determinative effect on the cell. For instance, most tissue cells are not viable without a solid support [31]. The physical topology in the cellular microenvironment provides important cues that influence cell differentiation and migration in events such as development and wound healing [32].

We used fish epidermal keratocytes, a model system for the study of cell motility [26] in experiments to investigate laser microfabrication for dynamic control of cell migration. Here we constructed the fence-like protein microstructures out of a solution of 300 mg ml^{-1} BSA using a frequency doubled Nd:YAG, a laser capable of efficiently fabricating structures in protein solution without added photosensitizer.

Fence structures were made within microns of targeted cells. The geometry of the structures was determined by the programmed parameters of a piezo nanopositioning stage which oscillated in the in vertical axis according to a sine function while moving at constant rates in the x,y plane. The amplitude of the sine function defined the height of the fence and the frequency, in conjunction with the rate of travel in the x,y directions, could control the density of vertical lines in the fence. To use the fence building routine, the user would select the desired path of the fence in relation to cells in the microscope field of view as observed by the CCD. On command, fences would be fabricated according to the parameters programmed into the piezo scanner. With this system, fences could be used to corral individual cells. This process is shown in Figure 3.3 where a box was built by parts around a migrating keratocyte. The piezo z-axis was driven by a sine function with the amplitude of 5 μm and a frequency of 25 Hz which (for the piezo x,y translation rate of 5 μm s^{-1}) meant that the focal volume made 10 vertical passes for every 1 μm of travel in the x,y plane. The actual height of the fence was not precisely defined because the axial resolution of this fabrication system was not characterized and the axial starting positions for the fence structures were estimated visually.

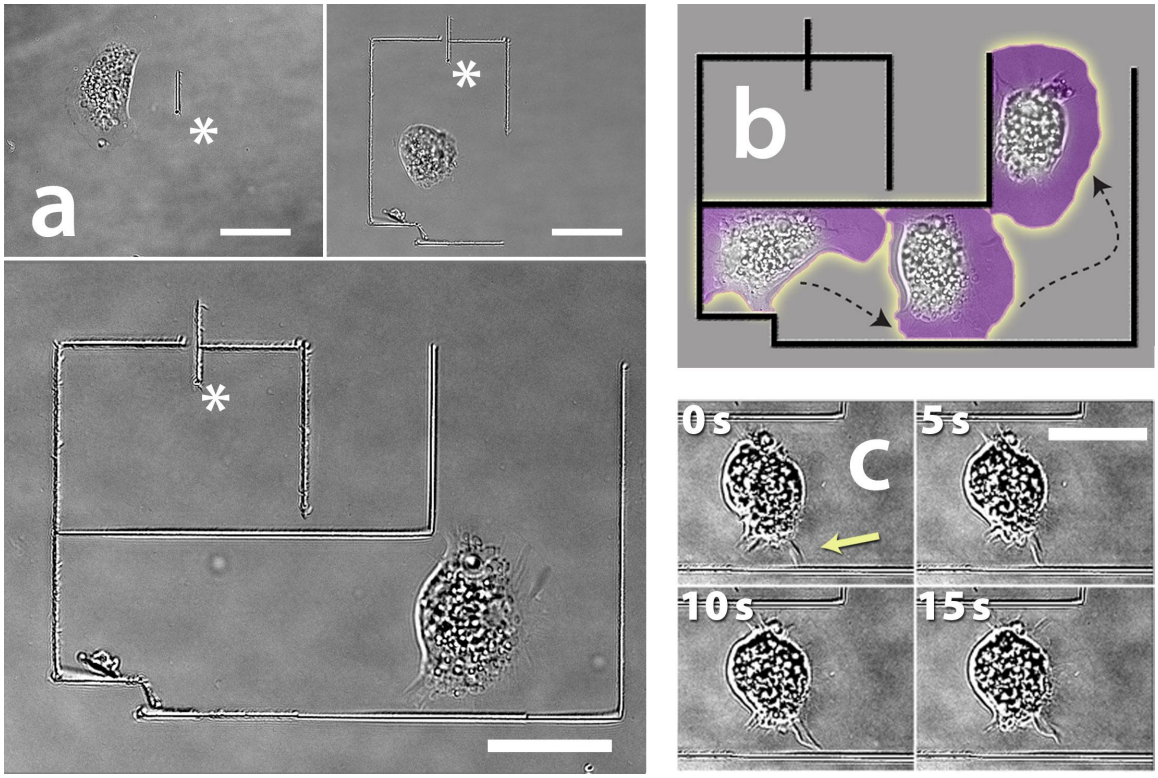

Figure 3.3: Control of cell migration with dynamic microfabrication. (a) DIC images showing ~5 µm high fences, fabricated from a BSA precursor solution, built sequentially around a migrating fish epidermal keratocyte. The asterisk highlights the original fence segment in each of the images. There is an approximate 5 min interval between each image. (b) Illustration depicting how the protein structures redirect migrating cells. (c) Sequence of images, 5 seconds apart, depicting a characteristic interaction of the cell lamellipodium with the protein structure. The arrow highlights a more prominent region of the lamellipodium that forms, interacts with the protein fence in several locations and then retracts in under 30 seconds. All scale bars are 30 µm.

In these experiments rapidly migrating cells (~10 µm/min) that had moved clear of the tissue explant were selected and perturbed by microfabrication to constrain their direction of travel. A migrating keratocyte whose path was blocked by a protein fence was redirected after an interaction between the keratocyte's lamellipodium and the fence. A migrating cell impeded by a protein fence would stop when the lamellipodium

contacted the fence and then proceed in a different direction at a similar rate. This process (for these rapidly migrating cells selected for analysis) generally took around 5 min. For the structural dimensions of the fences examined in this experiment, the response of the cells was remarkably consistent. A cell trapped in an enclosed box would generally migrate around the inside, contacting and moving away from the walls in apparently random directions often for 3 to 4 hours, until the cell began to lose apparent viability. Conditions in these experiments were not optimized for the long term maintenance of cells on the microscope stage, which was unheated. Experiments would also occasionally end with the cell traversing the ostensibly 5 μm high fence.

A system such as this with unique abilities to test and control motile cells with micro-scale stimulation could be of interest to biological researchers. Future experiments could expand the experimental system described here. The response of cells to a variety of microstructure geometries on scales from tens of microns (such as mazes and corrals made from systems of fences) to the micron-scale (such as height, density and textures of the fence) could be assessed. The ability to select cells demonstrating particular morphologies or activities, and to test them with custom structures could enable unique experimental strategies not available to conventional lithographic techniques where the substrate modifications necessarily take place before the cells are plated.

It might seem peculiar to put a cell in a maze as one would place a rat in a maze. However, the establishment of stereotypical responses of an organism to a controlled and structured environment can provide important phenotypic information. Would migrating cells associated with mammalian connective tissues such as fibroblasts, or the mammalian immune system such as neutrophils, respond similarly? The response of

various cells in different conditions to microstructural stimuli could provide insight to the natural behavior of cells in tissue. Use of cell-lines amenable to genetic manipulation might provide routes for studying some of the complex mechanotransductive and biochemical events that must underlie the process of cell sensing and response to change in physical microtopography.

3.4 CONCLUSION

A potential advantage of the techniques described in this chapter is that through methodologies common to automated microscopy, such as programmed stage control, laser exposure, and computer image recognition, it should be feasible to greatly increase the rate at which cells are analyzed. It is much easier to move a manipulative probe rapidly through a cell culture if the probe consists of focused light instead of relatively massive mechanical devices such as micropipettes. Partial automation is already demonstrated in the case of microstructure fabrication to guide cell migration.

The capability of fabricating catalytically active protein matrixes provides a unique tool to tailor microenvironments. This approach offers the ability to create a broad range of chemically defined topographical features (e.g., cables, surface adherent lines, pads, fence geometries). Developing methods of creating microstructures with biomolecular gradients well enough defined to control cell behavior chemically is an ongoing research subject in the Shear lab.

The approaches explored in this work should provide new capabilities for studying a variety of cell functions, ranging from single-cell biochemistry and

development to perturbation and analysis of populations of cultured cells. The 3D control inherent to multiphoton cross-linking could eventually enable enzyme-based sensors to be fabricated within cellular environments in topographies that restrict diffusion of analytes from their cellular release sites, thus increasing the efficiency of mass-limited cellular analyses. Beyond its application to fundamental questions in cell biology, applications for this technology are likely to be found in regenerative medicine where precise chemical and physical control of cell proliferation and differentiation is required. Innovations in microfluidics promise to revolutionize the biosciences by providing new approaches to diagnostics [33], enzymatic assays [34], and cell biology [10, 11]; on-demand, high-resolution microfabrication complements and adds versatility to these technologies by providing a means to alter chemical and mechanical environments after fabrication of initial microfluidic architectures.

3.5 REFERENCES

1. Ghashghaei, H., C. Lai, and E. Anton, *Neuronal migration in the adult brain: are we there yet?* Nature Reviews Neuroscience, 2007. **8**: p. 141-151.

2. Song, H. and M. Poo, *Signal transduction underlying growth cone guidance by diffusible factors.* Curr. Opin. Neurobiol, 1999. **9**: p. 355-363.

3. Tessier-Lavigne, M., *The molecular biology of axon guidance.* Science, 1996. **274**(5290): p. 1123-1133.

4. Cairns, R., R. Khokha, and R. Hill, *Molecular mechanisms of tumor invasion and metastasis: an integrated view.* Curr Mol Med, 2003. **3**(7): p. 659-671.

5. Gregor, T., et al., *Stability and nuclear dynamics of the bicoid morphogen gradient.* Cell, 2007. **130**(1): p. 141-152.

6. Janmey, P., *The cytoskeleton and cell signaling: component localization and mechanical coupling.* Physiological Reviews, 1998. **78**(3): p. 763-781.

7. Geiger, B., et al., *Extracellular matrix cytoskeleton crosstalk.* Nature Reviews Molecular Cell Biology, 2001. **2**: p. 793.

8. Lohof, A., et al., *Asymmetric modulation of cytosolic cAMP activity induces growth cone turning.* Journal of Neuroscience, 1992. **12**(4): p. 1253-1261.

9. Zhang, X. and M. Poo, *Localized synaptic potentiation by BDNF requires local protein synthesis in the developing axon.* Neuron, 2002. **36**(4): p. 675-688.

10. Takayama, S., et al., *Selective chemical treatment of cellular microdomains using multiple laminar streams.* Chem. Biol, 2003. **10**(2): p. 123–130.

11. Takayama, S., et al., *Subcellular positioning of small molecules.* Nature, 2001. **411**(6841): p. 1016.

12. Kane, R., et al., *Patterning proteins and cells using soft lithography.* Biomaterials, 1999. **20**(23): p. 2363-76.

13. Whitesides, G., et al., *Soft lithography in biology and biochemistry.* Annual Review of Biomedical Engineering, 2001. **3**(1): p. 335-373.

14. Khademhosseini, A., et al., *Microscale technologies for tissue engineering and biology.* Proceedings of the National Academy of Sciences, 2006. **103**(8): p. 2480-2487.

15. Li, N., A. Tourovskaia, and A. Folch, *Biology on a chip: microfabrication for studying the behavior of cultured cells.* Crit. Rev. Biomed. Eng, 2003. **31**(5-6): p. 423–488.

16. Kawata, S., et al., *Finer features for functional microdevices - Micromachines can be created with higher resolution using two-photon absorption.* Nature, 2001. **412**(6848): p. 697-698.

17. Serbin, J., et al., *Femtosecond laser-induced two-photon polymerization of inorganic-organic hybrid materials for applications in photonics.* Optics Letters, 2003. **28**(5): p. 301-303.

18. Baldacchini, T., *Acrylic-based resin with favorable properties for three-dimensional two-photon polymerization.* Journal of Applied Physics, 2004. **95**(11): p. 6072.

19. Galajda, P. and P. Ormos, *Complex micromachines produced and driven by light.* Lasers and Electro-Optics, 2002. CLEO'02. Technical Digest. Summaries of Papers Presented at the, 2002: p. 634-635.

20. Basu, S. and P. Campagnola, *Enzymatic activity of alkaline phosphatase inside protein and polymer structures fabricated via multiphoton excitation.* Biomacromolecules, 2004. **5**(2): p. 572-9.

21. Pitts, J., et al., *Submicron multiphoton free-form fabrication of proteins and polymers: studies of reaction efficiencies and applications in sustained release.* Macromolecules, 2000. **33**(5): p. 1514-1523.

22. Kochevar, I., et al., *Singlet oxygen, but not oxidizing radicals, induces apoptosis in HL-60 cells.* Photochemistry and Photobiology. **72**(4): p. 548-553.

23. Paulino, T., et al., *Use of visible light-based photodynamic therapy to bacterial photoinactivation*. Biochemistry and Molecular Biology Education, 2005, ASBMB. p. 46-49.

24. Kaehr, B., et al., *Guiding neuronal development with in situ microfabrication.* Proceedings of the National Academy of Sciences of the United States of America, 2004. **101**(46): p. 16104-16108.

25. Kaehr, B., et al., *Direct-write fabrication of functional protein matrixes using a low-cost q-switched laser.* Analytical Chemistry (Washington, DC), 2006. **78**(9): p. 3198-3202.

26. Svitkina, T., et al., *Analysis of the actin-myosin II system in fish epidermal keratocytes: mechanism of cell body translocation.* The Journal of Cell Biology, 1997. **139**(2): p. 397-415.

27. Folch, A., et al., *Microfabricated elastomeric stencils for micropatterning cell cultures.* Journal of Biomedical Materials Research, 2000. **52**(2): p. 346-353.

28. Hui, L. and K. Roy, *Biomimetic three-dimensional cultures significantly increase hematopoietic differentiation efficacy of embryonic stem cells.* Tissue Engineering, 2005. **11**(1/2).

29. Silva, G., et al., *Selective differentiation of neural progenitor cells by high-epitope density nanofibers*. Science, 2004, American Association for the Advancement of Science. p. 1352-1355.

30. Song, H., C. Stevens, and F. Gage, *Astroglia induce neurogenesis from adult neural stem cells.* Nature, 2002. **417**: p. 39-44.

31. Discher, D., P. Janmey, and Y. Wang, *Tissue cells feel and respond to the stiffness of their substrate*. Science, 2005, American Association for the Advancement of Science. p. 1139-1143.

32. Li, S., J. Guan, and S. Chien, *Biochemistry and biomechanics of cell motility.* Annu Rev Biomed Eng, 2005. **7**: p. 105-150.

33. Chiem, N., C. Colyer, and D. Harrison, *Microfluidic systems for clinical diagnostics.* Solid State Sensors and Actuators, 1997. Transducers '97 Chicago., 1997 International Conference on, 1997. **1**.

34. Seong, G., J. Heo, and R. Crooks, *Measurement of enzyme kinetics using a continuous-flow microfluidic system.* Anal Chem, 2003. **75**(13): p. 3161-7.

Chapter 4: Dynamic Mask-Based Microfabrication*

This chapter describes a strategy for rapidly producing microstructures using multiphoton lithography directed by a computer-controlled dynamic mask. Morphological descriptions of 3D structures, including biological specimens and designed tissue analogues, are encoded in 2D slice data that are used to create a sequence of reflective photomasks on a digital micromirror device (DMD). By scanning a laser focus across the face of these intrinsically aligned masks, tomographic and computed data can be translated into protein-based 3D reproductions having micrometer feature sizes within minutes. This straightforward and highly versatile approach may provide improved routes for the development of custom tissue replacements, design of 3D cellular scaffolds, and rapid prototyping of microanalytical devices.

4.1 INTRODUCTION

Multiphoton lithography is a unique microfabrication strategy capable of generating high-resolution 3D microstructures through a laser direct-write process [1]. The nonlinear dependence of multiphoton excitation on photon flux provides inherent optical sectioning for fluorescence microscopy [2] and photofabrication [3]. Recently, the Shear lab showed that by directing multiphoton photo-cross-linking with transparency-based photomasks, 3D microstructures and chambers composed of cross-linked proteins could be designed, fabricated and evaluated in minutes, allowing rapid iteration of

* Adapted from Nielson, Kaehr and Shear *Angewante Chemie* **2007** (*submitted*)

prototype geometries that guide cellular motion or trap single cells for extended incubation of clonal populations [4]. The basis of this technique was the placement of a physical mask in the path of a raster scanned laser beam that was directed into microscope optics. The mask was aligned at the intermediate image plane before a tube lens and high NA infinity corrected microscope objective. Therefore, the scanning beam would reproduce the mask image in reduced proportions onto the specimen plane.

This ability to rapidly fabricate micro-forms composed of biological building blocks [5, 6] could be important in a variety of applications. However, because the image displayed on a multiphoton mask determines the pattern of cross-linked protein at the specimen plane, transparency masks must be replaced sequentially in a laborious procedure to achieve variations in microstructure topography. As a result, this procedure has been well suited to fabrication of structures requiring only one or two photomasks but is not practical for creating more complex materials such as tissue micro-constructs.

To achieve the levels of complexity necessary to replicate complex structures such as micro-scale tissue morphology, we have designed a system based on a DMD automated reflectance mask [7]. This device, which is manufactured for image projection in consumer electronics, consists of an array of over 5×10^5 aluminum micromirrors which mechanically switch between two orientations. Light rays impinging on the mirrors are either sent along an optical path or into a beam block according to the orientation of the individual mirrors. This provides a means of video-rate mask switching. Similar dynamic-mask lithographic approaches recently have been used to pattern (broadband) UV light for a number of applications including micro-array fabrication and stereolithography [8-11]. Our approach combines dynamic mask microfabrication with

the advantages offered by multiphoton lithography allowing 3D fabrication in aqueous environments. To accomplish this, a femtosecond pulsed laser light is raster scanned in a rectangular pattern across the face of a DMD positioned at the intermediate image plane (Figure 4.1). The image displayed on the DMD using the graphic output from a personal computer is reproduced on the specimen plane of the objective with a reduction of scale approximately determined by the ratio of the focal lengths of the objective and tube lens. In combination with the intrinsic 3D resolution of multiphoton lithography, this approach allows sequential horizontal fabrication planes to be rapidly layered with precise, automated alignment—in contrast to traditional photo-lithography which requires high accuracy physical alignment for sequential masks. Here, we demonstrate the versatility of this straightforward fabrication approach for 3D micro-prototyping and micro-replication.

4.2 EXPERIMENTAL METHODS

4.2.1 Instrumentation

The output from a mode-locked Ti:S laser (Spectra-Physics, Tsunami) tuned to 730 – 740 nm was aligned into a confocal scan box (Biorad, MRC600) where galvanometer-driven mirrors scanned the beam in a raster pattern of ~500 lines in 1 or 3 s depending on the setting. The DMD used in these experiments (Texas Instruments, 0.55SVGA) was a component of a partially dismantled business projector (Benq, MP510). The reflective surface of the DMD was an 848 x 600 array of 16 μm x 16 μm aluminum mirrors. Each individual mirror could switch between “on” and “off” states

corresponding to a ±10º tilt angle. The individual mirrors were controlled by the intact projector electronics which were programmed to display (by modulating between the off and on states) the graphic output of a computer. A 15.2 cm focal length lens focused the laser onto the DMD which resulted in an estimated beam diameter on the chip face of ~30 μm. The beam spot scanned over approximately a quarter of the DMD mirrors. The DMD reflectivity when duplicating a white display was ~40%. Light reflected down the optical path was collimated by a 15.2 cm focal length tube lens and sent into an inverted microscope (Zeiss Axiovert). A Zeiss Fluar, 100x/1.3 NA, oil immersion objective was used for all fabrication data presented except Figure 4.7 which was fabricated with an Olympus LUMPlanFl, 100x/1.0 NA, water immersion objective. Laser powers measured at the back aperture of the microscope objective typically were 50 – 60 mW. The irradiated area at the sample plane was ~60 μm by ~40 μm.

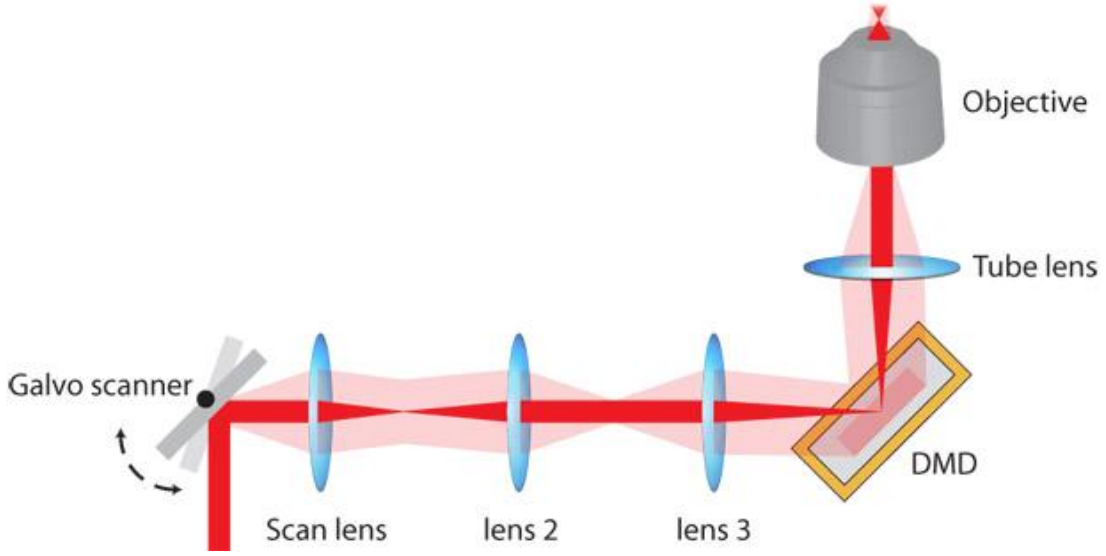

Figure 4.1: Simplified schematic of the optical alignment of the DMD-directed multiphoton lithography system. On the left side of the diagram is a depiction of the x,y galvo scanner (only one scanning mirror is shown). The highlighted region represents the extent of the beam translation. The scan lens and lens 2 have focal lengths of 2.5 cm and 10.2 cm, respectively. The beam focused by lens 3 scans the face of the DMD. After reflection off of the DMD the beam is collimated by the tube lens (focal lengths of lens 3 and tube lens, 15.2 cm). To ensure that a collimated beam pivots at the back aperture, the distance between the galvo mirror and the back aperture of the objective is approximately twice the sum of the focal lengths of the four lenses. Mirrors in the beam path have been omitted for simplicity.

4.2.2 Microstructure Fabrication

Structures were fabricated on no. 1 1/2 coverglass (Erie Scientific Co.). The coverglass was boosted ~35 – 190 µm over a lower coverglass by using microsphere or coverglass spacers. The low profile chamber was filled with a solution containing 400 mg ml^{-1} BSA (Equitech-Bio) and 5 mM MB (Sigma) in PBS (pH ~7.5). Structures were fabricated from the top coverglass (to avoid focusing through the nascent structure) over

60 to 150 individual scan planes stepped by 0.1 to 1.0 μm increments (along the optical axis) using a motorized focus driver (Prior, H122). Vertical heights of the structures could be extended to as much as 150 μm with low-micrometer (axial) and submicrometer (radial) minimum feature sizes using this approach.

4.2.3 Image and Stage Control

The modified projector displayed the same computer output as a monitor, allowing observation and control of the DMD display. Most of the images displayed were in JPEG format and had been adjusted using Adobe Photoshop to correct for an observed ~5º skew (discussed below). In addition, most tomographic input data were processed to reduce resolution until features of the plane slice data roughly matched the spatial resolution of the system. The batch processing capacities of Photoshop were convenient for preparing the groups of images necessary to define the multiple plane structures.

The display of images, stage translation, and shutter activation were controlled with software written in-house using Labview (National Instruments). For multiple plane structures, x,y and z stage translation was coordinated with the display of plane slice data that corresponded to the appropriate features of the microstructure. The fabrication of extended 2D structures made by stitching together multiple planes used a program that segmented images into smaller parts. Programs written with Labview accomplished these image processing routines. Labview software was also used to present animations of trigonometrically defined shapes which were used to specify 3D structures plane by plane. For example, to create the slice data for an enclosed 3D ramp that ascended at 30°,

the Labview display window would be programmed to show white field inset with a black box. The dimensions of the box represented a horizontal slice through the intended tunnel structure. The position of the Labview display window corresponded with the laser-scanned region on the DMD chip (which shared the computer output with the monitor). Each iteration of the program was coordinated with a z-axis step of s μm. The physical length at the specimen plane was calibrated with the display resolution of the monitor, giving a conversion factor p (pixels μm^{-1}) (for example if the display resolution was set at 1280 by 1024 then p was ~12.5 pixels μm^{-1}). With each iteration, a structure cross-section would be fabricated on the specimen plane, then the stage would step up by s μm and the position of the box would shift on the monitor in a defined direction by $ps(\tan(30°))^{-1}$ pixels. From multiple fabricated planes a ramp would be constructed. This basic principle could be extended to create a variety of 3D objects.

4.2.4 Scanning Electron Microscopy (SEM)

Samples for SEM were prepared by sequential immersion (15 min. per solution) in 5% glutaraldehyde (Ted Pella, Redding CA), phosphate buffered saline (PBS, pH 7.4), deionized water, 50% methanol (MeOH), and 100% MeOH. After air drying overnight the samples were sputter coated with Au/Pd to a nominal thickness of 15 nm and imaged with a LEO 1530 SEM (Leo Electron Microscopy Ltd., Zeiss, Oberkochen, Germany). Preparation of structures for electron microscopy in some instances resulted in settling of minimally supported features.

4.2.5 Multiphoton Fluorescence Microscopy

Multiphoton excitation (MPE) fluorescence images were acquired using a stage scanning system mounted on a Nikon Eclipse TE2000-E inverted microscope. A nanopositioning stage (Physik Instrumente, P-527) driven by a digital piezo controller (Physik Instrumente, E-710) raster scanned the sample relative to a Ti:S beam (750 nm) focused using a 1.4 NA objective. Fluorescence detection was accomplished using a PMT (HC125-02, Hamamatsu) and multichannel scaler (SR-430, Stanford Research Systems) that was synchronized via trigger signals from the piezo controller. In general, images were acquired at ~3000 pixels/s. Stage translation, signal acquisition, and image reconstruction were accomplished using a custom Labview program.

Fluorescence data could also be acquired during fabrication of each plane of a protein structure. In this case, BSA solution was spiked with BSA-FITC, and the multiphoton excited fluorescence emitted during fabrication of each plane was recorded using a CCD (Photometrics Coolsnap HQ). ImageJ software was used for image processing and 3D renderings from slice data [12].

4.2.6 Bacterial Cell Culture

E. coli strain RP9535 (ΔcheA, kindly provided by J. S. Parkinson, Dept. of Biology, University of Utah), were streaked on 1.5% agar (214050, Becton Dickinson) containing T-broth (1% Tryptone [211705, Becton Dickinson], 0.5% wt/vol NaCl) and grown at 32°C. Single-colony isolates were used to inoculate 2 ml of T-broth, which were grown to saturation on a rotary shaker (200 rpm) at 32°C. An aliquot was diluted

1:100 into another 2 ml of T-broth and grown ~4.5 h. to mid-exponential phase. Bacteria solutions were diluted for experiments 1:10 to 1:100 in motility buffer (10 mM KPO4, 67 mM NaCl, 0.1 mM EDTA, 10 mM sodium lactate, pH 7.0). Cells collected in the microchamber depicted in Fig. 4 were incubated at ambient temperature (~20 °C) in T-broth in a 1 ml dish.

4.3 RESULTS AND DISCUSSION

4.3.1 Plane-Defined 3D Structures

The system for dynamic mask microfabrication could be used to quickly build complex 3D microstructures in a process that required no specific programming from input data that required minimal processing. Figure 4.2(a, b) shows scanning electron micrographs of tissue replicas composed of photo-cross-linked BSA that were defined by images derived from X-ray computed tomographic (CT) data. Input data depicting from 60 to 120 CT image planes were used to direct fabrication of microstructures on glass substrates using step sizes of between 0.1 and 0.5 μm per z–step, a process that required less than 4 minutes per structure.

Figure 4.2c provides a qualitative assessment of the 3D fabrication fidelity. The left sides of the middle and bottom rows show reconstructions of the 110 images of image processed CT slices that provided plane data for the fabrication of the pincushion protea. The side view of the mask data 3D reconstruction (middle row, left side) can be compared to the low angle SEM micrograph of the finished structures (top row) and fluorescence data acquired during fabrication (middle row, right). The bottom row

compares a z-projection of the mask data (left) with MPE fluorescence x,y slices of the final structure (right).

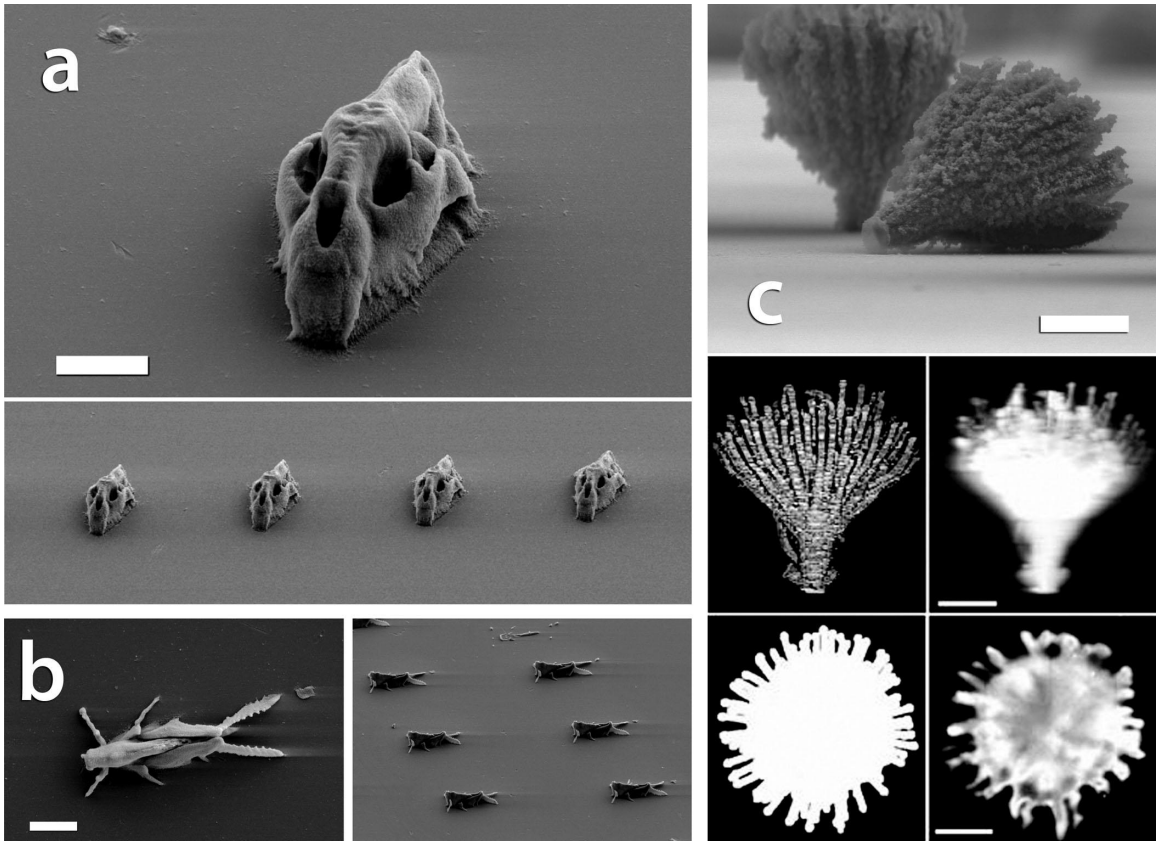

Figure 4.2: Micro-reconstructions of biological organisms. The synchronization of DMD image sequences (high resolution X-ray CT data; digimorph.org) with vertical sample plane steps enables replicas composed of photo-cross-linked BSA to be fabricated rapidly (1 – 2 s plane^{-1}). (a) On top is a 3D replica of a puma skull (puma concolor), while below is a group of duplicate puma skulls. (b) A spotted bird grasshopper (Schistocerca emarginata) replica (left) and group of facsimiles (right). (c) Depictions of pincushion protea (Leucospermum tottum). On the top row is a low angle SEM micrograph (one of the structures fell during sample preparation). The middle row shows a 3D reconstruction of mask data used for fabrication (left) and a 3D reconstruction from fluorescence acquired during fabrication (right). The bottom row shows a z-projecton of the slice data (left) and z-projection from MPE fluorescence optical sections of finished structure (right). Scale bars,10 μm.

4.3.2 Resolution and Artifacts

Because of geometric limitations in focusing with typical microscope optics the focal volume is inevitably longer (along the optical axis) then it is wide [13]. In fabricated structures this results in an axial distortion in sufficiently small features. The finer features (0.5 – 0.75 μm) of the beetle in the left panel of Figure 4.3 represent the minimum size of defined features with the fabrication system. The minimum axial features (middle panel) were approximately 3 to 4 times larger. This distortion can be observed in the beetle mandibles, which in the mask data are not elongated in the axial directions (right panel, top). With the initial optical set-up the back aperture of the objective was not completely filled, which results in a non-diffraction limited focus and a degradation of lateral and axial resolution. Overfilling the back aperture in future configurations should result in improved lateral and axial resolution.

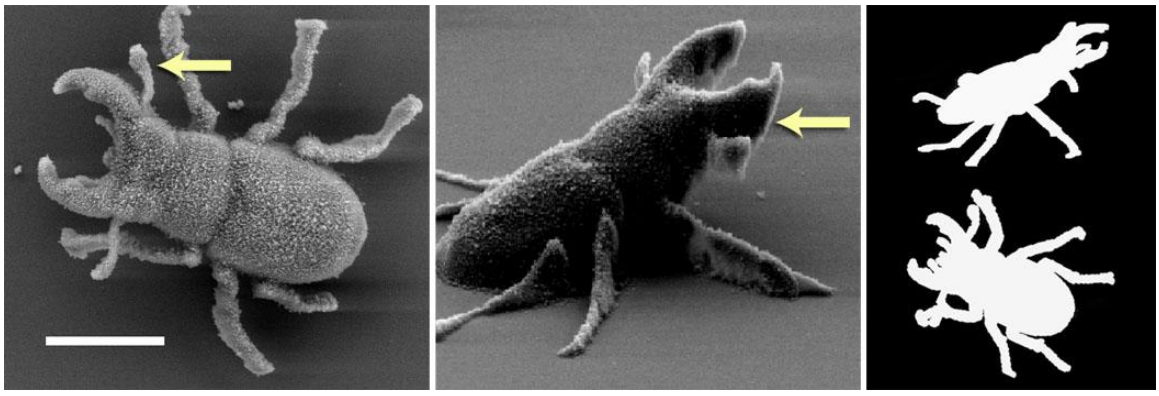

Figure 4.3: BSA structures showing axial distortion. Left and middle, SEM micrographs of replicas of the staghorn beetle (Lucanus sp.). Submicron resolution was regularly achieved in the lateral (left image) but not in the axial dimensions (middle image). Arrows highlight fine features. Right image, 3D reconstruction of mask data in orientations similar to SEM images. Scale bar, 10 μm.

The reflection geometry of the DMD chip resulted in a skew in the projected image on the specimen plane. Two separate, parallel rays reflecting off of a single plane will maintain the same relative spatial relationship before and after reflection. This is not the case for two parallel beams reflecting off separate micromirrors on a DMD chip. The mirrors, which tilt on separate axes, are not in the same plane. Therefore the relative distance between beams is changed after reflection. The result is a ~5º skew in the image projected onto the specimen plane (Figure 4.4). This is easily corrected by added a counter skew to the slice data.

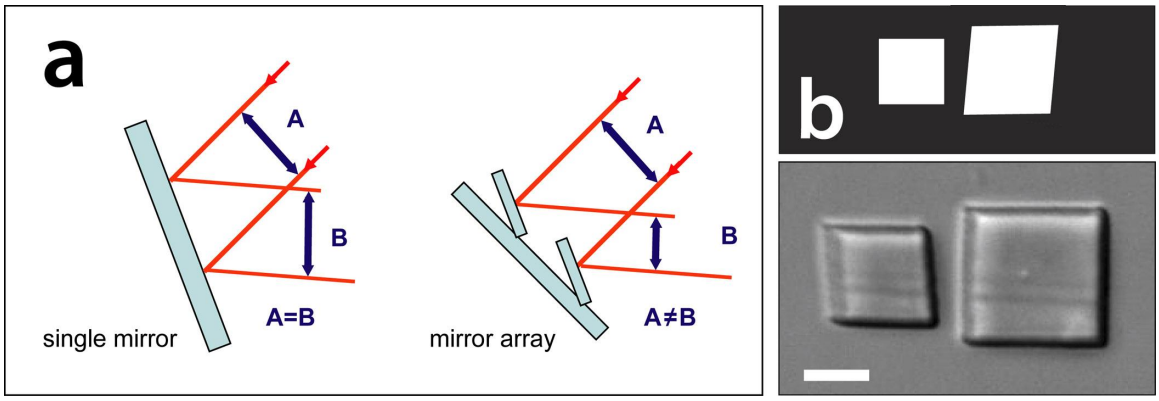

Figure 4.4: Reflection geometry distortion. (a) Diagram of change in spatial relationship of parallel beams with reflection from separate planes. (b) Skew correction. The square mask produces a skewed structure while the skewed mask produces an approximately squared structure. Scale bar, 10 μm.

Grayscale effects similar to those observed with a DMD in its intended use as an image projection system were not attained with the laser fabrication system. It would be advantageous to have the capability of continuous attenuation of laser exposure at defined

micro-regions designated by grayscale patterns on the chip; however, with the current configuration exposure is essentially binary. This is because of an artifact stemming from the fact that the laser does not sample the mirrors of the DMD continuously. Grayscale shading effects are achieved with DMD projection systems by adjusting the duty cycles of individual micromirrors which is known as pulse width modulation (PWM) [7]. According to information from the manufacturer, the DMD projector is programmed to operate at a frequency of approximately 50 to 80 Hz. A time period *T* can be defined as the inverse of the projector frequency. To achieve shading, the mirrors are in the "on" position for a fraction of *T*. For brighter shades, the mirrors are in the "on" position for a larger fraction of *T*, and for darker shades, a lesser fraction. The dwell time of the beam spot on an individual mirror is microseconds, far less then *T*. Thus micromirrors scanned during the "off" portion of their duty cycles will not send light to the specimen plane. By using a scanning, focused light source the effects of the micromirror PWM are not averaged as they would be for a broadly distributed continuous source. The result is the development of interference patterns as seen in Figure 4.5. The projector frequency was ambiguously defined making the interference patterns difficult to predict. Future configurations will have galvanometer scanning mirrors with continuously adjustable frequencies. This should allow the minimization of the interference patterns or the use of interference patterns for designed periodic structures.

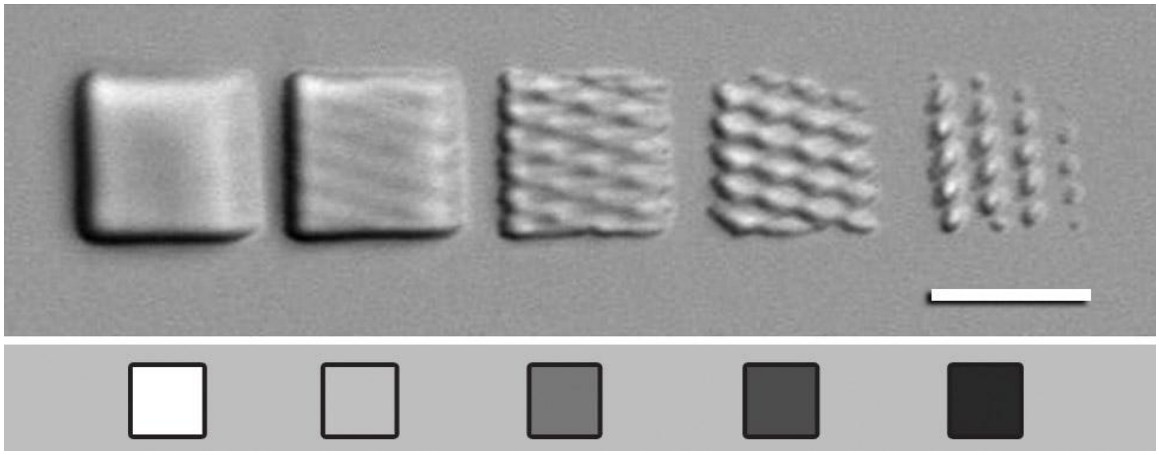

Figure 4.5: Interference patterns. Effects caused by scanning focal spot sampling of grayscaled micromirrors. The lower panel depicts the shades that gave rise to the patterns in the row above. Scale bar, 10 μm.

4.3.3 Extended 2D Structures

The micrometer resolution possible with DMD-based multiphoton lithography enables structural features to be incorporated into materials at subcellular scales. In the design of tissue replicas or cell-culture environments, it could be useful to extend such microengineered materials over lateral dimensions larger than a single-scan plane, which in the current studies are ~$(50\ \mu m)^2$. To achieve such capabilities, we have created automated procedures for coordinating x,y stage movements with sequential display of DMD masks, providing a route for "quilting" multiple horizontal scan planes into larger integrated patterns. The quilted structures were fabricated from an acrylic-based resin that consisted of equal volumes ethoxylated(6) trimethy-lolpropane triacrylate (Sartomer) and tris(2-hydroxyethyl)isocyanurate triacrylate (Sartomer) with 2% trimethylbenzophenone UV photoinitiator [14]. Figure 4.6a depicts the image segmentation process for piecemeal

fabrication. The purpose of expanding and overlaying the segments is to obscure joints, the main cause of which are positioning inaccuracies in the motorized stage. With more accurate stage positioning it should be feasible to quilt materials that cover square millimeters on a time-scale of tens of minutes. Figure 4.6b shows structures fabricated from Sartomer resin. The quilting and overlapping procedures were easier to optimize for the resin because it was less prone than protein to accumulation of material with repeated laser exposure. The resin was also used out of convenience when developing new fabrication procedures, because of the long shelf life of the solution. The axial resolution of the structures made with the resin was very poor (~8 μm minimum feature size, from SEM analysis). Therefore, the resin was not a good precursor material for 3D structure fabrication.

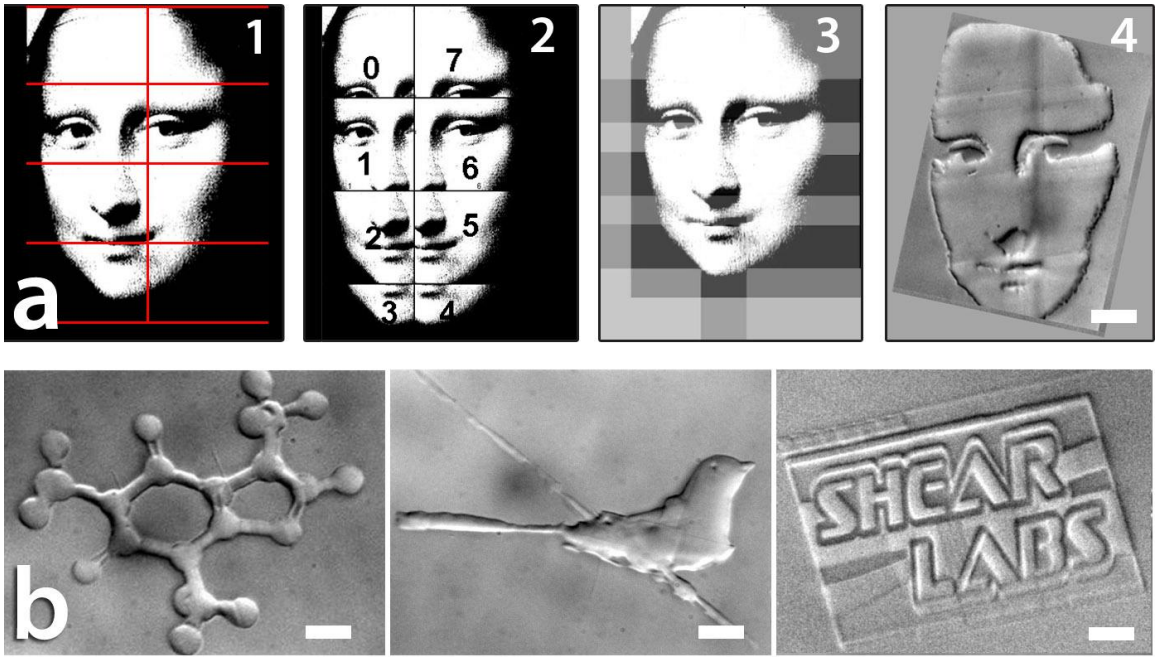

Figure 4.6: Quilted structures fabricated from acrylic-based resin. (a) Steps in a Labview program that segments an image for fabrication by parts. (1) Shows the segmented regions. (2) Depiction of expansion of segmented regions (now labeled by order of fabrication). (3) Depicts the amount of overlap between fabricated structures. (4) Shows the finished structure stitched together from eight separate masks. (b) Eight-segment quilted structures made from JPEG files. From left: model of caffeine, flycatcher on wire, and Shear Lab logo. Scale bars, 10 μm.

4.3.4 Animation Defined Structures

Simple DMD mask sequences can be designed for constructing complex 3D protein topographies such as braided filaments. These microstructural motifs are of particular relevance for tissue engineering applications, serving, for example, as regrowth scaffolds whose mechanical and cell-infiltration properties can be tuned using a range of geometric design parameters [15-17]. To fabricate a triple-fiber braid, a DMD animation

was created using LabView software that displayed three squares translating through interwoven ‘figure 8’ patterns; by coordinating the mask sequence with precise steps of the focal plane along the optical axis, a protein microbraid with a desired pitch was rapidly produced (Figure 4.7). In contrast to the significant computational encoding that would be needed to fabricate such structures using conventional direct-write procedures, DMD-directed masking is accomplished simply and with the flexibility to modify or iterate rapidly by changing basic parameters (e.g., size, shape, and overlap of geometric components), providing a facile approach for materials prototyping.

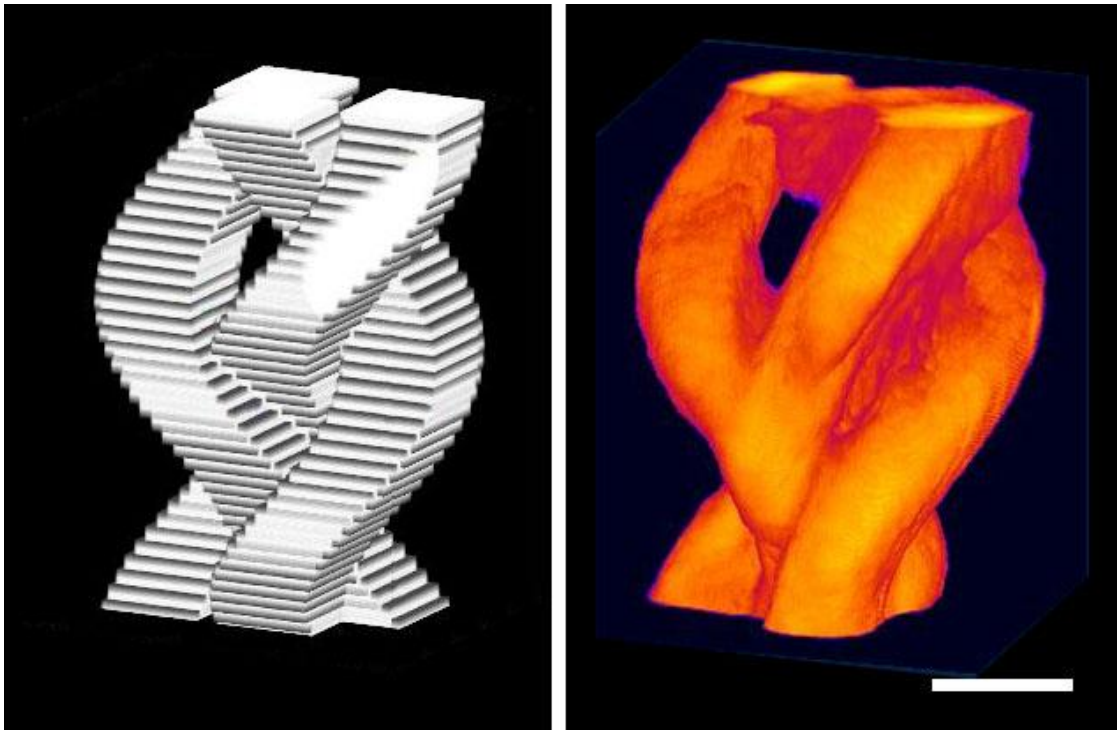

Figure 4.7: A simple mask sequence creates a complex 3D object. Left: 3D reconstruction of 40 masks spaced by the equivalent of 1 μm. The mask data for each plane was formed by three squares that moved in interlocked "figure 8" patterns. Right: Reconstruction of optical slices obtained by MPE fluorescence optical sectioning of the fabricated structure. Scale bar, 10 μm.

The complex nature of interactions between biological cells and their microenvironments (e.g., those affecting stem-cell differentiation, neuronal development, and formation of bacterial biofilms) has created a demand for tissue analogues that serve as more advanced 3D models for exploring cell activity in culture [18]. To evaluate the use of DMD-directed masking in the generation of functional cell-culture interfaces, we created a mask-sequence animation that could be modified rapidly to prototype new 3D topographies in a culture of motile (*E. coli*) cells. The programmed animations displayed

individual slices of a 3D structure which, when fabricated, consisted of a protein cylinder containing a spiraling tunnel and a central receptacle (Figure 4.8).

Because geometric parameters describing the cylinders, including width, height, and pitch of the transit tunnel, were defined by simple trigonometric functions, they could be readily modified to identify conditions for guiding cell migration through the tunnel in three dimensions to the central receptacle. Incremental iteration of tunnel heights resulted in optimization of chamber dimensions for reproducible entry, guidance, and trapping of smooth-swimming *E. coli*. Analogous prototyping schemes would be valuable in development and optimization of various bacterial interfaces, including microstructures designed for the study of population-based behavior, diagnostic separation of bacterial species or phenotypes, and development of bacteria-powered micro-electromechanical and microfluidic devices [19].

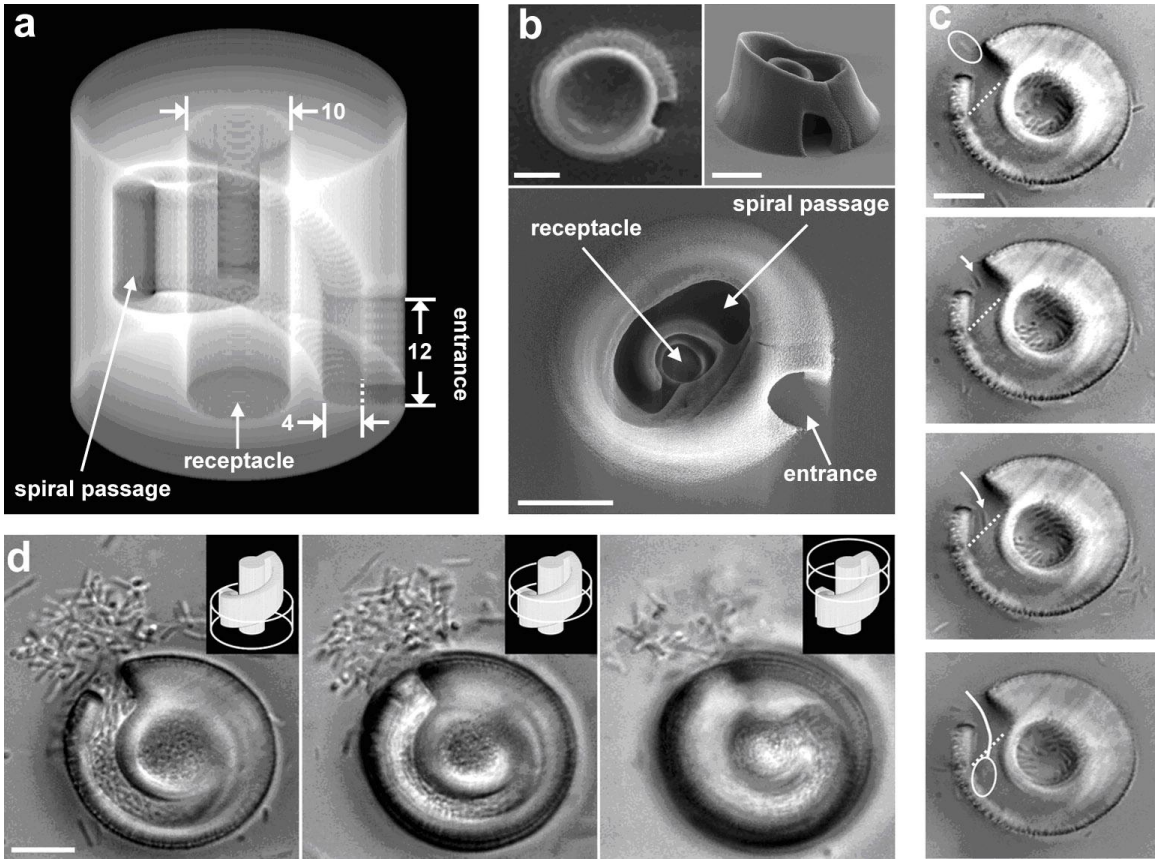

Figure 4.8: Prototyping of microarchitectures for directing cell motility and molding 3D cell colonies. (a) 3D reconstruction (based on mask images) of a microchamber prototype with a single entrance into a spiral ramp (20° pitch, 270° twist) leading up and into the top-front of the enclosed central receptacle (labels are dimensions in micrometers). (b) SEMs of microchamber prototypes with intact (top left panel) and sectioned (top right and bottom panels) tops. (c) DIC image sequence of a single, smooth-swimming *E. coli* bacterium (oval) that passes the entrance and is directed up the spiral passage. Dotted line denotes the top edge of the passageway; elapsed time for sequence is 1 s. (d) Overnight incubation in T-broth of *E. coli* within the microchamber (from panel c) results in growth of a molded cell colony conforming to the shape of the internal architecture. Insets show a schematic of the cell colony and position of focus for each panel. All structures were fabricated from solutions of BSA in ~2 min. using a sequence of 120 masks, with the specimen stepped by 0.3 μm along the optical axis between masks. Nominal structure height (c and d), 32 microns. Scale bars, 10 μm.

4.4 CONCLUSION

In conclusion, we have demonstrated that DMD-directed multiphoton microreplication and prototyping provide new capabilities for facile development and optimization of biologically interactive microstructures. The capability of this system to rapidly translate tomographic data and computer-generated topographies into biological microstructures is an important step toward the creation of custom tissue replacements and culture scaffolds that mimic complex 3D biological environments, such as bronchial, intestinal, and oral tissue. The use of such a technique promises an unprecedented degree of flexibility and accuracy in the ex vivo study of biological processes.

4.5 REFERENCES

1. LaFratta, C., et al., *Multiphoton fabrication.* Angewandte Chemie, 2007. **46**(33): p. 6238.

2. Denk, W., J.H. Strickler, and W.W. Webb, *Two-photon laser scanning fluorescence microscopy.* Science, 1990. **248**(4951): p. 73-6.

3. Kawata, S., et al., *Finer features for functional microdevices.* Nature, 2001. **412**(6848): p. 697-8.

4. Kaehr, B. and J.B. Shear, *Mask-directed multiphoton lithography.* J Am Chem Soc, 2007. **129**(7): p. 1904-5.

5. Kaehr, B., et al., *Direct-write fabrication of functional protein matrixes using a low-cost Q-switched laser.* Anal Chem, 2006. **78**(9): p. 3198-202.

6. Kaehr, B., et al., *Guiding neuronal development with in situ microfabrication.* Proceedings of the National Academy of Sciences of the United States of America, 2004. **101**(46): p. 16104-16108.

7. Van Kessel, P., et al., *A MEMS-based projection display.* Proceedings of the IEEE, 1998. **86**(8): p. 1687-1704.

8. Singh-Gasson, S., et al., *Maskless fabrication of light-directed oligonucleotide microarrays using a digital micromirror array.* Nature Biotechnology, 1999. **17**: p. 974-978.

9. Sun, C., et al., *Projection micro-stereolithography using digital micro-mirror dynamic mask.* Sensors and Actuators A: Physical, 2005. **121**(1): p. 113-120.

10. Lu, Y., et al., *A digital micro-mirror device-based system for the microfabrication of complex, spatially patterned tissue engineering scaffolds.* Journal of Biomedical Materials Research, Part A, 2006. **77A**(2): p. 396-405.

11. Chung, S., et al., *Optofluidic maskless lithography system for real-time synthesis of photopolymerized microstructures in microfluidic channels.* Applied Physics Letters, 2007. **91**: p. 041106.

12. Abramoff, M., P. Magelhaes, and S. Ram, *Image processing with ImageJ.* Biophotonics Int, 2004. **11**(7): p. 36-42.

13. Hell, S., *Toward fluorescence nanoscopy.* Nature Biotechnology, 2003. **21**(11): p. 1347-1355.

14. Baldacchini, T., *Acrylic-based resin with favorable properties for three-dimensional two-photon polymerization.* Journal of Applied Physics, 2004. **95**(11): p. 6072.

15. Cooper, J., et al., *Fiber-based tissue-engineered scaffold for ligament replacement: design considerations and in vitro evaluation.* Biomaterials, 2005. **26**(13): p. 1523-1532.

16. Freeman, J.W., M.D. Woods, and C.T. Laurencin, *Tissue engineering of the anterior cruciate ligament using a braid-twist scaffold design.* J Biomech, 2007. **40**(9): p. 2029-36.

17. Lu, H.H., et al., *Anterior cruciate ligament regeneration using braided biodegradable scaffolds: in vitro optimization studies.* Biomaterials, 2005. **26**(23): p. 4805-16.

18. Griffith, L.G. and M.A. Swartz, *Capturing complex 3D tissue physiology in vitro.* Nat Rev Mol Cell Biol, 2006. **7**(3): p. 211-24.

19. Weibel, D., W. DiLuzio, and G. Whitesides, *Microfabrication meets microbiology.* Nature Reviews Microbiology, 2007. **5**: p. 209-218.

Chapter 5: Parallel Chemical Dosing of Subcellular Targets*

To characterize the role of spatially heterogeneous signaling in cellular function, methods are required for differentially exposing distinct regions of individual cells to externally applied reagents. Although a range of standard approaches exists for generating localized chemical gradients in culture, including puffer pipette spritzing and photolytic release of caged effectors, each is limited in key respects. Here, we report development of a cell-dosing strategy that addresses these limitations, providing the means to create steep gradients of any aqueous-miscible compound at essentially unlimited numbers of sites in parallel. In this approach, cells are cultured on a micrometer-thick polymer membrane that serves as a barrier between two stacked laminar-flow channels: one containing the cell culture and the other serving as a reagent flow cell. By focusing a pulsed laser beam onto one or more selected membrane positions, micrometer-diameter pores can be ablated upstream of desired cellular targets. Nascent pores thus serve as ports of entry into the culture environment for reagent streams capable of modifying subcellular features at positions potentially hundreds of micrometers from ablation sites. Importantly, individual reagent streams also can be rapidly eliminated by photo-cross-linking a protein plug over a selected pore. This versatile strategy for dynamically reshaping the chemical microenvironments in which cells reside should be useful in a variety of cell biology applications, ranging from neurotrophic modulation of neurite pathfinding to stimulation of cellular networks.

---

* Adapted from Nielson and Shear *Anal. Chem.* **2006**, 78(17) 5987 -5993

5.1 INTRODUCTION

Controlled chemical dosing of cells in culture is an indispensable tool in the study of cell differentiation, growth, activity, and death. Agents for selectively perturbing second-messenger signaling, gene-transcription rates, and metabolic processes are used to probe cellular function in a defined fashion [1, 2]. Although entire culture dishes commonly are dosed with a reagent via perfusion or pipette, there is growing understanding for a need to exert greater spatio-temporal control over interactions between chemicals and cells. In particular, studies focused on signaling within and between individual cells, chemotaxis, and neuritic pathfinding have benefited from a battery of methods for creating localized chemical signals. In addition, the ability to deliver labeling reagents to subcellular domains has the potential to clarify mechanisms involved in processing and transport of macromolecules and organelles [3, 4].

Various strategies have been used to locally target chemical agents within cell-culture environments. Of these, puffer-pipette expulsion and photolytic cleavage of caged cellular effectors both have been adopted as relatively routine tools for dosing with subcellular resolution. While both methods present important capabilities, each suffers from serious limitations. Micropositioned puffer pipettes can be used to accurately target nanoliter volumes to subcellular coordinates and, consequently, have been used extensively in studies of polarized cellular responses, including growth-cone turning and localized stimulation of neurons [5, 6]. It generally is not feasible, however, to independently position more than several pipettes in tandem or to rapidly reposition

fragile tips to new sites of interest. For chemical uncaging, dosing volumes can be as small as ~1 fL and the site at which effectors are photolytically created can be rapidly selected and changed in a manner unattainable with puffer pipette [7, 8]. Nevertheless, the applicability of uncaging is severely limited by the need to synthesize a new caged precursor for every effector of interest, many of which cannot be caged using current strategies. For dosing using either micropipettes or uncaging, it typically is not feasible to establish steep concentration gradients that are sustainable for extended periods.

Microfluidic technologies have been used control chemical gradients in microfabricated chambers amenable to cell culture [9-12]. Whitesides and coworkers developed a method in which parallel laminar-flow streams formed within a microfluidic environment could be used to dose subcellular regions of cells with reagent [13, 14]. In this approach, the interfacial region between streams remains sharp, with mixing across stream boundaries limited to the small amount of diffusional transport that occurs as streams rapidly traverse a confluence channel. Unlike dosing using micropipettes or uncaging, steep gradients can be easily established and sustained indefinitely.

Despite its advantages, the microfluidic approach has important limitations. Most significantly, the complexity of the chemical environment is constrained by the initial design of the microfluidic device, and, as with the use of puffer pipettes, practical considerations most likely limit simultaneous dosing to a few independent subcellular sites. Moreover, although stream-interface positions can be manipulated laterally within a confluence channel, stream directionality must be oriented along the channel's longitudinal axis. As a consequence, a structure such as a neurite growing longitudinally in a channel would either have to be dosed along its entire extent or not at all.

Chapter 3 of this dissertation described a technique that used protein structures that were fabricated in the presence of cultured cells, enzymatically functionalized, and exposed to laminar flows of dissolved substrate to create localized gradients. The ability to generate diffusible gradients on arbitrary 3D microstructures in cell culture may one day be an important tool for creating cell scaffolding and tissue analogs. However, before this technique can fulfill its promise several challenges must be met. One problem is the nonspecific adsorption of the protein fabrication precursor which degrades the ability to spatially localize enzymes. Another issue, similar to that of caged compounds, is that the effector needs to be biologically inert until reaction with a specific enzyme. This is a stringent chemical requirement that would limit choice of reagents in experiments. Considering these challenges, it is reasonable to concurrently pursue complimentary cell dosing strategies.

Here, I describe an approach for cellular dosing that fundamentally extends existing capabilities. Cells are cultured on an ultrathin polymer membrane that separates two stacked laminar-flow chambers (Figure 5.1a). Brief application of a train of focused femtosecond laser pulses rapidly introduces a pore in the membrane, producing a laminar-flow effector stream that enters the lower-pressure cell-culture chamber. Because membrane ablation can be performed in the presence of cultured cells, features of interest (e.g., cell bodies, synaptic terminals, growth cones) can be specifically targeted for chemical dosing. In contrast to other chemical dosing approaches, this strategy is amenable to creation of essentially unlimited numbers of laminar-flow streams at arbitrarily selected positions. Importantly, the design of this system should be readily modified to provide on-the-fly control of flow directionality and access for patch pipettes.

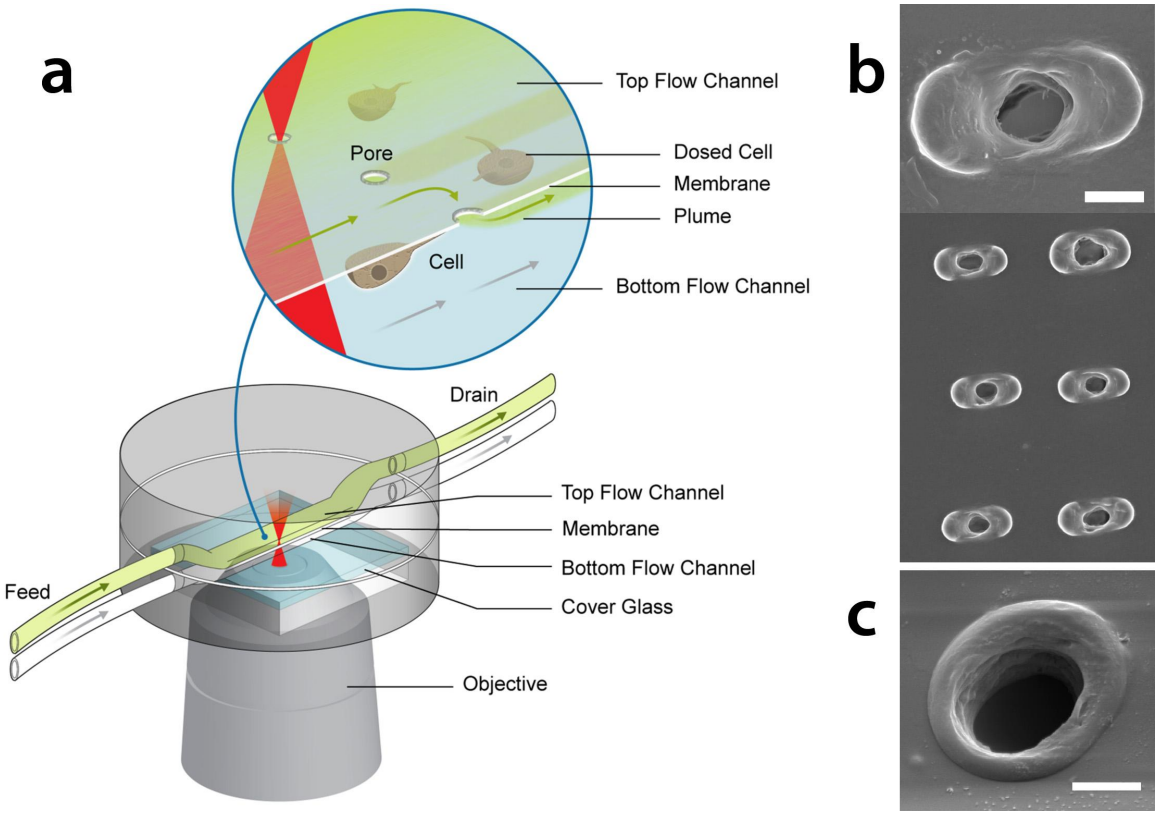

Figure 5.1: Strategy for producing laminar-flow dosing streams via ablation of polymer membranes. (a) PDMS device design. Cells are cultured on a several-micrometer-thick membrane, which is inserted into the device with the cells on the underside of the membrane facing a microscope objective. A femtosecond pulsed laser beam (red cone) is focused by the objective onto the membrane to create an ablation pore at a desired position. Effector solution from the higher pressure top flow channel is forced through the pore, producing a tightly defined reagent stream that propagates across the membrane surface within the cell culture environment. (b) SEMs of ablation pores created in 6 µm-thick polycarbonate membranes showing oblong damage regions surrounding central pores. The scale bar for the top image is 4 µm. An array of pores is shown to the right. (c) A higher magnification SEM showing the more symmetric and smaller pores created in 2.5 µm thick Mylar. Scale bar, 2 µm.

5.2 EXPERIMENTAL METHODS

5.2.1 Device Configuration

In the initial device design, a 2 mm by 8 mm field of cells (see below) was sandwiched between two parallel PDMS flow channels. The membrane acted both as a substrate for support of adherent cells and as a barrier between the two flow channels. A standard microscope coverglass served as the bottom of the lower channel. Because the membrane was situated within the working distance of the microscope objective (~100 μm above the coverslip), it was possible to both image cells and to focus a laser beam on the membrane for ablation. The low profile of the channel also resulted in low Reynolds number (laminar) flow even at the highest flow rates examined, a condition important for creating well-defined reagent streams as solution emerges through pores from the upper chamber. The comparatively large width of the channel (2.5 mm) readily accommodated an extended field of cultured cells, providing many potential cellular targets for dosing and the possibility for creating extensively networked neuronal cultures. To enable rapid exchange of solutions for cell dosing, a similar flow-channel design was adopted for the upper chamber. A positive pressure gradient was created between the upper and lower chambers by constricting the drain tube of the upper flow cell, thus ensuring that solution flowed downward through a pore into the cell culture region. Viton tubing (1.6 mm inner diameter; Cole-Parmer, Vernon Hills, IL) provided a fluidic connection between the chambers and a syringe pump (BS-9000, Braintree Scientific, Braintree, MA).

5.2.2 Device Fabrication

Flow channels were fabricated using modifications to standard PDMS molding processes [15]. To provide a positive relief for the upper channel a strip of transparency film 2.5 mm wide, 22 mm long and 0.1 mm thick was fastened to the bottom of a 5.5 cm diameter polystyrene Petri dish using a thin application of silicone rubber adhesive (RTV 108, GE silicones, Niskayuna, NY). Masters for the drain and feed channels were created with pieces of polyurethane coated wire (0.9 mm diameter) glued next to the ends of the transparency strip in an orientation initially normal to the surface. At a height of ~3 mm the wires were bent parallel to the surface and extended away from the channel master. PDMS (RTV 615 parts A and B, GE Silicones) was mixed at a 10:1 ratio of monomer to curing agent then degassed by centrifuging at 2000 rpm for 10 min. The mixture then was poured into the Petri dish mold to a height of ~6 mm and further degassed in a vacuum chamber. PDMS was cured at 70 ºC for 1 h.; hardened polymer was separated from its masters/mold and was cut to its final dimensions using a razor. The resulting form was a PDMS block 40 mm long, 14 mm wide and 6 mm high which encased a rectangular channel accessed by additional channels to feed and drain solution. The lower channel was fabricated in a similar manner except that after the addition of a thin layer of PDMS, a 22 mm by 22 mm No. 1 1/2 coverglass (Erie Scientific Company, Portsmouth, NH) was compressed onto the transparency film that formed the master for the lower channel. Additional PDMS mixture was added, burying the coverglass and filling the Petri dish mold to the height of ~2.5 mm. After curing, PDMS was separated

from the Petri dish and the masters/mold. A 15 mm by 15 mm wide window for the microscope objective was made by cutting through and removing the PDMS on the side opposite the channel, thereby exposing part of the coverglass that was embedded in the elastomer. The finished bottom flow channel was 0.1 mm high, 2.5 mm wide and 22 mm long, with the optically transparent coverglass serving as the floor of the channel.

The eight port flow channel was constructed in much the same manner except the master for the channel was made by conventional photolithography. An SU-8 precursor was spin-coated onto a glass substrate. The desired asterisk-like shape was polymerized into the precursor by UV light patterned with a printed transparency mask. After development, the SU-8 master had wires attached to the ends of the channel molds to function as inlet/outlet ports in the finished flow channel. PDMS was used to form the body of the flow channel. There were four 2 mm wide, 0.15 mm thick and 22 mm long channels that crossed in the middle forming an asterisk-shape in the finished structure. The finished structure was ~40 mm on a side and ~10 mm high.

5.2.3 Chemicals

Except where noted, all chemicals were purchased from Sigma-Aldrich (St. Louis, MO). BSA was obtained from Equitech-Bio (Kerrville, TX). Mitotracker Green FM (M7514) was purchased from Molecular Probes, Inc. (Eugene, OR).

5.2.4 Cell Culture

Substrates for cell culture consisted of 2.5 μm thick Mylar polyester membranes (SPI Supplies, West Chester, PA) or 6 μm thick polycarbonate membranes (Goodfellow, Devon, PA). Pieces of polymer membrane were held taut by taping them to plastic frames that formed 18 mm wide by 50 mm long rectangular openings. PDMS wells were placed in the center of the pieces of membrane, forming a stable seal by means of surface adhesion. The wells created ~1 ml containers for growth medium. The bottom of the wells had 2 mm by 8 mm rectangular apertures which provided a means to pattern adherent cells onto the polymer membrane. The PDMS well/polymer membrane adhesion structures were washed multiple times with ethanol and de-ionized water. Wells were filled for 20 min. with 33 μg ml^{-1} collagen from rat tail (C7661, Sigma) in HBS (10 mM Hepes, 135 mM NaCl, 5 mM KCl, 2 mM MgCl2, 2 mM CaCl2, 10 mM D glucose, pH 7.4) then rinsed several times with plain HBS before the addition of the cell suspension.

Neuroblastoma-glioma (NG108-15) cells were purchased from the American Type Culture Collection (Manassas, VA) and cultured in DMEM (Mediatech, Inc., Herndon, VA) supplemented with 10% fetal-bovine serum (FBS), penicillin (100 mg/L), and streptomycin (100 kUnits/L) purchased from Invitrogen (Carlsbad, CA). Flasks were maintained at 37 °C in a 10% CO2 atmosphere with saturated H2O. Cells were suspended in a low-serum (1% FBS) growth medium at a concentration of ~30,000 cells ml^{-1}, placed into the PDMS wells on the polymer membrane and incubated for 1 – 3 days in the low-serum medium to induce neuronal differentiation.

5.2.5 Cell Loading

After incubation, cells were loaded into the flow channels by inverting the membrane on which the cells had been plated; the PDMS well then was removed, leaving a hanging drop that bathed the plated cells. The two flow channels were aligned on either side of the cell field and compressed to sandwich the membrane. A block with two screws was used to hold and compress the mated channels onto a heated microscope stage, reinforcing a seal between the channels and the membrane. This process yielded two channels ~100 μm high and 2.5 mm wide that were separated by a polymer membrane, with a field of cells adhered to the underside of the membrane. The lower channel feed tube was secured to the heated stage and the temperature was adjusted so that solution exiting the lower channel was 37 °C.

5.2.6 Pore Formation

Pores in membranes were produced by ablation using the output from one of two light sources. The first was a Ti:S laser (Coherent Mira, Santa Clara, CA) tuned to 750 nm. The laser repetition rate was 76 MHz and the pulse duration was ~150 fs. The second laser was a frequency doubled (532 nm) microchip Nd:YAG laser (Teem Photonics). Both beams were aligned into a Zeiss Axiovert (inverted) microscope. The beams were expanded and collimated so that they approximately filled the back aperture of a 40x objective (Olympus UPlanFl, 0.75 NA). The average power of the Ti:S beam ranged from 200 to 350 mW (measured before the objective), yielding an approximate intensity at the focal spot of ~2.5 – 4 TW cm^{-2}. While the average power for the frequency doubled Nd:YAG was typically 10 mW which yielded an intensity of ~0.6 TW cm^{-2}. Laser

exposure periods were controlled using a Uniblitz UHS1 shutter (Vincent Associates, Rochester, NY).

5.2.7 Microscopy

Light transmission photomicrographs were obtained on the Axiovert using a cooled CCD camera (C4742-98; Hamamatsu, Bridgewater, NJ). Fluorescence images were acquired using a Zeiss HBO 100 mercury lamp and a FITC filter set. Confocal images of plumes were obtained using a Leica SP2 AOBS confocal microscope (Wetzlar, Germany). Image analysis was performed using ImageJ [16].

To obtain SEM images of ablated pores, polymer membranes were washed with ethanol and air dried. Afterward, membranes were sputter coated with gold to a nominal thickness of 9 nm and imaged using an LEO 1530 scanning electron microscope (Leo Electron Microscopy Ltd., Zeiss, Oberkochen, Germany).

5.3 Results and Discussion

5.3.1 Membrane Ablation

The pore forming process is accompanied by localized melting of the membrane and the formation of a gas bubble. As discussed in Chapter 2, such phase changes require a significant deposition of energy and the predominant mechanism for this is most likely multiphoton and avalanche ionization. In the current studies, a 40x air objective was used to create pores in Mylar and polycarbonate membranes that separated adjoining flow cells. For most of the experiments described in this chapter ablation of polymer

membranes was accomplished by focusing a high repetition rate (76 MHz) Ti:S beam approximately midway into a membrane. In studies using 6 μm-thick polycarbonate membranes, exposure was limited to a period of ~150 ms using a laser power of ~200 mW (measured before the objective). For ablation of 2.5-μm-thick Mylar, various exposure conditions were evaluated to achieve minimum pore sizes and to optimize the regularity and reproducibility of pore shapes. Ultimately, a procedure was adopted in which the membrane was irradiated by a train of ten 1 ms exposures at 350 mW average power, spaced by 50 ms intervals. Insertion of these extended "dark" periods appeared to reduce cumulative exposure effects, resulting in more regularly sized pores than were attained using continuous exposure. Pore size did not appear to depend strongly on laser power, so long as laser power was set to a level significantly above the threshold for ablation. The precise positioning of the laser focus within the membrane likely affected pore size, although detailed studies on this effect were not conducted in this initial study.

High-resolution analysis of pores formed in polycarbonate and Mylar using these procedures was performed using scanning electron microscopy (SEM). As shown in Figure 1b, in polycarbonate a somewhat elongated central pore (pore area, 12 ± 4 μm^2) is created surround by an asymmetric lip. The appearance and relatively large diameter of the pores (~4 μm diameter; more than 10-fold larger than the focal spot diameter) indicate that the ablation process likely involves both dielectric breakdown and an accompanying thermal process [17]. The apertures in 2.5-μm thick Mylar (Figure 5.1c) were both smaller (pore area, 3.2 ± 0.7 μm^2) and less oblong. Standard deviations in membrane pore areas were determined via SEM measurements on series of pores fabricated within single polycarbonate and Mylar membranes. Provided that the laser

focal point remained stationary with respect to the membrane during pore ablation, this level of variability appears similar to that fabricated in other membranes (on different days) as observed using optical microscopy.

When ablation is performed with aqueous solutions in both the upper and lower chambers, gas bubbles often adhere to the lip surrounding the pore, obstructing flow through the aperture. Such blockage can be avoided by filling the upper chamber with air during laser exposure, an approach that requires the chamber to be re-filled with solution after formation of the pore.

5.3.2 Laminar Stream Characteristics

Confocal fluorescence microscopy was used to characterize the 3D properties of laminar-flow streams created by flow of 1 μM fluorescein through representative pores in 6 μm thick polycarbonate membranes. Figure 5.2a shows streams emerging from three pores laterally spaced by ~30 μm. Using a lower-chamber flow rate of 1.0 ml min^{-1} (calculated to be 15 μm ms^{-1} at a distance of 4 μm from the membrane), well-defined streams are created that extend from pores for hundreds of microns with minor broadening. The mean 1/e stream radius 10 μm downstream from the pore edge at a nominal distance of 4 μm from the membrane was measured to be ~6 μm. Laminar-flow streams run parallel to the membrane, with dye detectable at a maximum distance of ~8 μm from the membrane surface. Within experimental error, the concentration of the dye at the center of the laminar-flow stream 10 μm downstream from the pore was equivalent to the concentration of dye supplied to the upper chamber. As expected, at a lower flow rate (0.15 ml min^{-1}; 2.3 μm ms^{-1} 4 μm from the membrane), plumes were

more diffuse, with fluorescein fanning out significantly tens of microns downstream from the pore. However, within 10 μm of the pore the dye stream remained well defined, with a measured lateral radius of ~7 μm. As a consequence, specific targets can be dosed with reasonably high resolution even at lower flow rates.

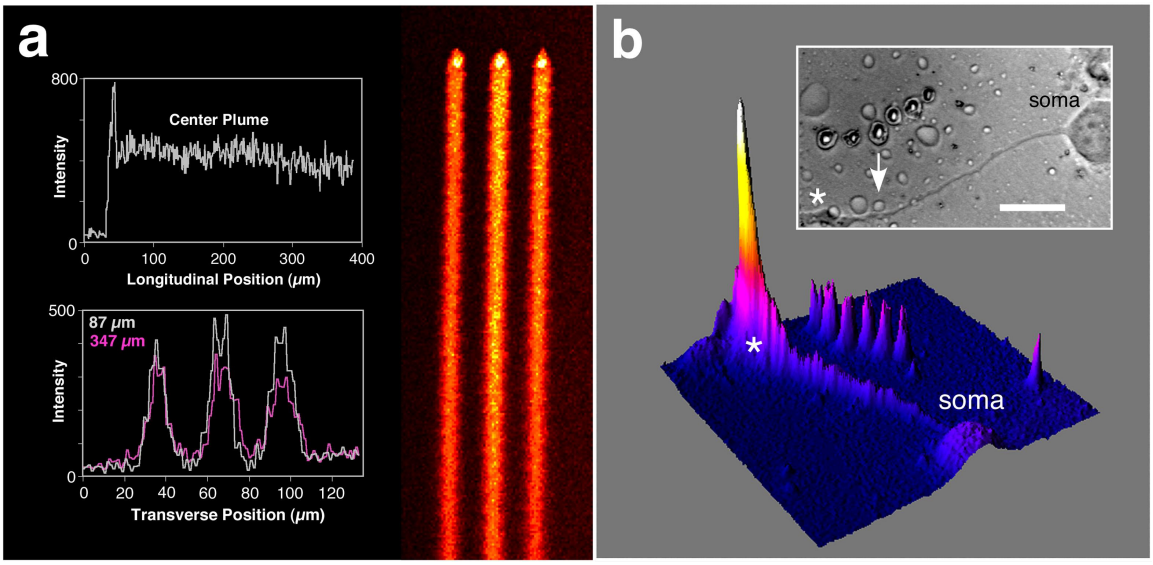

Figure 5.2: Formation of laminar-flow streams through photoablated pores. (a) Confocal fluorescence microscopy of 1 µM fluorescein streams emerging through pores created in a 6 µm-thick polycarbonate membrane. The image in the right panel was created by summing a stack of confocal images ranging from the membrane to tens of micrometers into solution. Measurements were acquired using a 20x, 0.7 NA air objective with 0.34 µm steps between stack images. The panel at the upper left plots intensity along a line running from the top of the image downward through the center of the middle plume. Fluorescein intensity decreases by ~20% over the 350 µm length of stream shown. The plot on the lower left shows intensity along transverse lines running left to right across the image at two positions downstream from the pores (87 and 347 µm). Note the relatively minor increase in stream widths at the more distal position. (b) Differential interference contrast image (inset) and fluorescence intensity surface plot demonstrating the use of a series of pores to dose an extended region of a cultured cell. A varicosity region (asterisk, both images) and neurite of an NG108-15 cell cultured on a polycarbonate membrane is labeled with 50 µM carboxyfluorescein diacetate (a membrane-permeant stain) over ~75 µm using a set of six pores. Flow direction is represented by the downward arrow (inset). The varicosity region is labeled most intensely, as it lies both in the direct path of the dye stream and is significantly larger in volume than the neurite. HBS buffer was flowed through the cell chamber at a volume flow rate of 0.15 ml min^{-1}. Scale bar (inset), 30 µm.

Initial characterization of laminar streams emerging through pores formed in Mylar indicates that stream radii decrease as a consequence of the smaller and more symmetric ablation pores. Using widefield fluorescence to estimate stream dimensions via de-quenching of fluorescein emission (as a consequence of a pH differential between the two flow channels), 1/e radii of flow streams ~10 μm downstream from the pore edge are estimated to be smaller than 5 μm.

Notably, the dimensions of laminar-flow streams are consistently larger than their corresponding aperture diameters, even at positions immediately adjacent to pores. Various factors in addition to pore diameter likely influence the concentration distribution and morphology of laminar-flow streams, including the shape of the pore and its surrounding burr, the cross-sectional area of the pore and the pressure drop between the chambers.

In these initial studies, it was not feasible to dictate the diameter of pores with a high degree of control. In both Mylar and polycarbonate, pores having the minimum achievable diameters (Figure 5.1b–c) can be created with good reproducibility and over a limited range, pore size can be increased by using larger average laser powers or longer exposure times. Ultimately, however, threshold values are reached at which violent ablation results in membrane cratering, a process that yields apertures with diameters several-fold larger than pores fabricated below threshold. From a utilitarian standpoint, however, we found it feasible to create wider plumes by ablating arrays of densely packed small pores (Figure 5.2b).

5.3.3 Termination of Flow through Selected Pores

An ability to "valve-off" selected laminar streams while continuing to flow reagents through other pores would provide valuable on-the-fly control over the chemical landscapes that can be created with this approach. To eliminate flow through selected pores in cellular environments without use of complex, pre-fabricated microfluidics, we have adapted biocompatible protein microfabrication as a means to seal off selected pores. To accomplish this, we introduced a solution of 100 mg ml^{-1} BSA and 5 mM FAD into the reagent chamber. By focusing ~50 mW from the Ti:S laser (measured before the objective) onto the aperture entrance, BSA plugs (Figure 5.3a) could be fabricated within less than 1 s that eliminated all apparent flow through a desired pore without visibly damaging the polymer membrane. Figure 3b demonstrates a series in which plumes of BSA are sequentially eliminated in this manner. In addition, we have attempted to re-open pores by removing BSA plugs through a subsequent ablation event. Although pore re-opening is readily feasible, our preliminary studies have produced somewhat larger pores than were originally created in the membrane.

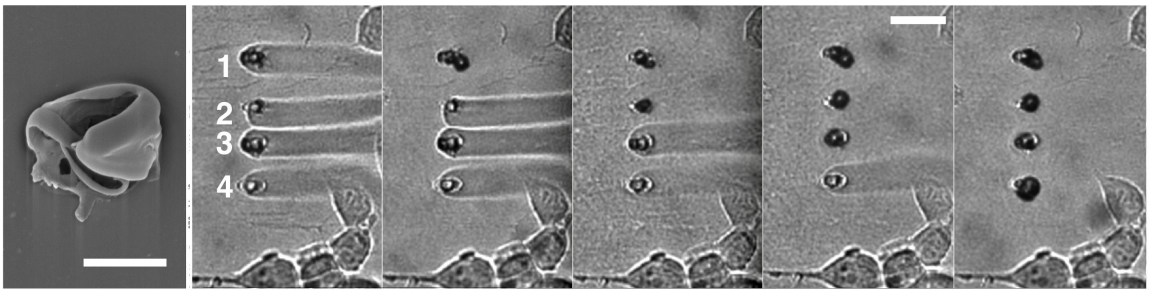

Figure 5.3: Closure of pores using protein photo-cross-linking. Left panel: an SEM of a BSA plug fabricated to obstruct a pore formed in Mylar. Scale bar, 5 μm. Right five panels: sequential plugging of laminar-flow BSA streams (1-4) in a culture of NG108-15 cells using multiphoton-excited protein photo-cross-linking. FAD was used as a nontoxic photosensitizer to promote BSA cross-linking at the entrances to pores ablated in a polycarbonate membrane. From left, sequential images were acquired at t = 0 s, t = 132 s, t = 185 s, t = 190 s, and t = 206 s. HBS buffer flowed through the cell chamber at a volume flow rate of 0.15 ml min^{-1}. Scale bar, 30 μm.

5.3.4 Cell Dosing Studies

For moderate solution flow rates, we found that flow had little or no effect on cells as assessed by adherence, morphology, and metabolic viability (see carboxyfluorescein diacetate studies, below). At flow rates above ~0.5 ml min^{-1} (~0.8 cm s^{-1} at a position 4 μm from the membrane) visible effects of shear stress could be observed on some NG108-15 cells plated on Mylar (e.g., minor deformation, partial lifting of neuritic structures) and at flow rates greater than 1.0 ml min^{-1} a significant fraction of cells lost adherence within 10 min.

An initial assessment of the biocompatibility of the membrane ablation process was made by examining morphological properties of NG108-15 cells plated on Mylar during and after pore formation. Retraction of neurites and other signs of physical distress often are apparent when pores are made in direct proximity to cells (i.e., at spacings of

less than 5 μm), but generally are not evident at somewhat greater distances (> 10 μm). Provided that cells appear healthy immediately after ablation, they typically display no morphological degradation for experiments that last more than an hour. Were it advantageous to create a pore within 5 μm or less of a cell, the pressure differential between flow chambers could be reversed to minimize exposure of cells to membrane debris during pore formation. It also would be of value in future studies to evaluate transient temperature increases in the vicinity of a pore that accompany the ablation process.

The ability to dose specific cells and subcellular regions with a labeling reagent was evaluated using 5-carboxyfluorescein diacetate (CFDA) (Molecular Probes, C1361), a membrane-permeable dye that is converted to its fluorescent form after hydrolysis by cytosolic esterases. Because visualization of this dye relies both on the continued functioning of metabolic components and a reasonably leak-free plasma membrane [18, 19], use of this dye served the additional role of further probing the viability of cells downstream of newly created pores. In these studies, 2.5 μm thick Mylar served as the barrier between flow chambers. To avoid occlusion of the pore by adherent bubbles, ablation was performed with the reagent chamber filled with air. Within several seconds of pore formation, CFDA was pumped into the upper flow cell, resulting in formation of a laminar-flow stream in the lower chamber directed at a selected target. CFDA was replaced with plain HBS buffer in the upper chamber after a dosing period of ~1 min., and the procedure was repeated several times to sequentially dose targets at desired spatio-temporal coordinates. As shown in Figure 5.4a, cellular features of specific

interest—a neurite terminal and three cell bodies—could be directly targeted, as evidenced by an increase in fluorescein emission.

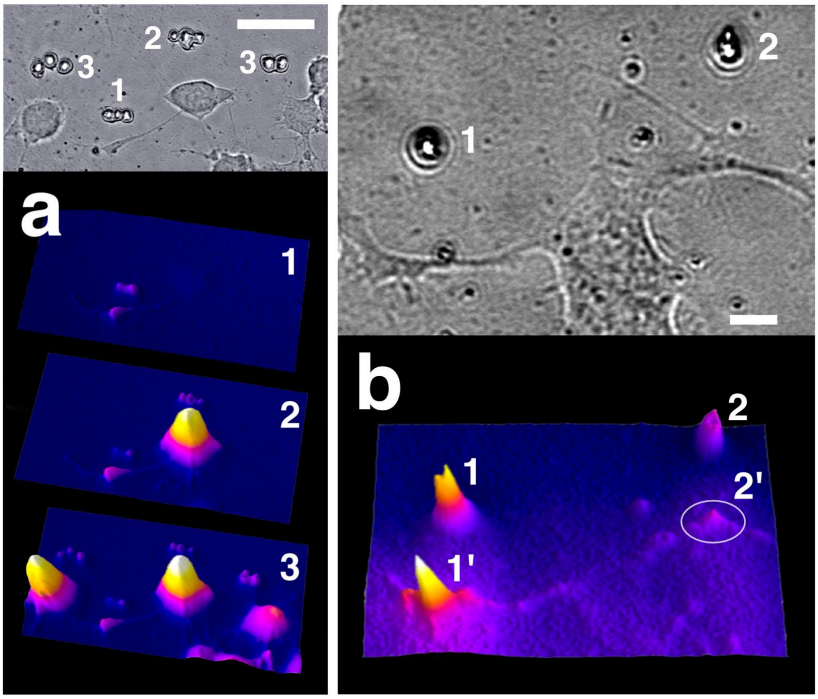

Figure 5.4: Subcellular labeling of neuronally differentiated cells using multiple laminar-flow streams. (a) NG108-15 dosing using the plasma membrane permeant fluorescein dye, CFDA. Four sets of pores are visible in the transmission image (top), with clusters numbered according to the sequence in which they were created. After formation of pore clusters 1-3 in the Mylar substrate, CFDA laminar-flow streams were established to selectively dose subcellular regions; following 1 min, exposures to 50 µM CFDA and dye washout, fluorescence data were acquired using wide-field imaging. Fluorescence intensities are displayed as surface plots corresponding to t = 0 (top plot, pore cluster 1), after ~14.5 min (middle, pore cluster 2), and after ~27 min (bottom, pore clusters 3). Scale bar, 50 µm. (b) Point labeling of opposing neurites on an NG108-15 cell using Mitotracker Green FM. Two pores (1 and 2) were created in the Mylar substrate, seen as concentric circles (top, transmission image) and fluorescence peaks (bottom, fluorescence intensity surface plot). Subcellular sites labeled by pores 1 and 2 are designated in the fluorescence image as 1' and 2', respectively. Fluorescence data were acquired after a 1 min exposure to 2 µM Mitotracker followed by ~1 min of dye washout. Scale bar, 10 µm. For the studies shown in parts a and b, HBS buffer flowed through the cell chamber during the dosing period at rates of 0.15 and 0.45 ml min^{-1}, respectively.

In general, we found that CFDA delocalized throughout the cytosol within minutes, a finding consistent with expected diffusion rates for this compound [20]. For example, the neuritic fluorescence created by pore cluster 1 dissipated almost completely in the period between the initial CFDA exposure and dosing after creation of pore cluster 2 (data not shown). Only after CFDA flow was re-initiated did the neuritic structure once again become fluorescent.

We also found it feasible to selectively dose precise regions within cultured cells using Mitotracker Green FM (Molecular Probes, M7415), a dye that, at the concentrations used here, has been reported to localize to a variety of cellular structures. Because this dye is fluorescent principally when incorporated into lipid environments (e.g., organelles), cellular staining from this species delocalizes less rapidly than for cytosolic fluorophores with similar molecular masses, such as CFDA. To evaluate Mitotracker labeling, NG108-15 cells cultured on Mylar were dosed in a procedure similar to that used for CFDA except that the volumetric flow rate was increased to 0.45 ml min^{-1}. As shown in Figure 5.4b, it is possible to target narrow regions (extending ~10 μm) on two neurites on opposing sides of a cell body without appreciable staining of the soma itself.

To test the ability of this system to selectively target cells for disruption, ethanol was flowed through the reagent chamber and a single pore was introduced near a cluster of cells plated on polycarbonate (Figure 4.5). Within several seconds of pore formation, a cell positioned directly downstream of the pore underwent extensive dehydration. The last (right-most) image in this sequence, taken ~25 s after creation of the pore, shows that

even after this relatively long period no additional cells within the field displaed signs of morphological damage.

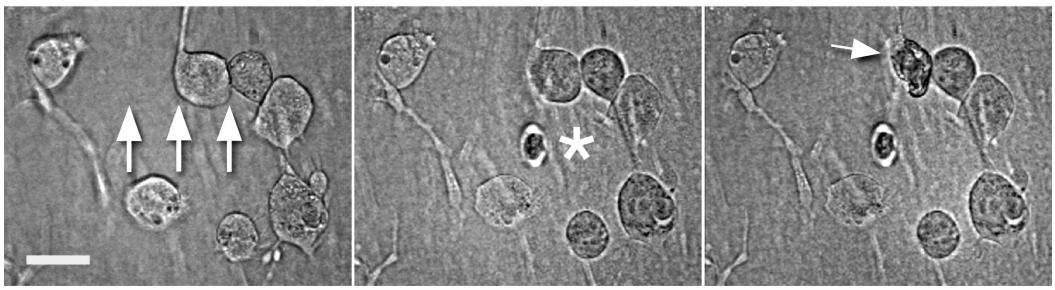

Figure 5.5: Sequence showing selective dehydration of an NG108-15 cell. A laminar-flow ethanol stream was introduced through a pore (asterisk, middle image) formed in a polycarbonate substrate. Based on the direction of flow (arrows, left panel), ethanol was delivered to the cell identified in the final panel (acquired 25 s after pore formation). Throughout dosing, HBS buffer flowed through the cell chamber at a rate of 0.15 ml min^{-1}. Scale bar, 30 μm.

5.3.5 Multiport System

In complex neuronal cultures, accessibility to some sites of interest would be improved by incorporating into the system a means to control flow orientation. The membrane-based system developed here is readily amenable to modifications that provide such control. This was demonstrated with an eight port flow chamber in which four channels (with dimensions similar to those in single channel set-up) were arranged in an orientation where the channels intersected in the middle and were off-set 45° at the ends, giving the flow chamber an asterisk-like appearance. The chamber was regulated with pinch valves so that fluid could flow in either direction through any of the four channels. This was done by having two inlets at the end of every channel, one to feed and one to drain. The inlets were connected to the syringe pump or to the waste container by

silicon tubing. The corresponding feed and drain tubing for each channel direction was controlled by the same pinch valve, so that opening a valve would allow liquid flow in one direction through a particular channel. An array of eight electronically controlled pinch valves allowed fluid flow to be controlled in at least eight orientations through the four-channel flow cell. With the ablation of a pore and the flow of separate solutions through the upper and lower channels, the result was a plume whose orientation could be changed in less than 1 s. In addition more orientations could be obtained by activating several channels simultaneously (Figure 5.6).

Modifications for future configurations may include an opening in the central region to provide greater mechanical access to cells to, for example, to enable electrophysiology to be conducted in parallel with chemical dosing. These designs necessitate cells plated on the top side of the membrane which has been the preferred configuration in recent experiments. Others have demonstrated that flow cell systems with open-air canals can provide rapid, laminar-flow exchange of solution while maintaining access for patch-clamp measurements [21]. Preliminary studies seem to indicate the laminar flow characteristics can be reasonably well maintained in open flow cells.

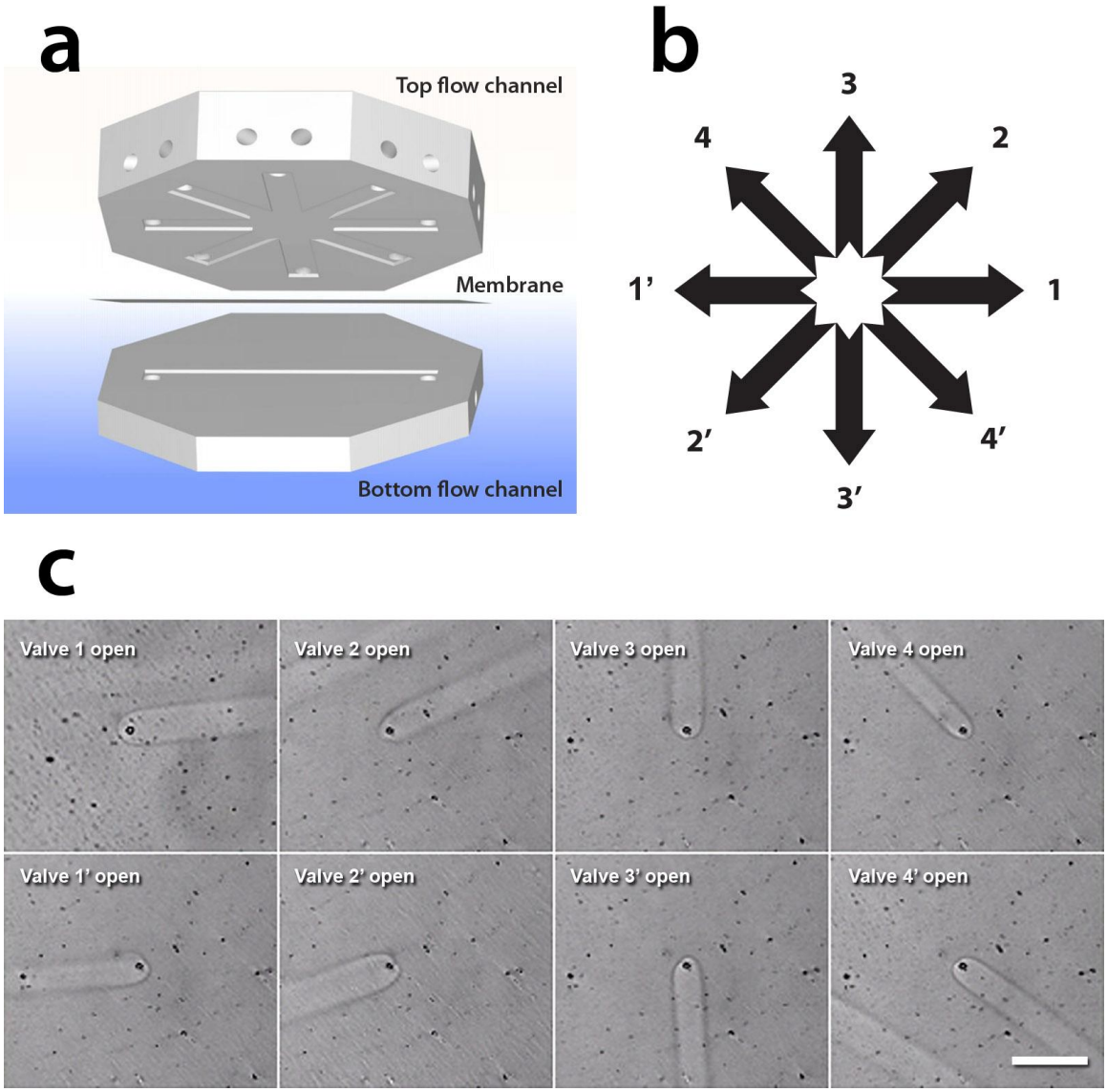

Figure 5.6: Multiport flow chamber for control of plume orientation. (a) Exploded view showing the four channel upper flow chamber, separating membrane, and single channel bottom flow chamber. (b) Diagram of flow orientations controlled by eight valves (c) Eight separate orientations for 6% BSA plumes emerging into aqueous buffer as different flow directions are activated. The pores were formed in 2.5 µm thick Mylar with a frequency doubled Nd:YAG (estimated intensity at focus, ~0.6 TW cm^{-2}). The volumetric flow rate in the channel was 0.1 ml min^{-1}. Scale bar, 50 µm.

5.4 CONCLUSION

In these studies, we demonstrate that stable, well-defined reagent streams can be created in parallel within cell culture environments. Although larger pores are created in polycarbonate membranes than in Mylar, more systematic studies will be required to determine the individual contributions of material composition and membrane thickness to pore size. Because ablation and plugging of pores that gate reagent delivery can be accomplished under biologically benign conditions, this procedure provides fundamentally new capabilities for chemically interfacing with cells without requiring complex, prefabricated microfluidic networks. Creation of sustainable and steep concentration gradients in neuronal environments may have a substantial impact in numerous applications, including multisite chemical stimulation of neuronal networks, induction of receptor clustering, neurotrophic mediation of neurite pathfinding, and tracking of axonal transport processes [22-24].

5.5 REFERENCES

1. Ito, H., et al., *Neurotrophins facilitate synthesis of choline acetyltransferase and tyrosine hydroxylase in cultured mouse neural stem cells independently of their neuronal differentiation.* Neuroscience Letters, 2003. **339**: p. 231-234.

2. Contestabile, A. and E. Ciani, *Role of nitric oxide in the regulation of neuronal proliferation survival and differentiation.* Neurochemistry International, 2004. **45**: p. 903-914.

3. Karten, B., et al., *Neuronal models for studying lipid metabolism and transport.* Methods, 2005. **36**: p. 117-128.

4. Brown, A., *Slow axonal transport: stop and go traffic in the axon.* Nature Reviews Molecular Cell Biology, 2000. **1**: p. 153-156.

5. Zheng, J.Q., J. Wan, and M.M. Poo, *Essential role of filapodia in chemotropic turning of growth cone induced by a glutamate gradient.* Journal of Neuroscience, 1996. **16**: p. 1140-1149.

6. Wang, G.X. and M.M. Poo, *Requirement of TRPC channels in netrin-1-induced chemotropic turning of nerve growth cones.* Nature, 2005. **434**: p. 898-903.

7. Matsuzaki, M., et al., *Dendritic spine geometry is critical for AMPA receptor expression in hippocampal CA1 pyramidal neurons.* Nature Neuroscience, 2001. **4**(11): p. 1086-1092.

8. Callaway, E. and R. Yuste, *Stimulating neurons with light.* Current Opinion in Neurobiology, 2002. **12**: p. 587-592.

9. Peterman, M.C., et al., *Localized chemical release from an artificial synapse chip.* Proceedings of the National Academy of Sciences of the United States of America, 2004. **101**(27): p. 9951-9954.

10. Wu, H., B. Huang, and R.N. Zare, *Generation of complex, static solution gradients in microfluidic channels.* Journal of the American Chemical Society, 2006. **128**(13): p. 4194-4195.

11. Jeon, N.L., et al., *Neutrophil chemotaxis in linear and complex gradients of interleukin-8 formed in a microfabricated device.* Nature Biotechnology, 2002. **20**(8): p. 826-830.

12. Taylor, A.M., et al., *Microfluidic multicompartment device for neuroscience research.* Langmuir, 2003. **19**(5): p. 1551-1556.

13. Takayama, S., et al., *Subcellular positioning of small molecules.* Nature, 2001. **411**: p. 1016.

14. Takayama, S., et al., *Selective chemical treatment of cellular microdomains using multiple laminar flows.* Chemistry & Biology, 2003. **10**: p. 123-130.

15. Duffy, D.C., et al., *Rapid prototyping of microfluidic systems in polydimethylsiloxane.* Anal. Chem., 1998. **70**: p. 4974-4984.

16. Abramoff, M.D., P.J. Magelhaes, and S.J. Ram, Biophotonics Int., 2004. **11**: p. 36-42.

17. Schaffer, C.B., et al., *Structural changes induced in transparent materials with ultrashort laser pulses*. Ultrafast Lasers, G. Sucha, Editor. 2003, Marcel Dekker Inc.: New York. p. 395-418.

18. Satoh, T., et al., *Flow cytometric analysis of serum deprivation-induced apoptosis of PC12 cells, with special reference to the role of bcl-2.* Neuroscience Letters, 1995. **201**: p. 119-122.

19. Provinciali, M., G.D. Stefano, and N. Fabris, *Optimization of cytotoxic assay by target cell retention of the flourescent dy carboxyfluorescein diacetate and comparison with conventional CR release assay.* Journal of Immunological Methods, 1992. **155**: p. 19-24.

20. Verrechia, F., et al., *ATP counteracts the rundown of gap junctional channels of rat ventricular myocytes by promoting protein phosphorylation.* Journal of Physiology, 1999. **516**: p. 447-459.

21. Hsu, C., C. Chen, and A. Folch, *"Microcanals" for micropipette access to single cells in microfluidic environments.* Lab Chip, 2004. **4**: p. 420-424.

22. Chada, S.R. and P.J. Hollenbeck, *Nerve factor signaling regulates motility and docking of axonal mitochondria.* Current Biology, 2004. **14**: p. 1272-1276.

23. Gallo, G. and P.C. Letourneau, *Localized Sources of Neurotrophins Initiate Axon Collateral Sprouting.* Journal of Neuroscience, 1998. **18**(14): p. 5403-5414.

24. Vogt, A.K., et al., *Synaptic plasticity in micropatterned neural networks.* Biomaterials, 2005. **26**: p. 2549-2557.

Bibliography

Abramoff, M. D., P. J. Magelhaes, and S. J. Ram. Biophotonics Int., 11 (2004): 36-42.

Abramoff, MD, PJ Magelhaes, and SJ Ram. "Image processing with ImageJ." Biophotonics Int., 11, no. 7 (2004): 36-42.

Allen, R. "Pertubation and analysis of biological microenvironments." University of Texas, 2005.

Allen, R, R Nielson, DD Wise, and JB Shear. "Catalytic three-dimensional protein architectures." *Analytical Chemistry (Washington, DC)* 77, no. 16 (2005): 5089-5095.

Amborski, LE, and DW Flierl. "Physical properties of polyethylene terephthalate films." *Industrial & Engineering Chemistry* 45, no. 10 (1953): 2290-2295.

Baldacchini, T. "Acrylic-based resin with favorable properties for three-dimensional two-photon polymerization." *Journal of Applied Physics* 95, no. 11 (2004): 6072.

Basu, S, and PJ Campagnola. "Enzymatic activity of alkaline phosphatase inside protein and polymer structures fabricated via multiphoton excitation." *Biomacromolecules* 5, no. 2 (2004): 572-9.

Baudelet, M, L Guyon, J Yu, JP Wolf, T Amodeo, E Fréjafon, and P Laloi. "Femtosecond time-resolved laser-induced breakdown spectroscopy for detection and identification of bacteria: a comparison to the nanosecond regime." *Journal of Applied Physics* 99 (2006): 084701.

Ben-Yakar, A, A Harkin, J Ashmore, RL Byer, and HA Stone. "Thermal and fluid processes of a thin melt zone during femtosecond laser ablation of glass: the formation of rims by single laser pulses." *Journal of Physics D: Applied Physics* 40, no. 5 (2007): 1447-1459.

Berland, KM, PT So, and E Gratton. "Two-photon fluorescence correlation spectroscopy: method and application to the intracellular environment." *Biophysical Journal* 68, no. 2 (1995): 694-701.

Birge, RR. "One-photon and two-photon excitatioin spectroscopy." *Ultrasensitive Laser Spectroscopy. Edited by David S. Kliger. Published by Academic Press, a subsidiary of Harcourt Brace Jovanovich, New York, 1983, p. 109* (1983).

Boudaïffa, B, P Cloutier, D Hunting, MA Huels, and L Sanche. "Resonant formation of DNA strand breaks by low-energy (3 to 20 Ev) electrons." *Science* 287, no. 5458 (2000): 1658.

Brown, A. "Slow axonal transport: stop and go traffic in the axon." *Nature Reviews Molecular Cell Biology* 1 (2000): 153-156.

Cairns, RA, R Khokha, and RP Hill. "Molecular mechanisms of tumor invasion and metastasis: an integrated view." *Curr Mol Med* 3, no. 7 (2003): 659-671.

Callaway, E., and R. Yuste. "Stimulating neurons with light." *Current Opinion in Neurobiology* 12 (2002): 587-592.

Cao, Y, Q Chu, and J Ye. "Determination of hydroxyl radical by capillary electrophoresis." *Anal Bioanal Chem* 376 (2003): 691-695.

Chada, S. R., and P. J. Hollenbeck. "Nerve factor signaling regulates motility and docking of axonal mitochondria." *Current Biology* 14 (2004): 1272-1276.

Chichkov, BN, C Momma, S Nolte, F von Alvensleben, and A Tünnermann. "Femtosecond, picosecond and nanosecond laser ablation of solids." *Applied Physics A: Materials Science & Processing* 63, no. 2 (1996): 109-115.

Chiem, N, C Colyer, and DJ Harrison. "Microfluidic systems for clinical diagnostics." *Solid State Sensors and Actuators, 1997. Transducers '97 Chicago., 1997 International Conference on* 1 (1997).

Chirico, G, F Olivini, and S Beretta. "Fluorescence excitation in two-photon microsccopy by autocorrelation spectroscopy and photon counting histogram."*Applied Spectroscopy* 54, no. 7 (2000): 1084-1090.

Chung, BG, LA Flanagan, SW Rhee, PH Schwartz, AP Lee, ES Monuki, and NL Jeon. "Human neural stem cell growth and differentiation in a gradient-generating microfluidic device." *Lab Chip* 5 (2005): 401-406.

Chung, SE, W Park, H Park, K Yu, N Park, and S Kwon. "Optofluidic maskless lithography system for real-time synthesis of photopolymerized microstructures in microfluidic channels." *Applied Physics Letters* 91 (2007): 041106.

Contestabile, A., and E. Ciani. "Role of nitric oxide in the regulation of neuronal proliferation survival and differentiation." *Neurochemistry International* 45 (2004): 903-914.

Cooper, JA, HH Lu, FK Ko, and JW Freeman. "Fiber-based tissue-engineered scaffold for ligament replacement: design considerations and in vitro evaluation." *Biomaterials* 26, no. 13 (2005): 1523-1532.

Cremers, DA, and LJ Radziemski. *Handbook of Laser-Induced Breakdown Spectroscopy*: John Wiley, 2006.

Cukierman, E, R Pankov, DR Stevens, and KM Yamada. "Taking cell-matrix adhesions to the third dimension." *Science* 294, no. 5547 (2001): 1708.

Cumpston, G. H., S. P. Ananthavel, S. Barlow, D. L. Dyer, J. E. Ehrlich, L. L. Erskine, A. A. Heikal, S. M. Kuebler, I. Lee, and S. McCord-Maughon. "Two-photon polymerization initiators for three-dimensional optical data storage and microfabrication." *Nature* 398 (1999): 51-54.

Davies, KJ. "Protein damage and degradation by oxygen radicals. I. General aspects." *Journal of Biological Chemistry* 262, no. 20 (1987): 9895-9901.

Davies, MJ. "Reactive species formed on proteins exposed to singlet oxygen." *Photochem. Photobiol. Sci* 3, no. 1 (2004): 17–25.

Davies, MJ, and RJ Truscott. "Photo-oxidation of proteins and its role in cataractogenesis." *J Photochem Photobiol B* 63, no. 1-3 (2001): 114-25.

Denk, W, DW Piston, and WW Webb. "Two-photon molecular excitation in laser-scanning microscopy." *Handbook of Biological Confocal Microscopy*, ed. J Pawley. New York: Plenum Press, 1995.

Denk, W., J. H. Strickler, and W. W. Webb. "Two-photon laser scanning fluorescence microscopy." *Science* 248, no. 4951 (1990): 73-6.

Discher, DE, P Janmey, and Y Wang. "Tissue cells feel and respond to the stiffness of their substrate." *Science*, 310, 1139-1143: American Association for the Advancement of Science, 2005.

Dittrich, PS, K Tachikawa, and A Manz. "Micro total analysis systems. Latest advancements and trends." *Analytical Chemistry* 78, no. 12 (2006): 3887-908.

Duffy, D. C., J. C. McDonald, O. J. A. Schueller, and G. M. Whitesides. "Rapid prototyping of microfluidic systems in polydimethylsiloxane." *Anal. Chem.* 70 (1998): 4974-4984.

Dvorak, HF. "How tumors make bad blood vessels and stroma." *American Journal of Pathology*, 162, 1747-1757: ASIP, 2003.

El-Ali, J, PK Sorger, and KF Jensen. "Cells on chips." *Nature* 442, no. 7101 (2006): 403-411.

Fang, HL, and RL Swofford. "The thermal lens in absorption spectroscopy." *Ultrasensitive Laser Spectroscopy*, ed. D Kliger. New York: Academic Press, 1983.

Folch, A, BH Jo, O Hurtado, DJ Beebe, and M Toner. "Microfabricated elastomeric stencils for micropatterning cell cultures." *Journal of Biomedical Materials Research* 52, no. 2 (2000): 346-353.

Freeman, J. W., M. D. Woods, and C. T. Laurencin. "Tissue engineering of the anterior cruciate ligament using a braid-twist scaffold design." *J Biomech* 40, no. 9 (2007): 2029-36.

Gabrielli, D, E Belisle, D Severino, AJ Kowaltowski, and MS Baptista. "Binding, aggregation and photochemical properties of methylene blue in mitochondrial suspensions." *Photochemistry and Photobiology* 79, no. 3: 227-232.

Galajda, P, and P Ormos. "Complex micromachines produced and driven by light." *Lasers and Electro-Optics, 2002. CLEO '02. Technical Digest. Summaries of Papers Presented at the* (2002): 634-635.

Gallo, G., and P. C. Letourneau. "Localized sources of neurotrophins initiate axon collateral sprouting." *Journal of Neuroscience* 18, no. 14 (1998): 5403-5414.

Garrison, WM. "Reaction mechanisms in the radiolysis of peptides, polypeptides, and proteins." *Chemical Reviews* 87, no. 2 (1987): 381-398.

Geiger, B, A Bershadsky, R Pankov, and KM Yamada. "Extracellular matrix cytoskeleton crosstalk." *Nature Reviews Molecular Cell Biology* 2 (2001): 793.

Getoff, N. "Pulse radiolysis of aromatic amino acids—State of the art." *Amino Acids* 2, no. 3 (1992): 195-214.

Ghashghaei, HT, C Lai, and ES Anton. "Neuronal migration in the adult brain: are we there yet?" *Nature Reviews Neuroscience* 8 (2007): 141-151.

Gratton, E, S Breusegem, N Barry, Q Ruan, and J Eid. "Fluctuation correlation spectroscopy in cells: determination of molecular aggregation, 2004." Biophotonics-Optical Science and Engineering for the 21st Century.

Gregor, T, EF Wieschaus, AP McGregor, W Bialek, and DW Tank. "Stability and nuclear dynamics of the bicoid morphogen gradient." *Cell* 130, no. 1 (2007): 141-152.

Griffith, L. G., and M. A. Swartz. "Capturing complex 3D tissue physiology in vitro." *Nat Rev Mol Cell Biol* 7, no. 3 (2006): 211-24.

Gu, M. *Advanced Optical Imaging Theory*. New York: Springer, 2000.

Haug, E., and W Nakel. *The Elementary Process of Bremsstrahlung*. Vol. 73 World Scientific Notes in Physics. London: World Scientific, 2004.

Hell, SW. "Toward fluorescence nanoscopy." *Nature Biotechnology* 21, no. 11 (2003): 1347-1355.

Hess, ST, and WW Webb. "Focal volume optics and experimental artifacts in confocal fluorescence correlation spectroscopy." *Biophysical Journal* 83, no. 4 (2002): 2300-2317.

Hill, R., J. Lyon, R. Allen, K. Stevenson, and J. Shear. "Microfabrication of three-dimensional bioelectronic architectures." *Journal of the American Chemical Society* 127 (2005): 10707-10711.

Hsu, C., C. Chen, and A. Folch. ""Microcanals" for micropipette access to single cells in microfluidic environments." *Lab Chip* 4 (2004): 420-424.

Huels, MA, B Boudaiffa, P Cloutier, D Hunting, and L Sanche. "Single, double, and multiple double strand breaks induced in DNA by 3-100 eV electrons." *J. Am. Chem. Soc* 125, no. 15 (2003): 4467–4477.

Hui, L, and K Roy. "Biomimetic three-dimensional cultures significantly increase hematopoietic differentiation efficacy of embryonic stem cells." *Tissue Engineering* 11, no. 1/2 (2005).

Igarashi, N, S Onoue, and Y Tsuda. "Photoreactivity of amino acids: tryptophan-induced photochemical events via reactive oxygen species generation." *Analytical Sciences* 23, no. 8 (2007): 943-948.

Ito, H., H. Nomoto, Y. Furukawa, and S. Furukawa. "Neurotrophins facilitate synthesis of choline acetyltransferase and tyrosine hydroxylase in cultured mouse neural stem cells independently of their neuronal differentiation." *Neuroscience Letters* 339 (2003): 231-234.

Janmey, PA. "The cytoskeleton and cell signaling: component localization and mechanical coupling." *Physiological Reviews* 78, no. 3 (1998): 763-781.

Jeon, Noo Li, Harihara Baskaran, Stephan K. W. Dertinger, George M. Whitesides, Livingston Van De Water, and Mehmet Toner. "Neutrophil chemotaxis in linear and complex gradients of interleukin-8 formed in a microfabricated device." *Nature Biotechnology* 20, no. 8 (2002): 826-830.

Joglekar, A. P., H. Liu, G. J. Spooner, E. Meyhofer, G. Mourou, and A. J. Hunt. "A study of the deterministic character of optical damage by femtosecond laser pulses and applications to nanomachining." *Applied Physics B-Lasers and Optics* 77, no. 1 (2003): 25-30.

Juhasz, T, GA Kastis, C Suarez, Z Bor, and WE Bron. "Time-resolved observations of shock waves and cavitation bubbles generated by femtosecond laser pulses in corneal tissue and water." *Lasers Surg Med* 19, no. 1 (1996): 23-31.

Kaehr, B, R Allen, DJ Javier, J Currie, and JB Shear. "Guiding neuronal development with in situ microfabrication." *Proceedings of the National Academy of Sciences* 101, no. 46 (2004): 16104-16108.

Kaehr, B, N Ertas, R Nielson, R Allen, RT Hill, M Plenert, and JB Shear. "Direct-write fabrication of functional protein matrixes using a low-cost q-switched laser." *Anal Chem* 78, no. 9 (2006): 3198-3202.

Kaehr, B, and JB Shear. "Mask-directed multiphoton lithography." *J Am Chem Soc* 129, no. 7 (2007): 1904-5.

Kaiser, A, B Rethfeld, M Vicanek, and G Simon. "Microscopic processes in dielectrics under irradiation by subpicosecond laser pulses." *Physical Review B* 61, no. 17 (2000): 11437-11450.

Kane, RS, S Takayama, E Ostuni, DE Ingber, and GM Whitesides. "Patterning proteins and cells using soft lithography." *Biomaterials* 20, no. 23 (1999): 2363-76.

Karten, B., H. Hayashi, R. B. Campenot, D. E. Vance, and J. E. Vance. "Neuronal models for studying lipid metabolism and transport." *Methods* 36 (2005): 117-128.

Kawata, S., H. B. Sun, T. Tanaka, and K. Takada. "Finer features for functional microdevices." *Nature* 412, no. 6848 (2001): 697-8.

Khademhosseini, A, R Langer, J Borenstein, and JP Vacanti. "Microscale technologies for tissue engineering and biology." *Proceedings of the National Academy of Sciences* 103, no. 8 (2006): 2480-2487.

Knowles, A, and S Gurnani. "A study of the methylene blue-sensitized oxidation of amino acids." *Photochem Photobiol* 16, no. 2 (1972): 95-108.

Kochevar, IE, MC Lynch, S Zhuang, and CR Lambert. "Singlet oxygen, but not oxidizing radicals, induces apoptosis in Hl-60 cells." *Photochemistry and Photobiology* 72, no. 4: 548-553.

Kochevar, IE, and RW Redmond. "Photosensitized production of singlet oxygen." *Methods Enzymol* 319 (2000): 20-8.

Kuebler, S., M. Rumi, T. Watanabe, K. Braun, B. Cumpston, A. Heikal, L. Erskine, S. Thyumanavan, S. Barlow, S. R. Marder, and J. W. Perry. "Optimizing two-photon initiators and exposure conditions of three-dimensional lithographic microfabrication." *Photopolymer Science and Technology*. Chiba, Japan, 2001.

LaFratta, CN, JT Fourkas, T Baldacchini, and RA Farrer. "Multiphoton fabrication." *Angewandte Chemie* 46, no. 33 (2007): 6238.

LaFratta, CN, L Li, and JT Fourkas. "Soft-lithographic replication of 3D polymeric microstructures created with map." *Proceedings of SPIE* 6462 (2007): 646210.

Li, L, and JT Fourkas. "Multiphoton polymerization." *Materials Today* 10, no. 6 (2007): 30-37.

Li, N, A Tourovskaia, and A Folch. "Biology on a chip: microfabrication for studying the behavior of cultured cells." *Crit. Rev. Biomed. Eng* 31, no. 5-6 (2003): 423–488.

Li, S, JL Guan, and S Chien. "Biochemistry and biomechanics of cell motility." *Annu Rev Biomed Eng* 7 (2005): 105-150.

Lohof, AM, M Quillan, Y Dan, and MM Poo. "Asymmetric modulation of cytosolic camp activity induces growth cone turning." *Journal of Neuroscience* 12, no. 4 (1992): 1253-1261.

Lu, H. H., J. A. Cooper, Jr., S. Manuel, J. W. Freeman, M. A. Attawia, F. K. Ko, and C. T. Laurencin. "Anterior cruciate ligament regeneration using braided biodegradable scaffolds: in vitro optimization studies." *Biomaterials* 26, no. 23 (2005): 4805-16.

Lu, Yi, Gazell Mapili, Gerry Suhali, Shaochen Chen, and Krishnendu Roy. "A digital micro-mirror device-based system for the microfabrication of complex, spatially patterned tissue engineering scaffolds." *Journal of Biomedical Materials Research, Part A* 77A, no. 2 (2006): 396-405.

Manevich, Y, KD Held, and JE Biaglow. "Coumarin-3-carboxylic acid as a detector for hydroxyl radicals generated chemically and by gamma radiation." *Radiation Research* 148, no. 6 (1997): 580-591.

Matsuzaki, M., G. Ellis-Davis, T. Nemoto, Y. Miyashita, and H. Kasai. "Dendritic spine geometry is critical for ampa receptor expression in hippocampal ca1 pyramidal neurons." *Nature Neuroscience* 4, no. 11 (2001): 1086-1092.

Muller, U, and D Nicolau. *Microarray Technology and Its Applications*: Springer, 2005.

Nagy, A, J Wu, and KM Berland. "Observation volumes and gamma-factors in two-photon fluorescence fluctuation spectroscopy." *Biophysical Journal* 89, no. 3 (2005): 2077-2090.

Nikogosyan, DN, and H Gorner. "Laser-induced photodecomposition of amino acids and peptides: extrapolation to corneal collagen." *Selected Topics in Quantum Electronics, IEEE Journal of* 5, no. 4 (1999): 1107-1115.

Nikogosyan, DN, D Oraevsky, and V Rubasov. "Two-photon ionization and dissociation of liquid water by powerful laser Uv radiation." *Chemical Physics* 77, no. 1 (1983): 131-143.

Noack, J, A Vogel, and MLC Lubeck. "Laser-induced plasma formation in water at nanosecond tofemtosecond time scales: calculation of thresholds, absorptioncoefficients, and energy density." *Quantum Electronics, IEEE Journal of* 35, no. 8 (1999): 1156-1167.

Parker, DH. "Laser ionization spectroscopy and mass spectrometry." *Ultrasensitive Laser Spectroscopy*, ed. D Kliger, 234-307. New York: Academic Press, 1983.

Paulino, TP, PP Magalhaes, G Thedei, AC Tedesco, and P Ciancaglini. "Use of visible light-based photodynamic therapy to bacterial photoinactivation." *Biochemistry and Molecular Biology Education*, 33, 46-49: ASBMB, 2005.

Peterman, Mark C., Jaan Noolandi, Mark S. Blumenkranz, and Harvey A. Fishman. "Localized chemical release from an artificial synapse chip." *Proceedings of the National Academy of Sciences of the United States of America* 101, no. 27 (2004): 9951-9954.

Pfefer, TJ, KF Chan, DX Hammer, and AJ Welch. "Dynamics of pulsed holmium: yag laser photocoagulation of albumen." *Physics in Medicine and Biology* 45, no. 5 (2000): 1099-1114.

Pitts, JD, PJ Campagnola, GA Epling, and SL Goodman. "Submicron multiphoton free-form fabrication of proteins and polymers: studies of reaction efficiencies and applications in sustained release." *Macromolecules* 33, no. 5 (2000): 1514-1523.

Plenert, ML, and JB Shear. "Microsecond electrophoresis." *Proceedings of the National Academy of Sciences* 100, no. 7 (2003): 3853-3857.

Provinciali, M., G. D. Stefano, and N. Fabris. "Optimization of cytotoxic assay by target cell retention of the flourescent dy carboxyfluorescein diacetate and comparison with conventional CR release assay." *Journal of Immunological Methods* 155 (1992): 19-24.

Satoh, T., S. Sakai, T. Kubo, Y. Enokido, Y. Uchiyama, and H. Hatanaka. "Flow cytometric analysis of serum deprivation-induced apoptosis of PC12 cells, with special reference to the role of BCL-2." *Neuroscience Letters* 201 (1995): 119-122.

Schaffer, C.B., A.O. Jamison, J.F. Garcia, and E Mazur. "Structural changes induced in transparent materials with ultrashort laser pulses." *Ultrafast Lasers*, ed. G. Sucha, 395-418. New York: Marcel Dekker Inc., 2003.

Schaffer, CB, A Brodeur, and E Mazur. "Laser-induced breakdown and damage in bulk transparent materials induced by tightly focused femtosecond laser pulses." *Measurement Science and Technology* 12, no. 11 (2001): 1784-1794.

Schönle, A, and SW Hell. "Heating by absorption in the focus of an objective lens." *Optics Letters* 23 (1998): 325-327.

Schou, J, S Amoruso, and JG Lunney. "Plume dynamics." *Laser Ablation and Its Applications*, ed. C Phipps, 67: Springer, 2007.

Schüssler, H, S Navaratnam, and L Distel. "Pulse radiolysis studies on histones and serum albumin under different ionic conditions." *Radiation Physics and Chemistry* 61, no. 2 (2001): 123-128.

Schüssler, H, and M Puchala. "Oxygen effect in the radiolysis of proteins: v. histones." *Radiation Physics and Chemistry* 69, no. 1 (2004): 45-53.

Seet, BKK, V Mizeikis, S Matsuo, S Juodkazis, and H Misawa. "Three-dimensional spiral-architecture photonic crystals obtainedby direct laser writing." *Microporous Mesoporous Mater* 58 (2003): 105.

Sengupta, P, J Balaji, S Mukherjee, R Philip, GR Kumar, and S Maiti. "Determination of the absolute two-photon absorption cross section of tryptophan." *Proc. SPIE* 4262 (2001): 336-339.

Seong, GH, J Heo, and RM Crooks. "Measurement of enzyme kinetics using a continuous-flow microfluidic system." *Anal Chem* 75, no. 13 (2003): 3161-7.

Serbin, J., A. Egbert, A. Ostendorf, B. N. Chichkov, R. Houbertz, G. Domann, J. Schulz, C. Cronauer, L. Frohlich, and M. Popall. "Femtosecond laser-induced two-photon polymerization of inorganic-organic hybrid materials for applications in photonics." *Optics Letters* 28, no. 5 (2003): 301-303.

Shah, L, J Tawney, M Richardson, and K Richardson. "Self-focusing during femtosecond micromachining of silicate glasses." *Quantum Electronics, IEEE Journal of* 40, no. 1 (2004): 57-68.

Shen, HR, JD Spikes, P Kopecekova, and J Kopecek. "Photodynamic crosslinking of proteins. I. Model studies using histidine-and lysine-containing N-(2-hydroxypropyl) methacrylamide copolymers." *J Photochem Photobiol B* 34, no. 2-3 (1996): 203-10.

Shen, HR, JD Spikes, P Kopeckova, and J Kopecek. "Photodynamic crosslinking of proteins. II. Photocrosslinking of a model protein-ribonuclease A." *J Photochem Photobiol B* 35, no. 3 (1996): 213-9.

Shen, R. Y. *The Principles of Non-Linear Optics*. New York: John Wiley and Sons, 1983.

Silva, GA, C Czeisler, KL Niece, E Beniash, DA Harrington, JA Kessler, and SI Stupp. "Selective differentiation of neural progenitor cells by high-epitope density nanofibers." In *Science*, 303, 1352-1355: American Association for the Advancement of Science, 2004.

Sims, C, and N Allbritton. "Analysis of single mammalian cells on-chip." *Lab on a Chip* 7 (2007): 423-440.

Singh-Gasson, S, RD Green, Y Yue, C Nelson, F Blattner, MR Sussman, and F Cerrina. "Maskless fabrication of light-directed oligonucleotide microarrays using a digital micromirror array." *Nature Biotechnology* 17 (1999): 974-978.

Sohn, YS, A Goodey, EV Anslyn, JT McDevitt, JB Shear, and DP Neikirk. "A microbead array chemical sensor using capillary-based sample introduction: toward the development of an “electronic tongue”." *Biosensors and Bioelectronics* 21, no. 2 (2005): 303-312.

Song, H, CF Stevens, and FH Gage. "Astroglia induce neurogenesis from adult neural stem cells." *Nature* 417 (2002): 39-44.

Song, HJ, and MM Poo. "Signal transduction underlying growth cone guidance by diffusible factors." *Curr. Opin. Neurobiol* 9 (1999): 355-363.

Stuart, BC, MD Feit, S Herman, AM Rubenchik, BW Shore, and MD Perry. "Nanosecond-to-femtosecond laser-induced breakdown in dielectrics." *Physical Review B* 53, no. 4 (1996): 1749-1761.

Stuart, BC, Feit MD, Rubenchik AM, Sore BW, and Perry MD. "Laser-induced damage in dielectrics with nanosecond to subpicosecond pulses." *Phys. Rev. Lett* 74 (1995): 2248.

Sun, C, N Fang, DM Wu, and X Zhang. "Projection micro-stereolithography using digital micro-mirror dynamic mask." *Sensors and Actuators A: Physical* 121, no. 1 (2005): 113-120.

Sun, HB, and S Kawata. "Two-photon photopolymerization and 3D lithographic microfabrication." *Adv. Polym. Sci* 170 (2004): 169-273.

Svitkina, TM, AB Verkhovsky, KM McQuade, and GG Borisy. "Analysis of the actin-myosin II system in fish epidermal keratocytes: mechanism of cell body translocation." *The Journal of Cell Biology* 139, no. 2 (1997): 397-415.

Takayama. "Selective chemical treatment of cellular microdomains using multiple laminar streams." *Chem. Biol* 10, no. 2 (2003): 123–130.

Takayama, S., E. Ostuni, P. LeDuc, K. Naruse, D. E. Ingber, and G. M. Whitesides. "Subcellular positioning of small molecules." *Nature* 411 (2001): 1016.

Taylor, Anne M., Seog Woo Rhee, Christina H. Tu, David H. Cribbs, Carl W. Cotman, and Noo Li Jeon. "Microfluidic multicompartment device for neuroscience research." *Langmuir* 19, no. 5 (2003): 1551-1556.

Teh, WH, U Dürig, U Drechsler, CG Smith, and HJ Güntherodt. "Effect of low numerical-aperture femtosecond two-photon absorption on (Su-8) resist for ultrahigh-aspect-ratio microstereolithography." *Journal of Applied Physics* 97 (2005): 054907.

Tessier-Lavigne, M. "The molecular biology of axon guidance." *Science* 274, no. 5290 (1996): 1123-1133.

Tien, AC, S Backus, H Kapteyn, M Murnane, and G Mourou. "Short-pulse laser damage in transparent materials as a function of pulse duration." *Physical Review Letters* 82, no. 19 (1999): 3883-3886.

Tsai, CH, A Stern, JF Chiou, CL Chern, and TZ Liu. "Rapid and specific detection of hydroxyl radical using an ultraweak chemiluminescence analyzer and a low-level chemiluminescence emitter: application to hydroxyl radical-scavenging ability of aqueous extracts of food constituents." *J Agric Food Chem* 49, no. 5 (2001): 2137-41.

Van Kessel, PF, LJ Hornbeck, RE Meier, MR Douglass, TI Inc, and TX Plano. "A mems-based projection display." *Proceedings of the IEEE* 86, no. 8 (1998): 1687-1704.

Verrechia, F., F. Duthe, S. Duval, I. Duchatelle, D. Sarrouilhe, and J. C. Herve. "ATP counteracts the rundown of gap junctional channels of rat ventricular myocytes by promoting protein phosphorylation." *Journal of Physiology* 516 (1999): 447-459.

Verweij, H, and J van Steveninck. "Model studies on photodynamic cross-linking." *Photochem. Photobiol* 35 (1982): 265–267.

Viravaidya, K, A Sin, and ML Shuler. "Development of a microscale cell culture analog to probe naphthalene toxicity." *Biotechnology Progress* 20, no. 1 (2004): 316-323.

Vogel, A, G Hiittman, and G Paltauf. "Femptosecond plasma-mediated nanosurgury of cells and tissues." In *Laser Ablation and Its Applications*, ed. C Phipps. New York: Springer, 2007.

Vogel, A, K Nahen, D Theisen, and J Noack. "Plasma formation in water by picosecond and nanosecond ND: yag laserpulses. I. Optical breakdown at threshold and superthreshold irradiance." *Selected Topics in Quantum Electronics, IEEE Journal of* 2, no. 4 (1996): 847-860.

Vogel, A., J. Noack, G. Huttman, and G. Paltauf. "Mechanisms of femtosecond laser nanosurgery of cells and tissues." *Applied Physics B-Lasers and Optics* 81, no. 8 (2005): 1015-1047.

Vogt, A. K., G. Wrobel, W. Meyer, W. Knoll, and A. Offenhauser. "Synaptic plasticity in micropatterned neural networks." *Biomaterials* 26 (2005): 2549-2557.

Vozzi, G, C Flaim, A Ahluwalia, and S Bhatia. "Fabrication of plga scaffolds using soft lithography and microsyringe deposition." *Biomaterials* 24, no. 15 (2003): 2533-40.

Wang, G. X., and M. M. Poo. "Requirement of TRPC channels in netrin-1-induced chemotropic turning of nerve growth cones." *Nature* 434 (2005): 898-903.

Weibel, DB, WR DiLuzio, and GM Whitesides. "Microfabrication meets microbiology." *Nature Reviews Microbiology* 5 (2007): 209-218.

Whitesides, G. M. "The origins and the future of microfluidics." *Nature* 442, no. 7101 (2006): 368-373.

Whitesides, GM, E Ostuni, S Takayama, X Jiang, and DE Ingber. "Soft lithography in biology and biochemistry." *Annual Review of Biomedical Engineering* 3, no. 1 (2001): 335-373.

Winters, BS, BK Raj, EE Robinson, RA Foty, and SA Corbett. "Three-dimensional culture regulates raf-1 expression to modulate fibronectin matrix assembly." *Molecular Biology of the Cell* 17, no. 8 (2006): 3386.

Wise, DD, and JB Shear. "Quantitation of nicotinamide and serotonin derivatives and detection of flavins in neuronal extracts using capillary electrophoresis with multiphoton-excited fluorescence." *Journal of Chromatography A* 1111, no. 2 (2006): 153-158.

Wu, ES, JH Strickler, WR Harrell, and WW Webb. "Two-photon lithography for microelectronic application." *SPIE Proc* 1674 (1992): 776.

Wu, Hongkai, Bo Huang, and Richard N. Zare. "Generation of complex, static solution gradients in microfluidic channels." *Journal of the American Chemical Society* 128, no. 13 (2006): 4194-4195.

Wu, S, J Serbin, and M Gu. "Two-photon polymerisation for three-dimensional micro-fabrication." *Journal of photochemistry and photobiology. A, Chemistry* 181, no. 1 (2006): 1-11.

Xu, C, and WW Webb. "Multiphoton excitation of molecular fluorophores and nonlinear laser microscopy." *Topics in Fluorescence Spectroscopy*, ed. J Lakowicz, 5, 471–540. New York: Springer, 1997.

Xu, YW, JR Zhang, YM Deng, LK Hui, SP Jiang, and SH Lian. "Fluorescence of proteins induced by two-photon absorption." *J Photochem Photobiol B* 1, no. 2 (1987): 223-7.

Zhang, X, and M Poo. "Localized synaptic potentiation by BDNF requires local protein synthesis in the developing axon." *Neuron* 36, no. 4 (2002): 675-688.

Zheng, J. Q., J. Wan, and M. M. Poo. "Essential role of filapodia in chemotropic turning of growth cone induced by a glutamate gradient." *Journal of Neuroscience* 16 (1996): 1140-1149.

Zipfel, WR, RM Williams, and WW Webb. "Nonlinear magic: multiphoton microscopy in the biosciences." *Nature Biotechnology* 21, no. 11 (2003): 1369-1377.

Vita

Rex Young Nielson was born in Provo, Utah on December 18, 1969 to Keith and Geraldine Nielson. He attended public schools in Orem, Utah and worked for several years before enrolling at the University of Utah, where he earned a Bachelor of Science in Chemistry (2002) as well as a Master of Science in Chemistry (2003). In 2003, he entered the Chemistry graduate program at the University of Texas at Austin.

Permanent address: 1519 Springdell Circle, Provo, UT 84604

This dissertation was typed by the author.